Effect of the Initial Out-of-Straightness on the Lateral Torsional Buckling Strength of Steel Beams

Ming Li

Thesis submitted to the
Faculty of Graduate and Postdoctoral Studies
in partial fulfillment of the requirements
for the degree of Master of Applied Science in Civil Engineering

Department of Civil Engineering
Faculty of Engineering
University of Ottawa

Abstract

The effect of initial out-of-straightness of steel beams with wide flange cross-sections on their elastic lateral torsional buckling strength is investigated analytically and numerically. A variational principle is first developed and then used to obtain the governing equilibrium conditions and associated boundary conditions for a beam with general patterns of initial out-of-straightness and initial angles of twist. The principle is then used to develop a finite element formulation to characterize the lateral torsional response of beams with initial out-of-straightness under general transverse loading. The validity of the finite element formulation is verified through comparison against results from models based thin-walled beam finite element and shell element models available in ABAQUS. Since the load lateral displacement responses do not exhibit a distinct point of loss of stability, two design criteria are proposed for the characterization of the failure. The first criterion is based on a threshold value for additional lateral displacement and the second criterial is based on a threshold value for the normal stresses. Both criteria are applied in conjunction with the analytical solution and finite element formulation in order to determine a moment resistance based on lateral torsional buckling that incorporates the effect of initial out-of-straightness. The moment capacity based on the displacement-based criterion is shown to solely depend on the ratio between the initial out-of-straightness component associated with the first buckling mode and the additional displacement threshold value specified. To the contrary, moment capacity based on the stress criterion, was found to depend upon the initial out-of-straightness magnitude, the normal stress threshold value and the geometry of the cross-section.

The effects of the above parameters on the predicted moment capacity were investigated for beams with common sections in a systematic parametric study. Possible means of modifying the present provisions of CAN-CSA S16 relating to elastic lateral torsional buckling to incorporate the effect of initial out-of-straightness effects are discussed and illustrated through examples.

The load-deformation plots for beams with initial out-of-straightens as predicted by the formulations developed in the present study are then used to extend the Southwell plot technique, originally developed for buckling of column with initial out-of-straightness, to the lateral torsional buckling of beams with initial out-of-straightness. The study shows that the plot, either experimentally or analytically obtained, of the applied load versus lateral displacement, at any point or angle of twist at any section, for a beam with initial out-of-straightness case can predict

(a) the elastic critical moment of an analogous initially straight beam, and (b) the first buckling mode contribution to the initial out-of-straightness.

Acknowledgements

I would have never accomplished my thesis without the guidance of my supervisor Dr. Magdi Mohareb. I would like to convey my profound gratitude to Dr. Magdi Mohareb for sharing his prominent knowledge and expertise in the technical problems and editing hence his great patience to guide me to finish a tough job like this thesis. I will always cherish those meetings we had and carry forward what I learned throughout my future study and work.

I would also like to thank my colleagues Dr. Arash Sahraei and Mr. Huade Cao for their help and suggestions.

Finally, I would like to thank my parents for their financial and moral support, and my girlfriend Tong Zeng for her sacrifice and encouragement through the tough moments.

TABLE OF CONTENTS

LIST OF SYMBOLS

A	area;
B	bimoment;
b	flange width;
C	moment gradient factor;
C_e	elastic buckling resistance for columns;
C_r	column buckling resistance;
C_w	warping constant;
$\{\mathbf{d}\}$	nodal displacement vector;
$\{\mathbf{d_0}\}$	initial nodal displacement vector;
d	total section height;
E	modulus of elasticity;
F_{cr}	elastic critical strength in American design provisions;
F_y	yield strength;
$\{\mathbf{F}(\mathbf{d_0})\}$	external force vector induced by the IOS ;
$\{\mathbf{f}\}$	nodal force vector;
G	shear modulus;
$\langle \mathbf{H}(\mathbf{z}) \rangle_{1\times 2}^{T}$	vector of linear shape functions;
I_x	moment of inertia about x-aixs
I_y	moment of inertia about y-aixs
J	Saint-Venant torsional constant;
K	effective length factor;
k_t	twist restraint factor;
k_l	load height factor;
k_r	lateral rotation restraint;
$[\mathbf{k_e}]$	elastic stiffness matrix;
$[\mathbf{k_g}]$	geometric stiffness matrix;
L	span;
l_e	effective length;
L_p	length between yield failure and inelastic LTB;
L_r	length between inelastic and elastic LTB;
m	sequence number;
$\mathbf{M^T}$	nodal moment vector;
M	applied moment;
M_i	inelastic lateral torsional buckling moment;
M_p	sectional plastic moment;

M_u	critical elastic moment;
M_Y	sectional yield moment;
$M_{\max}$	Maximum moment along the span;
M_A, M_B, M_C	Moment value at $L/4, L/2, 3L/4$
M_{cr}	elastic critical moment from the eigenvalue as determined from eigen-value analysis
M_{cri}	elastic critical moment for mode i;
M_1, M_2	Equivalent nodal moment;
M_x	strong axis bending moment;
M_y	weak axis bending moment about y-axis;
q	transverse load;
U	internal strain energy;
$\langle \mathbf{u_N} \rangle^T$	vector of nodal lateral displacement;
$\langle \mathbf{u_{0N}} \rangle^T$	vector of nodal initial lateral displacement;
$u(z)$	additional lateral displacement at section shear centre as a function of coordinate
$u_0(z)$	initial out-of-straightness (IOS) at section shear centre;
$u_{0-c}(z)$	IOS at the compression flange;
$u_c(z)$	additional peak lateral displacement at the compression flange;
$\bar{u}_c(z)$	total out-of-straightness at the compression flange;
$u_{0-t}(z)$	IOS at the tension flange;
$u_{0-p}(z)$	peak IOS at either flange;
$u_{0-q}(z)$	IOS at the other flange corresponding to u_{0-p};
$u_i(z)$	lateral buckling shape corresponding to mode i;
V	load potential energy;
v	transverse displacement;
w	web thickness;
z	longitudinal coordinate;
Z_e	effective section modulus;
α_{LT}	recommended imperfection factor;
α_m	moment modification factor in Australian Standard;
α_s	slenderness reduction in Australian Standard;
ε	stress fraction;
η_i	eigen vector for buckling mode i;
η_1	first buckling mode normalized by the peak IOS at the compression flange

η_3	third buckling mode normalized by the peak IOS at the compression flange
$\theta(z)$	additional angle of twist;
$\bar{\theta}(z)$	Total angle of twist;
$\theta_0(z)$	initial angle of twist (IAT);
$\theta_i(z)$	twisting buckling function for mode i;
$\langle \boldsymbol{\theta}_{\mathbf{N}} \rangle^T$	vector of nodal angles of twist;
$\langle \boldsymbol{\theta}_{\mathbf{0N}} \rangle^T$	vector of nodal initial angles of twist (IAT);
κ	fitting coefficient for the nominal moment equation in stress criterion
λ	load scaling factor;
λ_e	section slenderness in Australian Standards;
$\bar{\lambda}_{LT}$	slenderness parameter in Eurocode 3;
μ	yield to critical moment ratio;
π	total potential energy;
σ	normal stress;
τ	column slenderness
Φ_{LT}	intermediate coefficient in Eurocode 3;
φ	resistance factor;
χ	residual stress pattern factor for columns;
χ_{LT}	lateral torsional buckling reduction factor;
ϕ_i	scaling factor for mode i ;
ω	warping function of the cross-section

LIST OF ACRONYMS

IOS	Initial out-of-straightness;
IAT	Initial angle of twist;
LTB	Lateral torsional buckling;
TLOS	Total lateral out-of-straightness;
TAT	Total angle of twist;

LIST OF FIGURES

LIST OF TABLES

1. Introduction

1.1 Background

In the design for laterally unsupported steel beams, the resistance is often governed by the lateral torsional buckling (LTB) mode of failure. For the idealized case of a perfectly straight beam with a wide flange section subjected bent about the strong axis, the buckling point is associated with a distinct bifurcation point at which the beam exhibits a sudden change in the deformation pattern characterized by sudden lateral bending and twist. The buckling load level corresponding to such a point of instability is detected by solving an eigenvalue problem. Real steel beams possess inevitable initial out-of-straightness during the manufacturing process. Thus, unlike the idealized case of a perfectly straight beam, when real beams are subjected to strong axis bending, they do not exhibit a clear-cut point of bifurcation. Rather, such beams exhibit gradual lateral bending and twist as the applied transverse loads are incrementally increased. When the applied loads approach the theoretical buckling load of a perfectly straight beam, lateral displacements and twist tend to become excessive, typically attaining threshold displacement and/or stress values prior to attaining the critical loads determined for idealized perfectly straight beam. Thus, the lateral torsional buckling resistance of a real beam is, in principle, inferior to that of a comparable straight beam. The detrimental effect of initial crookedness on lateral torsional bucking resistance is reflected in some of the structural steel design standards, but is omitted in others. Thus, the present study intends to characterize the lateral torsional buckling strength reduction induced by the initial crookedness of the beams. The following sections thus provide a review of lateral torsional buckling provisions in international steel design standards with emphasis on aspects related to initial crookedness.

1.2 Lateral torsional buckling behavior of straight versus initially crooked beams

Consider a perfectly straight beam (configuration 1 in Figure 1.1). Upon the application of a transverse load P, the straight beam deflects vertically by a displacement v from configuration 1 to configuration 2. The applied load is then assumed to increase by a factor λ and attain the value λP at the onset of buckling (Configuration 3) where the pre-buckling displacement is assumed to increase to λv. At configuration 3, the section has a tendency to buckle to Configuration 4 by

moving laterally to displacement u_b and twisting through angle θ_b (Configuration 4). The corresponding load versus lateral displacement relation P - u_b is depicted in Figure 1.1b where no lateral displacements take place between 1-3 and a sudden displacement takes place between3-4. The buckling load λP is obtained through an eigenvalue analysis. In contrast, for beams with initial out-of-straightness u_0, θ_0 in the un-deformed state (configuration 1') by incrementally applying transverse load P, the section undergoes gradually increasing lateral displacement u and angle of twist θ as depicted by the nonlinear loading path 1-2'-3'4' and asymptotically approach the buckling load λP from below. The behavior is fundamentally different from that of a perfectly straight beam and no clear-cut buckling load exist. Thus, it would be of interest trace the nonlinear load deformation path 1'-2'-3'-4'. At a given lateral displacement (or a given stress), the difference ΔP between the buckling load based on a perfectly straight beam and that for an initially crooked beam is measure of loss of lateral torsional buckling loss of strength of the member due to initial out-of-straightness. As will be shown in the following sections, this loss in strength has been considered in some but not all structural steel design standards.

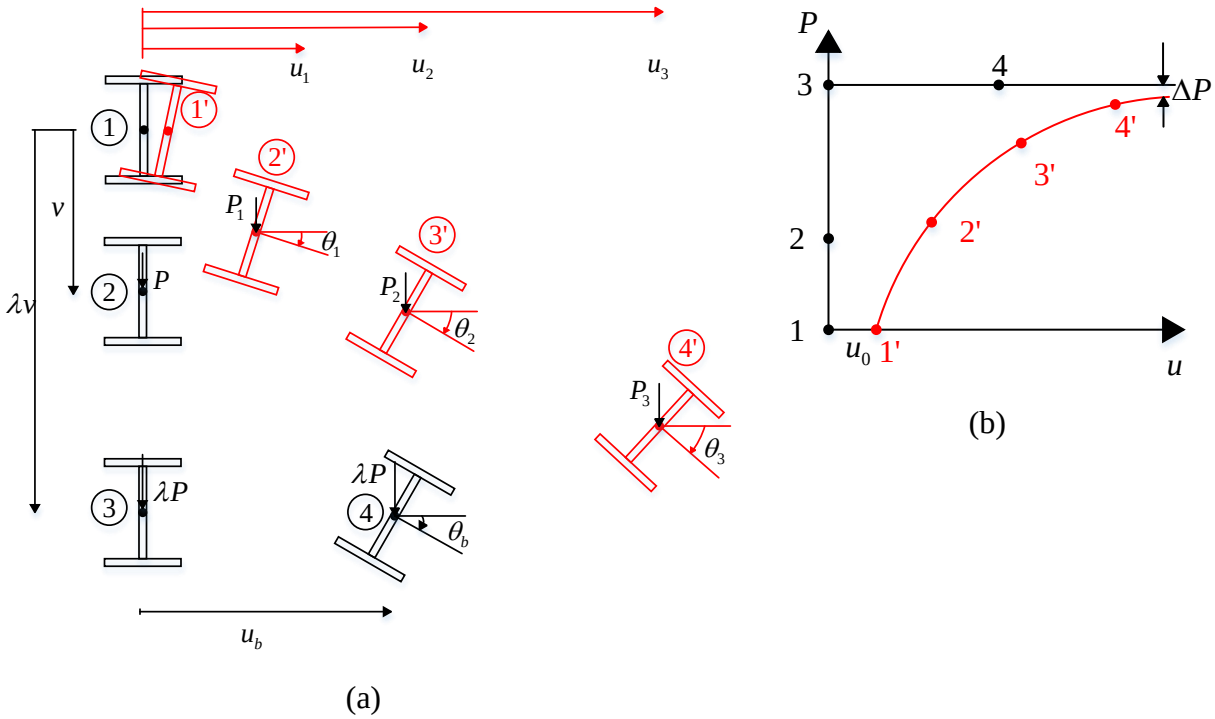

Figure 1.1 (a) Lateral torsional buckling configuration and (b) moment versus lateral displacement relationship for straight and initially crooked beams

1.3 Design standard provisions for beams

In various national design standards for steel members, discrepancies are observed in determining the LTB resistance for beams depending on whether the detrimental effect of the initial geometric imperfection has been accounted for or not. Thus, design provisions for beams are demonstrated to present the discrepancies in this section.

1.3.1 Canadian steel design standard

For laterally unsupported members with doubly symmetric sections subjected to bending in CAN/CSA S16-14, the moment resistance M_r is classified by the section class. For beams with class 1 and 2 sections, the moment resistance M_r is computed based on the sectional plastic moment M_p. For class 3 and 4 sections, the sectional yield moment M_Y is used in calculating the moment resistance. The following narrative is based on beams with class 1 and 2 sections. The boundary conditions are assumed simply supported with respect to the lateral displacement and the angle of twist. Three ranges governed by different failure modes are proposed for designing in the Canadian design provision standard. These ranges are distinguished by the sectional plastic moment M_p and the critical elastic moment M_u which is given by

$$M_u = \frac{C_{CAN}\pi}{L}\sqrt{EI_yGJ + \left(\frac{\pi E}{L}\right)^2 I_y C_w} \tag{1.1}$$

in which, L is the span between lateral torsional supports, E is the modulus of elasticity of steel, G is the shear modulus, I_y is the weak axis moment of inertia, J is the Saint-Venant torsional constant, and C_w is the warping constant. The coefficient C_{CAN} is a moment gradient coefficient given by $4M_{\max}\Big/\sqrt{M_{\max}^2 + 4M_a^2 + 7M_b^2 + 4M_c^2} \le 2.5$ and accounts for the increase in lateral torsional buckling resistance due to uniform bending moments, and M_a, M_b, M_c are the moments at quarter-span, half-span, and three-quarter span, respectively, and $M_{\max}$ is the maximum moment within the unsupported span L.

For comparatively long beams (i.e. $M_u \le 0.67M_p$ proposed in CAN/CSA S16-14), the moment resistance is governed by the elastic lateral torsional buckling failure mode and given by φM_u,

which is the primary focus of the present thesis. The resistance factor φ accounts for the material variability in the material properties (e.g. E, G, F_y etc.).

When $M_u > 0.67M_p$, the flexural resistance of the beams with intermediate spans is governed by inelastic lateral torsional buckling (LTB) failure mode. However, the inelastic lateral torsional buckling moment cannot exceed the resistance φM_p, i.e., the flexural resistance of very short beams is governed by yielding. To sum up, the moment resistance M_r proposed in CAN/CSA S16-14 is given by

$$M_r = \begin{cases} \varphi M_u & M_u \le 0.67M_p \\ M_i = \varphi 1.15M_p\left[1-\dfrac{0.28M_p}{M_u}\right] & M_u > 0.67M_p \\ \varphi M_p & M_i > M_p \end{cases} \tag{1.2}$$

The curve for Eq. (1.2) in CAN/CSA S16-14 is depicted in Figure 1.2 (a) with the elastic buckling curve from the bifurcation problem. For beams undergoing elastic LTB under uniform bending moments (i.e. $C_{CAN} = 1$) and the variability in material properties are omitted (i.e. $\varphi = 1$), Eq. (1.2) (a) is simplified as Eq. (1.1) by Timoshenko (1961) which accounts for no initial out-of-straightness. Thus, Eq. (1.2) (a) in CAN/CSA S16-14 is based on the eigenvalue solution which assumes a perfectly straight member. The fact that the Canadian standard provisions do not involve a reduction the elastic critical moment capacity $M_r = \varphi M_u$ is indicative of the fact that they do not capture the effect of initial out-of-straightness in the design equation for flexural members. This contrasts with approach taken by the Canadian standards for the design of compression members as will be outlined in the following section.

For a member with doubly symmetric cross-sections subjected to axial compression, the resistance C_r is given by

$$C_r = \varphi A F_y \left(1+\tau^{2\chi}\right)^{-1/\chi} \tag{1.3}$$

in which A is the gross cross-section area, F_y is the yield strength, $\tau = KL/\pi r\sqrt{F_y/E}$ is a slenderness factor characterizing the length of the member and the boundary conditions, K is a

effective length factor accounting for the effect of boundary conditions on the response of the axial compression member, r is the radius of gyration given by $\sqrt{I/A}$ (I_x or I_y based on the boundary conditions) and χ is a factor depending on the residual stress patterns in the member and is taken as 1.34 for hot-rolled sections and 2.24 for welded sections. In Figure 1.2 (b), the dimensionless resistance for columns $C_r/\varphi AF_y$ (normalized with respect to the factored yield strength) is plotted in terms of the slenderness KL/r. The dimensionless resistance is observed to be lower than the normalized elastic buckling curve $C_e / AF_y = \pi^2 E / F_y \left(KL/r\right)^2$ in Figure 1.3 (b). For example, when the weak axis slenderness $KL/r = 125.4$, the normalized resistances as given in Figure 1.2 (b) are C_r = 0.30 and C_e = 0.50. The percentage difference of 40.0% accounts for initial out-of-straightness. When KL/r increases to 170.9, the corresponding normalized resistance are C_r = 0.18 and C_e = 0.27, a 33.3% percentage difference. The lower reduction in this case, suggests that the strength reduction due to initial out-of-strength reduces as the column slenderness increases. The fact that the design equation plot coincides with the elastic buckling plot in Figure 1.2a, while the design equation plot is lower than the elastic buckling plot in Figure 1.2b, indicate that initial-out-of-straightness is omitted for beam design provisions but accounted for in compression member design provisions. This discrepancy is one of the motives of the present study.

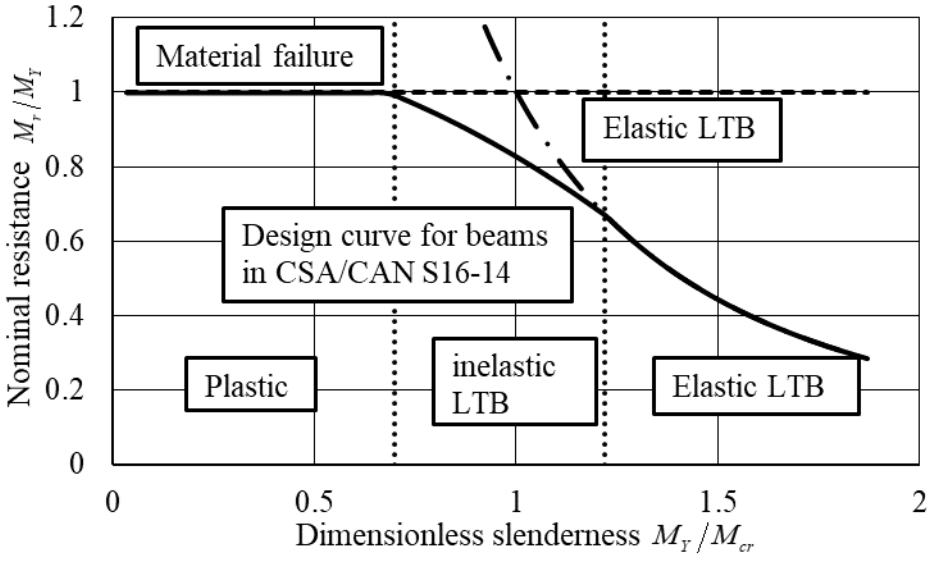

(a)

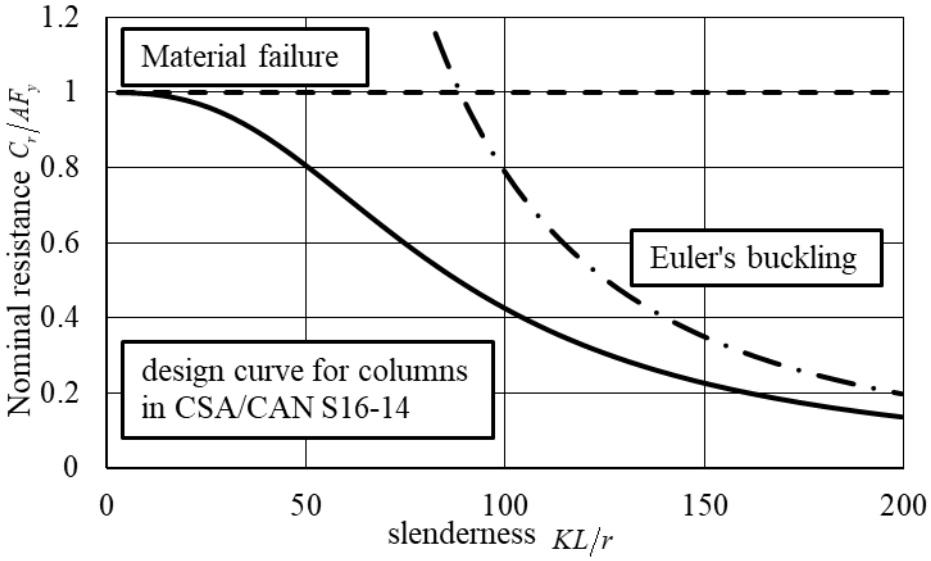

(b)

Figure 1.2 Comparison between the design curves in CAN/CSA S16-14 and the elastic buckling curve for (a) beams and (b) columns

1.3.2 American steel design standard

For members with doubly symmetric I-profile undergo bending about their strong axis, the American design provisions (ANSI/ASCI 360-16) distinguish the governing failure mode by lengths of the member. For beams with spans smaller than the limiting length $L_p = 1.76 r_y \sqrt{E/F_y}$, the moment resistance is deemed to be governed by yielding and is given by the sectional plastic

moment M_p. For beams with intermediate length, i.e., larger than L_p but smaller than L_r, The limiting length L_r is given by

$$L_r = 1.95 r_{ts} \frac{E}{0.7F_y} \sqrt{\frac{Jc}{S_x h_o} + \sqrt{\left(\frac{Jc}{S_x h_o}\right)^2 + 6.76\left(\frac{0.7F_y}{E}\right)^2}} \tag{1.4}$$

the resistance of the member is governed by the inelastic LTB. In Eq. (1.4) which, $r_{ts}^2 = \sqrt{I_y C_w / S_x}$ and $c = 1$ for doubly symmetric I-sections and $c = (h_o/2)\sqrt{I_y/C_w}$ for channels. When $L > L_r$, the moment resistance is governed by the elastic LTB given by $F_{cr} S_x$, in which F_{cr} is given by

$$F_{cr} = \frac{C_{ANSI}\pi^2 E}{\left(\frac{L}{r_{ts}}\right)^2} \sqrt{1 + 0.078 \frac{J_c}{S_x h_0}\left(\frac{L_b}{r_{ts}}\right)^2} \tag{1.5}$$

where C_{ANSI} is the moment gradient factor specified in ANSI/AISC 360-10 and given by $C_{ANSI} = 12.5M_{\max} / \left(2.5M_{\max} + 3M_{L/4} + 4M_{L/2} + 3M_{3L/4}\right)$, h_0 is the distance between the flange centroids. From the relation $r_{st} = \sqrt{I_y C_w} / S_x$, by substitution into Eq. (1.5) and multiplying both sides by S_x, one obtains

$$M_r = F_{cr} S_x = \frac{C_{ANSI}\pi}{L} \sqrt{\left(\frac{E\pi}{L}\right)^2 I_y C_w + E I_y G J \left(0.078 E\pi^2 \sqrt{C_w / I_y} / G h_0\right)} \tag{1.6}$$

Eq. (1.6) is similar in form as Eq. (1.1) except the term $\left(0.078 E\pi^2 \sqrt{C_w/I_y} / G h_0\right)$. For a doubly symmetric I-sections, it can be shown that the term $\left(0.078 E\pi^2 \sqrt{C_w/I_y} / G h_0\right) = 1$. Thus, Eq. (1.5) is another form of Eq. (1.1) and does not capture the initial out-of-straightness effects. To sum up, the nominal flexural resistance for members subjected to strong axis bending based on the American design provision is given by

$$M_r = \begin{cases} M_p & L \le L_p \\ C_{ANSI}\left[M_p - \left(M_p - 0.7F_yS_x\right)\left(\dfrac{L-L_p}{L_r-L_p}\right)\right] & L_r < L \le L_p \\ F_{cr}S_x & L > L_r \end{cases} \tag{1.7}$$

The nominal flexural resistance-span relationship based on Eq. (1.7) is plotted in Figure 1.3 (a). for a W200x36 cross-sections. For $L > L_r$, the lateral torsional buckling resistance based on ANSI/AISC 360-16 provisions coincides with the elastic critical moment, i.e., the no effects of initial imperfection are not accounted for in the design strength provisions. This observation contrasts with the approach taken in the same standard for compression which will be presented in the following

For compression members, the nominal compressive strength in the ANSI/AISC 360-16 is given by

$$C_r = F_{cr}A \tag{1.8}$$

in which the stress F_{cr} is given by

$$F_{cr} = \begin{cases} \left(0.658^{F_y/F_e}\right)F_y & KL/r \le 4.71\sqrt{E/F_y} \\ 0.877F_e & KL/r > 4.71\sqrt{E/F_y} \end{cases} \tag{1.9}$$

and $F_e = \pi^2 E/\left(KL/r\right)^2$ is the Euler's buckling stress as determined from an elastic (eigenvalue) buckling analysis which does not account for the detrimental effect of the initial out-of-straightness on the buckling strength. For $E = 200,000MPa$ and $F_y = 350MPa$, the threshold value is $4.71\sqrt{E/F_y} = 112.6$.

The adoption of an empirical fraction of the theoretical elastic buckling stress $0.877F_e$ for a perfectly straight column, the standard accounts for the strength reduction due to the initial geometric imperfection when determining the design strength for long columns. Figure 1.3 (b) depicts the normalized compressive resistance based on the American steel design standard in

terms of the slenderness KL/r for a W200x36 cross-section. Like the design curve for columns in CAN/CSA S16-14 (Figure 1.2 (b)), the nominal resistance for columns provides is lower than the elastic buckling resistance. The 12.3% difference in strength between the nominal design strength and the elastic buckling strength accounts for the strength reduction due to column out-of-straightness. In a manner similar to CAN/CSA S16-14, the design rules columns of American standard accounts for the detrimental effect of the initial out-of-straightness when characterizing the column nominal strength but not when characterizing the beam strength.

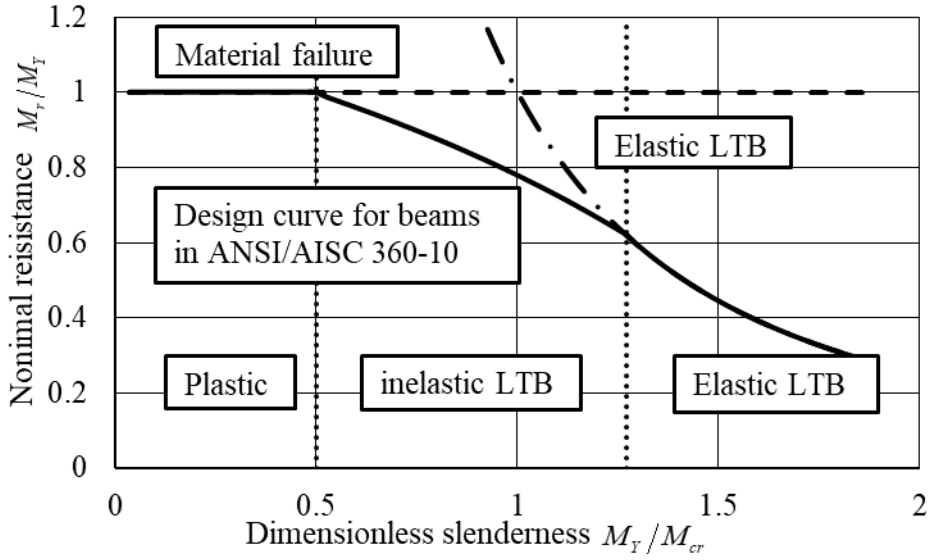

(a)

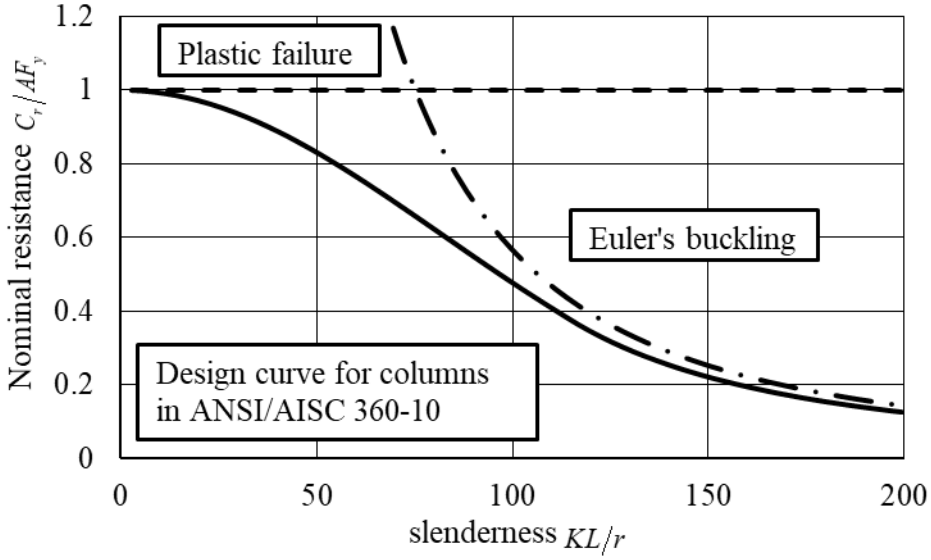

(b)

Figure 1.3 Comparison between the design curves in ANSI/ASCI S360-10 and the elastic buckling curve for (a) beams and (b) columns

1.3.3 Australian Standards

In the Australian Standard (AS 4100-1998), the nominal resistance M_r for a flexural member is given by

$$M_r = \alpha_m \alpha_s M_s \le M_s \tag{1.10}$$

where α_m is a moment modification factor (akin to moment gradient factor in CAN-CSA S16 2014) and is given by

$$\alpha_m = \frac{1.7 M_{\max}}{\sqrt{\left[\left(M_a\right)^2 + \left(M_b\right)^2 + \left(M_c\right)^2\right]}} \le 2.5 \tag{1.11}$$

In Eq. (1.11), the nominal moment resistance M_s is given by

$$M_s = F_y Z_e \tag{1.12}$$

in which, Z_e is the effective section modulus which is depends on the section slenderness λ_e defined as

$$\lambda_e = \left(\frac{b}{t}\right)\sqrt{\frac{F_y}{250}} \tag{1.13}$$

where b is the width of the element outstanding from the face of the supporting plate element or the width of the element between the faces of supporting plate elements, and t is the element thickness. The effective section modulus Z_e is given by

$$Z_e = \begin{cases} \min\left(Z_x, 1.5 S_x\right) & \lambda_e \le 82 \\ S_x + \left[\left(\dfrac{115 - \lambda_s}{33}\right)\left(\min\left(Z_x, 1.5 S_x\right) - S_x\right)\right] & 82 < \lambda_e \le 115 \\ S_x \left(\dfrac{115}{\lambda_s}\right)^2 & 115 < \lambda_e \end{cases} \tag{1.14}$$

In Eq. (1.11), α_s is a slenderness reduction factor which accounts for the reduction in strength due to yielding, The slenderness reduction factor α_s depends on the ratio of the nominal moment resistance M_s to the elastic critical moment M_o and takes the form

$$\alpha_s = 0.6\left[\sqrt{\left(\frac{M_s}{M_o}\right)^2 + 3} - \left(\frac{M_s}{M_o}\right)\right] \tag{1.15}$$

in which, the elastic critical moment is given by

$$M_o = \sqrt{\left[\left(\frac{\pi^2 EI_y}{l_e^2}\right)\left[GJ + \left(\frac{\pi^2 EC_w}{l_e^2}\right)\right]\right]} \tag{1.16}$$

and the effective length l_e of a segment is

$$l_e = k_t k_l k_r l \tag{1.17}$$

where k_t is a twist restraint factor, k_l is a load height factor and k_r is a lateral rotation restraint factor, all given in Table 1.1-Table A1.3 in Appendix 1.A. Figure 1.4 depicts the normalized flexural design strength for a beam with a W250x36 cross-section based on the Australian steel provisions as provided by Eq. (1.10). Overlain on the same plot are the elastic critical moment M_o and the flexural yield strength M_Y for comparison. Unlike CAN/CSA-S16 and ANSI/AISC-360, the Australian standards do not provide clear-cut slenderness limits for yielding, inelastic buckling, and elastic buckling. As, such, the threshold slenderness values based on CAN-CSA-S16 are overlain on the plot, which would correspond in this case to dimensionless slenderness ratios of 0.50 and 1.30.

Within the elastic range $\sqrt{M_Y/M_{cr}} > 1.30$, the nominal flexural resistance based on the Australian standard equation is lower than the elastic buckling resistance by a difference ranging from 15% at $\sqrt{M_Y/M_{cr}} = 1.87$ to 28% at $\sqrt{M_Y/M_{cr}} = 1.30$. The difference is indicative of the fact that the

Australian standards recognize the detrimental effect of initial out-of-straightness compared to the flexural resistance for perfectly straight beams.

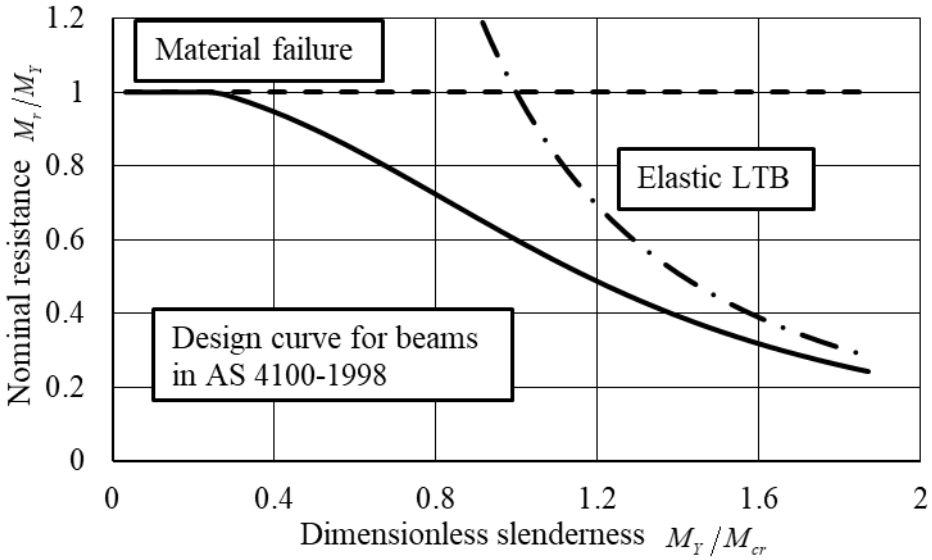

Figure 1.4 Comparison between the design curves in AS 4100-1998 for beams

1.3.4 The Eurocode Standard

According to the Eurocode 3 (2005), the design flexural resistance for laterally unsupported beams bent about the strong axis is given by

$$M_r = \chi_{LT} W_y \frac{F_y}{\gamma_{M1}} \tag{1.18}$$

where F_y is the yield stress, W_y is the section modulus about the strong axis, etc. The section modulus W_y depends upon the section class. For class 1 and 2 sections, the value of W_y is taken as the plastic section modulus Z_x and for class 3 sections, it is taken as the elastic section modulus S_x. For class 4 section, W_y is based on the effective elastic section modulus S_{eff}. In Eq. (1.18), γ_{M1} is a partial resistance factor (akin to the resistance factor $1/\varphi$ in CAN/CSA-S16) that accounts for the variability in the material properties and section dimensions, and will be taken as $\gamma_{M1} = 1.0$ in the present discussion given our focus on the nominal resistance. In Eq. (1.18), coefficient χ_{LT} is a reduction factor that accounts for lateral torsional buckling and is given by

$$\chi_{LT} = \frac{1}{\Phi_{LT} + \sqrt{\Phi_{LT}^2 - \bar{\lambda}_{LT}^2}} \tag{1.19}$$

where $\Phi_{LT} = 0.5\left[1 + \alpha_{LT}\left(\bar{\lambda}_{LT} - 0.2\right) + \bar{\lambda}_{LT}^2\right]$ with α_{LT} being a factor accounting for member imperfections as listed in Table 1.1 and ranges between 0.21 and 0.76, depending upon the manufacturing method and the height to width ratio. It accounts for misalignment and different residual stress distributions. For example, for the value $a = 0.21$, the nominal design resistance is found to be 78%-88% of the elastic buckling resistance for a perfectly straight beam. In Eq. (1.19) $\bar{\lambda}_{LT}$ is a slenderness parameter (akin to coefficient M_Y / M_o In the Australian standard) and is given by $\bar{\lambda}_{LT} = \sqrt{W_y F_y / M_{cr}}$ in which M_{cr} is the elastic critical moment and $W_y F_y$ is the moment resistance based on material failure, i.e., yield moment for W200x36. The nominal flexural resistance curves based on Eurocode 3 (EN 1993-1-1: 2005) are provided in Figure 1.5 based on the α_{LT} values listed in Table 1.1.

Table 1.1 Recommended values for imperfection factors for lateral torsional buckling curves

Buckling curve	a	b	c	d
Imperfection factor α_{LT}	0.21	0.34	0.49	0.76

* Descriptions of cross-sections a-d are given in Table 1.2

Table 1.2 Recommended values for lateral torsional buckling curves for cross-sections

Cross-section	Limits	Buckling curve
Rolled I-sections	$h/b \le 2$	a
	$h/b > 2$	b
Welded I-sections	$h/b \le 2$	c
	$h/b > 2$	d
Other cross-sections	N/A	d

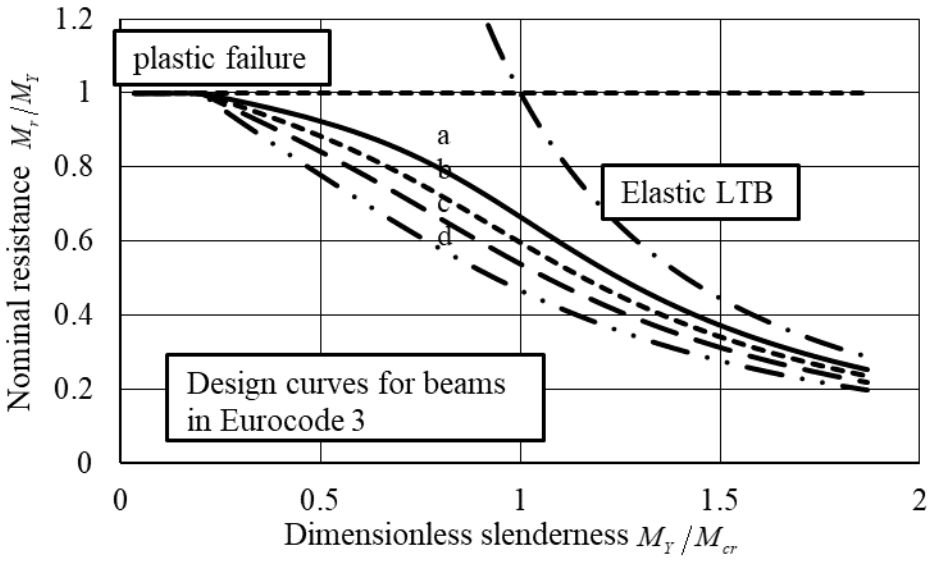

Figure 1.5 Comparison between the design curves in EN 1993-1-1: 1998 for beams for recommended imperfection factor $a = 0.21$, $b = 0.34$, $c = 0.49$ and $d = 0.76$ (curves for b,c and d not practical for W250X36 section)

1.3.5 Comparison of approaches of various standards

While Canadian and American standards recognize the detrimental effect of the initial out-of-straightness on column strength, such effects are not considered when characterizing the flexural member strength. In contrast, the effect of initial out-of-straightness is accounted for in the Australian and Eurocode standards. In the Australian design equation for beams, a slenderness factor α_s is introduced to quantify the influence of initial imperfections on the buckling resistance for beams whereupon a reduction is found when compared to the buckling resistance obtained from the eigenvalue solution. No clear statement regarding the types of initial imperfections is provided and no distinction is made between the treatment of rolled and welded cross-sections. This approach contrasts with that of the Eurocode 3, in which four levels of imperfection values α_{LT} are provided, depending on the manufacturing method and the sectional height to width ratio.

1.4 Motivation of present study

Present standards seem to be inconsistent in that the Eurocode and the Australian standards account for the effect of initial out-of-straightness when characterizing the LTB resistance of beams while the Canadian and American standards omit such effects. The present thesis thus aims at providing a theoretical foundation for quantifying the detrimental effects on initial out-of-straightens on LTB resistance by developing analytical and finite element solutions and applying them in conjunction

with proposed design criteria for possible future adoption in standards. The study focuses exclusively on elastic lateral torsional buckling and is thus intended for long span beams, as opposed to beams with intermediate spans where the presence of residual stresses may accelerate the yielding in portions of the cross-section.

1.5 Research Objectives

The specific objectives of the present study are to:

- Develop a finite element solution for the response of laterally unsupported steel beams subjected to various types of loads.
- Propose failure criteria based on displacement threshold and stress threshold values.
- Establish the relationship between the LTB resistance of perfectly straight beams and imperfect beams.
- Identify the parameters affecting design criteria and quantify their effects in a parametric study on common cross-sections in the W150 and W310 series of Handbook of steel construction (2014), and propose simplified design equations for both design criteria.
- Previously proposed methodologies (e.g., the Southwell plot (1931)) were devised to predict the buckling loads for ideal columns (without imperfections) from the experimental results on real columns (with initial-out-of-straightness). Since the present study establishes relations between the lateral torsional buckling strength of beams with initial imperfections and those that are perfectly straight, the study aims at assessing the extensibility of the Southwell plot technique, and variations thereof, to lateral torsional buckling of beams.

1.6 Outline of the thesis

Present Chapter 1 provided a comparative discussion of present standard provisions in the treatment of out-of-straightness effects when characterizing the lateral torsional buckling of strength of beams.

Chapter 2 provides a literature review on studies related lateral torsional buckling that account for the effect of initial out-of-straightness of steel beams. Studies related the inclusion of initial out-of-straightness into lateral torsional buckling strength in the Eurocode 3 provisions are also summarized given their relevance to the topic. Studies aiming at determining the critical loads (or

moments) for perfectly straight columns (or beams) from the load-displacements of members with initial crookedness are also surveyed given their relevance to the developments of Chapter 5.

Chapter 3 develops a finite element solution to capture the response of beams with initial geometric imperfections subjected to general transverse loads. The chapter also proposes two criteria, based on threshold displacements and threshold stresses, to characterize the effect of initial out-of-straightness on the elastic lateral torsional buckling strength of beams. The finite element solution is used in conjunction with the criteria proposed to investigate the effects of various geometric parameters on the moment capacity.

Chapter 4 presents the results of a parametric study on common cross-sections under three loading conditions: uniform moments, mid-span point loading, and uniformly distributed loading. The study investigates the effect of key parameters affecting the lateral torsional buckling resistance based on the both criteria proposed. Illustrative examples for incorporating the effect of initial-out-of-straightness into the present Canadian standards are provided.

Chapter 5 presents an extension of the Southwell plot technique that predicts the critical moments and initial geometric imperfections for an initially crooked beam. The extension of the Southwell plot technique is based on the finite element solution developed in Chapter 3. Various scenarios for initial out-of-straightness are examined to study the effect of higher modes on prediction in initial geometric imperfections.

Chapter 6 provides a summary of the work done, compiles the findings and conclusions of the study, and provides recommendations for future research.

Appendix 1. A

Table A1.1 Twist restraint factor k_t

Restraint arrangement	Factor k_t
FF, FL, LL, FU	1.0
FP, PL, PU	$1+\frac{\left[\left(\frac{d_1}{l}\right)\left(\frac{t_f}{2t_w}\right)^3\right]}{n_w}$
PP	$1+\frac{\left[2\left(\frac{d_1}{l}\right)\left(\frac{t_f}{2t_w}\right)^3\right]}{n_w}$

Table A1.2 Load height factor k_l for gravity loads

Longitudinal position of the load	Restraint arrangement	Load height position	
		Shear centre	Top flange
Within segment	FF, FP, FL, PP, PL, LL, FU, PU	1.0 1.0	1.4 2.0
At segment end	FF, FP, FL, PP PL, LL, FU, PU	1.0 1.0	1.0 2.0

Table A1.3 Lateral rotation restraint factor k_r

Restraint arrangement	Ends with lateral rotation restraints	Factor k_r
FU, PU	Any	1.0
FF, FP, FL, PP, PL, LL	None	1.0
FF, FP, PP	One	0.85
FF, FP, PP	Both	0.70

* F ≡ fully restrained, L ≡ laterally restrained, P ≡ partially restrained and U ≡ unrestrained

2. Literature review

The present study focuses on investigating the reduction effect of initial geometric imperfections on the lateral torsional buckling resistance of steel beams. Thus, Section 2.1 of this chapter presents a review of studies depicting mechanical or experimental approaches to capture the effect of initial geometric imperfections on the LTB problem. Section 2.2 provides an overview of studies related to the treatment for initial geometric imperfections in the Eurocode 3 (EN 1993-1-1(2005)). A review of studies investigating the probability and stochastics aspects of LTB problem is presented in Section 2.3. A summary of studies on experimental treatment to obtain the LTB critical load is provided in Section 2.4.

2.1 LTB for beams with initial geometric imperfections

Using the transfer matrix method, Yoshida and Maegawa (1983) determined the load-lateral displacement relationship of a laterally curved beam subjected to uniform moments. The beam radius of curvature was taken as constant and had a large magnitude compared to the dimensions of the cross section. The stress-strain was assumed to be perfectly elastic-plastic. The transfer matrix was derived based on the direct equilibrium approach of an infinitesimal element. To assess the validity of the analysis, the numerical results were compared to experimental results by Fukumoto and Nishida (1981) for IPE200, IPE250 and IPE600 sections.

Yoshida and Maegawa (1984) distinguished between the critical loads of perfectly straight members which are obtained an eigenvalue solution and the ultimate load for initially crooked members which are obtained from a non-linear analysis. The load-displacement relations were obtained based on the work of Yoshida and Maegawa (1983). The cases investigated involved (1) a beam with initial lateral deflection approximated by a circular arc, (2) a beam subjected to a mid-span point force acting on the top flange at horizontal offset from the center line of the section, (3) a beam subjected to vertical and a horizontal load acting at the same point on the top flange and (4) a beam with initial lateral out-of-straightness subjected to laterally eccentric point load acting at mid-span. The results were provided in a dimensionless form. The study investigated the effect of residual stress distribution, amplitude of the initial circular arc, loading conditions, and cross-section dimension. The influence of residual stress on the ultimate load was found to be low compared to initial imperfections and the dimensions of the cross section was found to have small effects on the ultimate strength.

Hasham and Rasmussen (1995) conducted two series of experiments on members under compression and major axis bending. Two spans were considered; 1990mm and 3990mm and different axial force to major axis bending moment ratios were applied on the specimens. The authors measured the sectional dimensions of the specimens and reported the average value and standard deviation. The authors also measured the initial out-of-straightness at the flange tips and section centroid. The axial force- bending moments interaction relations were plotted and compared against the predictions of AS4100 (1990), AISC-LRFD (1993) and Eurocode 3(1993) for the problem of out of plane lateral torsional buckling. The authors concluded that the design capacities based on AS4100, AISC-LRFD and Eurocode 3 were conservative when the bending moments to axial force ratios were comparatively high. In contrast, AISC-LRFD interaction relations were found to be overly conservative for series 2.

Dubina and Ungureanu (2002) performed nonlinear finite element analyses (FEA) on beams and columns with non-lipped and lipped channel sections which incorporate the effects of residual stresses and initial geometric imperfections. Two types of geometric imperfections were considered; transverse, and lateral/torsional imperfections and local-sectional imperfections in the form of web distortion. Local-section imperfections were introduced as symmetrical or asymmetric sine shapes along the web height as well as imperfections based on probabilistic analysis. The study investigated the reduction in the buckling strength due to imperfections and interactive buckling. Comparisons were conducted with the Australian and European standard predictions. The buckling strength based on the symmetric and asymmetric local imperfections were found to differ and the sinusoidal shape was not always appropriate for representing local-sectional imperfections. Also, the influence of local imperfections was found relatively low compared to global imperfections. The erosion of critical bifurcation load (ECBL) imperfection approach was found to be effective in charactering the geometric imperfections.

McCann et al. (2013) investigated the lateral torsional buckling (LTB) for beams with discrete lateral restraints that are vertically offset from the shear center. The model developed related to simply supported beams with doubly symmetric I-sections and linearly elastic lateral restraints. The solution was based the Rayleigh-Ritz method and the lateral displacement, angle of twist, and initial imperfections were expressed as Fourier series. Two eigen-value models were developed for perfectly straight beams; the first accounted for the flexibility of the lateral braces while the

second omitted their flexibility. A third solution was developed for beams with initial out of straightness. The work investigated the effect of bracing height on the required lateral restraint stiffness. Comparisons were performed against the predictions of LTBeam, a software for determining the critical moments of restrained beams. The comparison has shown that while a single harmonic solution may not be sufficient to predict the critical moments, the use of the full Fourrier series predictions in very good agreement with numerical results.

Nguyen and Chan et al. (2013) conducted geometric nonlinear FEA on I-section beams with Fibre Reinforced Polymer (FRP) and steel materials. The study examined the influence of load height effect and end warping fixity conditions on the critical lateral torsional buckling load and then incorporated the effect of initial lateral and twist imperfections in their analysis. The lateral out-of-straightness and the initial twist imperfection were assumed as half and quarter wave sinusoidal functions. The authors observed that the reduction in strength due to load height effects and the release of end warping fixity conditions to be more significant in FRP beams than in steel beams.

Ascione (2014) developed a finite element formulation wide flange beams with initial imperfections. The model was used to investigate the lateral torsional buckling of simply supported beams made of pultruded GFRP subjected to transverse uniformly distributed load acting at the top flange. Three types of imperfections were investigated; (1) lateral out-of-straightens and (2) non-orthogonality of the flanges and the web, and (3) combinations of both types of imperfections. The author observed that lateral out-of-straightness had a larger detrimental effect than the non-orthogonality of the flanges and the web.

2.2 Studies related to the Eurocode 3 buckling provisions for beams or beam-columns

Maquoi et al. (2001) presented a theoretical treatment for interaction equations of beam columns and provided a framework for generalizing the design provisions for beam-columns in Australia (AS 4100-1998), America (AISC 1966 and 1986), Europe (ECCS 1976 and 1978) and Germany (DIN 18800 1988). The proposed method can account for the lateral torsional buckling through amendments in computing the coefficients appearing in the interaction equations.

Boissonade et al. (2002) developed a second-order in-plane elastic analysis and used it to propose a new interaction equation as an alternative to that of the Eurocode 3 (1993). The alternative

interaction equation was developed by adopting the closed form solution developed by Maquoi and Rondal (1982) in conjunction with the interaction equation in the German steel standard provisions (DIN 18800). The work captured biaxial moments and plasticity effects. Finite element analyses on practical section dimensions were performed to assess the validity of the proposed solution. The proposed solution was found safe, efficient, and more accurate than that in EC 3 with the ability to account for lateral torsional buckling.

Aguero and Pallares (2007) summarized the approach methodology and simplified method used in the Spanish steel standard (NBE-EA-95) and Eurocode 3 (1992) for the ultimate strength of members in slender frames. A simplified method to capture second order effects was proposed by separating the analysis into sway and non-sway parts, and an auxiliary coefficient was developed to amplify the bending moments. The Dutheil's method (1952) was adopted to obtain equivalent imperfections. An illustrative example was presented for a beam with lateral and twist initial geometric imperfections subjected to biaxial bending. The accuracy of the proposed method was assessed by comparison against a closed form solution. The proposed solution was observed to be valid for predicting the ultimate limit state of slender members.

Szalai and Papp (2010) developed a generalization of the Ayrton-Perry Formula (APF) (Ayrton and Perry 1886) originally developed for predicting the buckling resistance for columns undergoing flexural buckling, and extended the APF to account for effect of initial imperfections on the lateral torsional buckling strength of beams and beam-columns.

Taras and Greiner (2010) conducted geometric and material nonlinear analyses for the lateral torsional buckling (LTB) analysis of beams. The results were found to be inconsistent with the Eurocode 3 solution. Based on the first yield criterion and a consistent derivation, the authors proposed new design curves.

By relating the stresses to the derivatives of the displacement fields, and adopting the first yield criterion based on von Mises stress, Aguero and Pallares (2015a) proposed initial lateral out-of-straight and angle of twist patterns for the design of members undergoing lateral torsional buckling. The proposed treatment simplified that design of members with initial out-of-straightness in a manner consistent with EC 3 and extended its scope to various load and boundary conditions.

Aguero and Pallares (2015b) implemented the Eurocode 3 in design members in frames by proposing a procedure to estimate the most adverse imperfection direction. A criterion was proposed to determine the number of buckling modes needed to define a proper imperfection shape based on the lowest buckling mode corresponding to a non-zero strain energy.

2.3 Probabilistic and Stochastic studies on LTB of beams with initial geometric imperfections

Kala and Melcher (2009) compiled statistical information on the measured yield strength and cross-sectional geometric parameters for Czech hot rolled steel I sections using various probabilistic distributions with S355 structural steel (yield strength =355MPa). The statistical characteristics compiled were subsequently used in Kala (2013) to investigate the lateral torsional buckling problems of simply supported beams with doubly symmetric-sections under major axis uniform bending moments. The authors assumed simple sinusoidal lateral and twist imperfections and provided a stress approach to predict the ultimate moment for initially crooked beams. A stochastic analysis was performed based on the Monte Carlo simulation to determine the stochastic characteristics of the critical moments. The lateral torsional buckling strength of I-section thin-walled members were reported to be sensitive to the magnitude of the initial imperfections

Papadopoulos and Soimiris et al. (2013) conducted finite element analyses for beam-columns and frames with I-sections in which members with imperfect geometry were modeled. The initial imperfections were given as non-homogeneous Gaussian fields and were generated based on the evolutionary power spectra using the method of separation. The relationship between local and the global imperfections were based on geometric equilibrium considerations. Two types of models were investigated (1) a column with an imperfection field under a compressive load and (2) a portal frames consisting of I-sections under a uniformly distributed vertical loading and a horizontal concentrated force. A Monte Carlo simulation was conducted on multiple initial imperfection scenarios were generated and a statistical description of the buckling load capacity and strength reduction were obtained.

2.4 The Southwell plot and its extension to lateral torsional buckling

A common challenge encountered when conducting buckling experiments on real (i.e., with initial of out straightness) columns or beams is that the obtained load deflection relation exhibits a

nonlinear relationship. The buckling behavior of such members is fundamentally different from that of ideal (i.e., perfectly straight members) for which theoretical eigenvalue analysis predicts a sudden change in the deformation pattern once the applied load attains a critical value. Several researchers have attempted to use the experimental nonlinear load deformation relations to predict the critical load of a perfectly straight members (e.g., Southwell (1931) method and its variations by Ariartnam 1960, Massey 1963, Meck 1977, and Mandal and Cadalin 2002). Such studies are discussed given that the present study will develop techniques to predict the magnitudes of lateral displacements and angles of twist for beams with initial lateral out-of-straightness and initial angle of twist. Such expressions will provide a basis to assess the seemingly conflicting variation of the Southwell plot solutions (Chapter 5).

Southwell (1931) developed a technique to estimate the critical load for pin-ended ideal perfectly straight column from the measured axial load-lateral displacement curves for real columns with initial out-of-straightness. The initial out-of-straightness of the column is assumed as a Fourier series. By omitting the contribution of higher modes on the lateral defection, Southwell observed a linear relationship between the lateral deflection-to-applied-load u/P ratio and the lateral deflection u . The Southwell method forms a basis to predict the critical load for columns from experimental results and was shown to compare well with classical buckling loads based on eigenvalue solution results.

Ariaratnam (1960) developed a theoretical framework to extend the work by Southwell plot methodology (Southwell 1931) for the prediction of the critical loads of plane frames and the torsional buckling loads for columns. Massey (1963) proposed a modified version of the Southwell plot technique, in which rather than adopting the $u/P - u$ plot, they advocated the use ϕ/M^2 versus ϕ plots to estimate the critical moments for beams with I-sections with initial lateral or twist imperfections subjected to a uniform bending moments. The method was further extended to account for material inelastic effects.

Meck (1977) proposed a modified method based on the original Southwell plot where they have advocated the use of u/P versus ϕ or ϕ/P versus u to predict the critical load for beams with initial lateral and twist imperfections. The load conditions investigated were extended to mid-span point load. By using a direct equilibrium method in conjunction with the principle of stationary

potential energy, a linear relation was observed between lateral displacement to moment ratio and the angle of twist. Also, the relation between the twist-to-moment ratio and the lateral displacement was found to be linear. These two sets of relations formed the basis of the proposed method to predict the LTB critical load for beams. The method was verified through comparison of experimental results with eigenvalue solution results.

Mandal and Calladine (2002) developed a theoretical framework for the evaluation of the work of Southwell (1931), that of Massey (1963) and that of Meck (1977). The analysis advocated the extension of the original $u/P - u$ Southwell plot, originally developed for columns, for the lateral torsional buckling analysis of beams with initial imperfects.

Table 2.1 Comparison of variations of the Southwell plot studies (simply supported beams)

Author	Buckling Type	Plot method	Load condition	Type of imperfections considered
Southwell (1931)	Flexural	δ/P versus δ	Axial force	u_0
Massey (1963)	LTB	θ/M^2 versus θ	Uniform bending moment	u_0 and θ_0
Meck (1977)	LTB	u/M versus θ and ϕ/P versus u	Uniform bending moment Midspan point load	u_0 and θ_0
Mandal and Cadalin (2002)	LTB	u/P versus u	Uniform bending moment	u_0 and θ_0

* δ, P are the deflection at mid-span and corresponding applied axial force respectively.

** θ, M are the angle of twist at mid-span and corresponding applied uniform bending moment.

2.5 Conclusions

As summarized in section 2.1, the behavior of beams with initial geometric imperfections has been studied in multiple studies for hot-rolled, FRP and cold-form sections through mechanical and experimental approaches. Capturing the effect of initial geometric imperfections on LTB behavior through the Ayrton-Perry formula has been well studied through various studies related to Eurocode 3 (EC 3) reported in Section 2.2. Scenarios investigated in these studies are limited to simply supported members subjected to uniform bending moment or point load at mid-span. Also,

the shapes of the initial geometric imperfections are assumed to be sinusoidal functions. Thus, a finite element solution investigating the LTB behavior of geometrical imperfect beams is developed in Chapter 3 accounting for imperfections given by superpositions of amplified buckling modes. Relatively fewer stochastic studies are reported to investigate beams with initial geometric imperfections as presented in Section 2.3 while no key parameters are found for design. In Chapter 4, a throughout parametric study for displacement and stress based design criteria is provided to depict key parameters in designing beams with initial geometric imperfections. Experimental treatments for estimating the critical load for practical members are well developed in studies summarized in Section 2.4. These studies focus on the prediction for the critical load and overlook the estimation for the initial geometric imperfections. A trial is presented in Chapter 5 to adopt the Southwell to estimate the initial geometric imperfections through the load-displacement curve generated in the finite element solution developed in Chapter 3.

3. Finite element for the lateral torsional response of beams with initial geometric imperfections

3.1 Scope and Objective

This chapter develops a simplified beam finite element formulation to predict the load-displacement response of laterally unsupported beams with initial crookedness subjected to general transverse loading. The present finite element solution is validated by comparison with results based on the commercial software ABAQUS. A parametric study is then presented to investigate the influence of various geometric parameters on the lateral torsional response of initially crooked beams.

3.2 Statement of the problem and Notation

A beam with a doubly symmetric I-section is assumed (Figure 3.1) with span L is assumed to have an initial lateral out-of-straightness (IOS) $u_0(z)$ and initial angle of twist (IAT) $\theta_0(z)$. The beam is subjected to transverse loads $q(z)$. Under such loads, the beam deforms from Configuration 1 to Configuration 2 (Figure 3.1) by undergoing displacements $v(z)$, $u(z)$ and twist $\theta(z)$. The bending moments associated with the transverse displacements $v(z)$ are $M(z)$. The loads are assumed to incrementally increase to $\lambda q(z)$, where λ is a scaling factor. The associated transverse displacement function is $\lambda v(z)$ and the corresponding bending moments is $\lambda M(z)$. As the beam deflects transversely, it undergoes lateral displacement $u(\lambda, z)$ and angle of twist $\theta(\lambda, z)$. Unlike the transverse response, $u(\lambda, z)$ and $\theta(\lambda, z)$ are nonlinear functions of the load parameter λ. It is required to determine the lateral and torsional response of the system $u(\lambda, z)$ and $\theta(\lambda, z)$. As a matter of notation, the sum of the IOS $u_0(z)$ and the lateral displacement $u(\lambda, z)$ is referred as the total lateral out-of-straightness $\bar{u}_c$ (TLOS). Also, the sum of the IAT $\theta_0(z)$ and the angle of twist $\theta(\lambda, z)$ is the Total Angle of Twist (TAT) (Figure 3.1). A right-handed Cartesian coordinate system is adopted in which the z-axis is oriented along the longitudinal direction and the *x* and *y*-axes (Figure 3.1) are parallel to lateral and transverse directions, respectively.

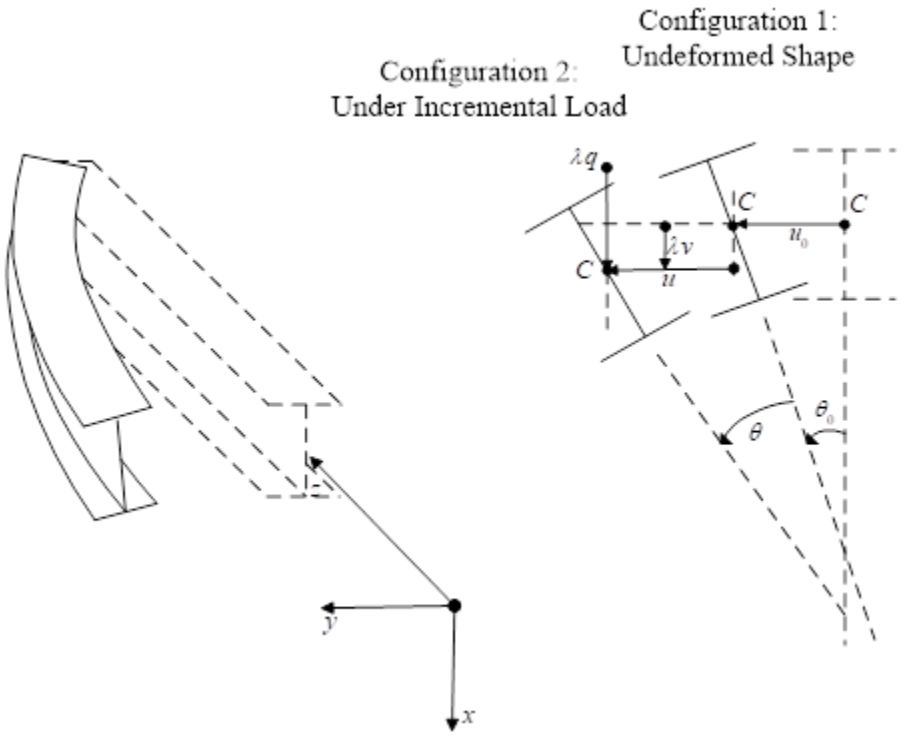

Figure 3.1 Model under investigation and deformed configurations

3.3 Assumptions

The following assumptions are adopted

1. The formulation is restricted to prismatic thin-walled members with doubly-symmetric sections.
2. The cross-section is assumed to move as a rigid disk in its own plane during deformation (i.e., the beam cross-section follows the first Vlasov hypothesis (Vlasov 1961))
3. The transverse shear deformation within the middle surface of the cross-section is neglected (i.e., the section is assumed to follow the second Vlasov hypothesis)
4. The material is linearly elastic isotropic and follows Hooke's law
5. When characterizing the destabilizing term due to lateral torsional buckling, pre-buckling effects are assumed to be negligible.

3.4 Formulation

3.4.1 Total potential energy

At a given load level λq, the total potential energy for the member is given by

$$\pi = U + V \tag{3.1}$$

in which U is the internal strain energy stored throughout the deformation of the member in going from the initial crooked configuration to the final deformed configuration and V is the load potential energy gained by the applied loads. The internal strain energy is given by

$$U = \frac{1}{2}\int_0^L EI_x\left(\lambda v''\right)^2 dz + \frac{1}{2}\int_0^L EI_y u''^2 dz + \frac{1}{2}\int_0^L GJ\theta'^2 dz + \frac{1}{2}\int_0^L EC_w\theta''^2 dz \tag{3.2}$$

in which E is the Young's modulus and G is the shear modulus and the relevant section properties are the strong axis moment of inertia $I_x = \int_A y^2 dA$, the weak axis moment of inertia $I_y = \int_A x^2 dA$, the Saint-Venant torsional constant $J = \sum\left(bt^3/3\right)$ and the warping constant is $C_w = I_x\left(d-t\right)^2/4$.

The load potential energy $V = V_1 + V_2$ gained by the loads is the sum of two components; $V_1 = -\int_0^L\left(\lambda q\right)\left(\lambda v\right)dz$ due to transverse forces λq undergoing transverse displacements λv and V_2 due to weak axis bending moments in the deformed configuration undergoing lateral curvatures.

In Figure 3.2 coordinate system oxy is fixed in space while coordinate system $ox'y'$ rotates with the section. The bending moments λM due to transverse loads, acting on a segment of beam of length dz are denoted by the double headed arrow in Figure 3.2 and are assumed to preserve their direction (i.e., conservative loading) as the beam deforms and rotates. As the cross section twists from angle θ_0 in the un-deformed configuration to angle $\theta_0 + \theta$, the bending moment λM acting about the un-deformed y axis induces a weak axis bending moment about the deformed x' axis. The projection of moment λM on the x' axis is $\lambda M_{x'} = -\lambda M\sin\left(\theta + \theta_0\right)$. For small angles $\left(\theta + \theta_0\right)$ one can write the approximation $\lambda M_{x'} \approx -\lambda M\left(\theta + \theta_0\right)$. The corresponding curvature (Figure 3.2(b)) is given by $-\left(u + u_0\right)''\Big/\left[1 + \left(u + u_0\right)'^2\right]^{3/2}$ which simplifies to $-\left(u + u_0\right)''$ for small

lateral deflections $u+u_0$. The load potential gain of an element of length *dz* due to weak axis moment $-M(\theta+\theta_0)$ undergoing curvature $-(u+u_0)''$ is $dV_2 = -M(\theta+\theta_0)\times\left[-(u+u_0)''\right]dz$, where the minus sign is consistent with the fact that the curvature depicted in Figure 3.2a is opposite to the direction of the weak axis moment $-\lambda M(\theta+\theta_0)$ and the total potential gain for the system is given by integration yielding $V_2 = \int_0^L \lambda M(z)(u+u_0)''(\theta+\theta_0)dz$, and

$$V = \int_0^L \lambda M(z)(u+u_0)''(\theta+\theta_0)dz - \int_0^L (\lambda q)(\lambda v)dz \tag{3.3}$$

Functions $u_0(z)$ and $\theta_0(z)$ are the IOS and IAT and are assumed to be known. In the first of term Eq. (3.3), the pre-buckling deformation effect have been neglected in line with most lateral torsional buckling solutions (e.g., Trahair 1993). The stationarity condition of the total potential energy is evoked by setting $\delta\pi = 0$. By performing integration by parts, one recovers the governing differential equations of equilibrium

$$EI_x v'''' + q = 0 \tag{3.4}$$

$$EI_y u'''' + \lambda\left[M(z)(\theta+\theta_0)\right]'' = 0 \tag{3.5}$$

$$EC_w\theta'''' + \lambda M(z)(u+u_0)'' - GJ\theta'' = 0 \tag{3.6}$$

The resulting boundary terms lead to the boundary conditions summarized in Table 3.1.

Table 3.1: Possible boundary conditions at ends $z = 0$ and $z = L$

Essential boundary conditions	Natural boundary conditions
$\delta v'$ is specified	$EI_x v'' = 0$
δv is specified	$EI_x v''' = 0$
$\delta u'$ is specified	$EI_y u'' + M(z)(\theta + \theta_0) = 0$
$\delta \theta'$ is specified	$EC_w \theta'' = 0$
δu is specified	$EI_y u''' + \left[M(z)(\theta + \theta_0) \right]' = 0$
$\delta \theta$ is specified	$GJ\theta' - EC_w \theta''' = 0$

In Eqs. (3.4), (3.5) and (3.6), the governing equilibrium equation for the vertical displacement $v(z)$ is observed to be independent from those of the lateral displacement $u(z)$ and the angle of twist $\theta(z)$. Thus, for a given transverse load $q = q(z)$, Eq. (3.4) can be used to independently solve for $v(z)$ In contrast, Equations (3.5) and (3.6) are coupled and characterize the lateral torsional buckling response of the beam. It can be verified that when the initial crookedness $u_0(z)$ and $\theta_0(z)$ vanish, one recovers the governing classical lateral torsional buckling neutral stability conditions for a perfectly straight beam (e.g., Trahair 1993).

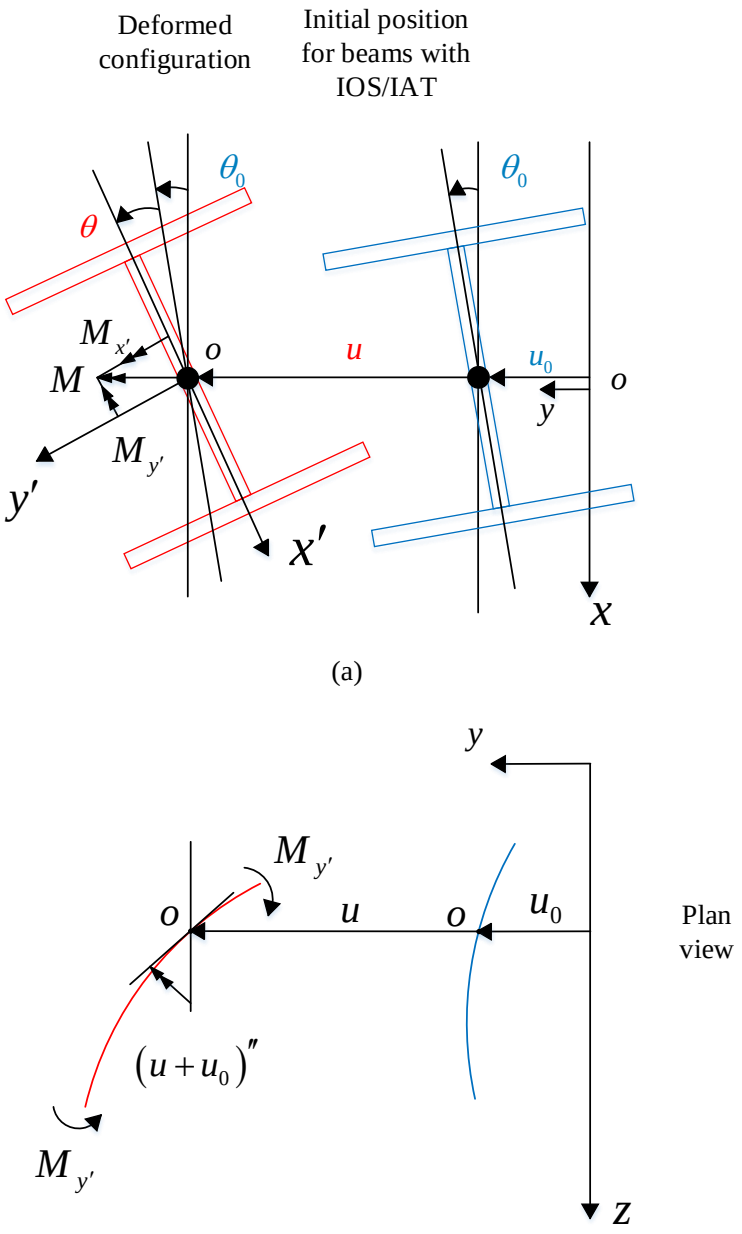

Figure 3.2 Displacement field for (a) cross-section and (b) plan view configuration for load potential energy expression

3.4.2 Closed form Solution for beam under uniform moments

A simply supported beam with initial out-of-straightness $u_0(z), \theta_0(z)$ is subjected to uniform bending moments $M(z) = M$. It is required to characterize the lateral displacement and angle of

twist in terms of the applied moments M . It is expedient to express the initial imperfection pattern as a linear summation of n buckling mode shapes for a perfectly straight beam, i.e., $\langle u_0(z) \quad \theta_0(z) \rangle^T = \sum_{m=1}^{n} \phi_m \langle u_m(z), \theta_m(z) \rangle^T$ where $u_m(z), \theta_m(z)$ are the buckling shapes for modes $m = 1, 2..n$ and ϕ_m is a scaling factor for mode m .

The mode shapes for a perfectly straight beam are obtained by setting $u_0(z), \theta_0(z)$ in Eqs. (3.5) and (3.6) to zero and +. The governing equations become $EI_y u''' + \lambda M \theta'' = 0$ and $EC_w \theta''' + \lambda M u'' - GJ\theta'' = 0$ and the corresponding boundary conditions are $u(0) = u''(0) = \theta(0) = \theta''(0) = 0$ $u(L) = u''(L) = \theta(L) = \theta''(L) = 0$. The solution of the above system of homogeneous of equations yields the critical moments M_{crm} and the buckling modes $u_m(z)$ and $\theta_m(z)$ are

$$M_{crm} = \lambda_m M = \frac{m\pi}{L}\sqrt{EI_y GJ + \left(\frac{m\pi E}{L}\right)^2 C_w I_y}$$
$$u_m(z) = \phi_m \sin\frac{m\pi z}{L} \qquad \theta_m(z) = \phi_m \left(\frac{\pi^2 EI_y}{M_{crm} L^2}\right) \sin\frac{m\pi z}{L} \; m = 1, 2, ..n \tag{3.7}$$

Using Fourier decomposition, a general IOS/IAT pattern can be expressed as a linear summation of mode shapes, i.e.

$$\langle u_0(z) \quad \theta_0(z) \rangle^T = \sum_{m=1}^{n} \phi_m \left\langle 1 \quad \left(\frac{\pi^2 EI_y}{M_{crm} L^2}\right) \right\rangle \left(\sin\frac{m\pi z}{L} \right) \tag{3.8}$$

where both sides of the above equation become equal as $n \to \infty$. For practical purposes, the series will be truncated by taking only the first few modes. From Eqs. (3.5) and (3.6), by setting $M(z) = M$ and substituting the IOS/IAT expressions from Eqs. (3.8), one obtains the additional displacements $u(z)$ and $\theta(z)$

$$u(z)=\frac{M}{EI_y}\sum_{m=1}^{n}\phi_m\frac{EI_yM+\left(\frac{\pi^2EI_y}{M_{crm}L^2}\right)EI_yEC_w\left(\frac{m\pi}{L}\right)^2+\left(\frac{\pi^2EI_y}{M_{crm}L^2}\right)EI_yGJ}{EC_wEI_y\left(\frac{m\pi}{L}\right)^4+EI_yGJ\left(\frac{m\pi}{L}\right)^2-M^2}\sin\left(\frac{m\pi z}{L}\right) \tag{3.9}$$

$$\theta(z)=\sum_{m=1}^{n}\phi_i\frac{\frac{M^2}{EI_y}\left(\frac{\pi^2EI_y}{M_{crm}L^2}\right)+M\left(\frac{m\pi}{L}\right)^2}{EC_w\left(\frac{m\pi}{L}\right)^4+GJ\left(\frac{m\pi}{L}\right)^2-\frac{M^2}{EI_y}}\sin\left(\frac{m\pi z}{L}\right) \tag{3.10}$$

For the special case where the initial geometric imperfections are assumed to be characterized by the first buckling mode as $\langle u_0(z)\quad \theta_0(z)\rangle^T=\phi_1\left[1,\left(\pi^2EI_y/M_{cr1}L^2\right)\right](\sin\pi z/L)$, Eq. (3.9) and (3.10) simplify to

$$u(z)=\frac{M}{EI_y}\phi_1\frac{EI_yM+\left(\frac{\pi^2EI_y}{M_{cr1}L^2}\right)EI_yEC_w\left(\frac{\pi}{L}\right)^2+\left(\frac{\pi^2EI_y}{M_{cr1}L^2}\right)EI_yGJ}{EC_wEI_y\left(\frac{\pi}{L}\right)^4+EI_yGJ\left(\frac{\pi}{L}\right)^2-M^2}\sin\left(\frac{\pi z}{L}\right) \tag{3.11}$$

$$\theta(z)=\phi_1\frac{\frac{M^2}{EI_y}\left(\frac{\pi^2EI_y}{M_{cr1}L^2}\right)+M\left(\frac{\pi}{L}\right)^2}{EC_w\left(\frac{\pi}{L}\right)^4+GJ\left(\frac{\pi}{L}\right)^2-\frac{M^2}{EI_y}}\sin\left(\frac{\pi z}{L}\right) \tag{3.12}$$

Equations (3.11) and (3.12) coincide with the work by Massay (1963).

3.4.3 Finite element formulation

The displacement fields $u(z)$, $\theta(z)$, and initial imperfections $u_0(z)$ and $\theta_0(z)$ are related to the nodal displacements, i.e.,

$$\begin{aligned} u(z)&=\langle\mathbf{N_u}(z)\rangle^T_{1\times4}\{\mathbf{u_N}\}, \qquad \theta(z)=\langle\mathbf{N_\theta}(z)\rangle^T_{1\times4}\{\boldsymbol{\theta}_\mathbf{N}\}\\ u_0(z)&=\langle\mathbf{N_u}(z)\rangle^T_{1\times4}\{\mathbf{u_{0N}}\}, \qquad \theta_0(z)=\langle\mathbf{N_\theta}(z)\rangle^T_{1\times4}\{\boldsymbol{\theta}_\mathbf{0N}\}\end{aligned} \tag{3.13}$$

where $\mathbf{N_u}(z)$, $\mathbf{N_\theta}(z)$ are the shape functions given by

$$\left\langle \mathbf{N_u}(z)\right\rangle_{1\times 4}^{T}=\left\langle 1-3z^2/L^2+2z^3/L^3 \;\vdots\; -z+2z^2/L-z^3/L^2 \;\vdots\; 3z^2/L^2-2z^3/L^3 \;\vdots\; -z^3/L^2+z^2/L\right\rangle$$

$$\left\langle \mathbf{N_\theta}(z)\right\rangle_{1\times 4}^{T}=\left\langle 1-3z^2/L^2+2z^3/L^3 \;\vdots\; z-2z^2/L+z^3/L^2 \;\vdots\; 3z^2/L^2-2z^3/L^3 \;\vdots\; z^3/L^2-z^2/L\right\rangle$$

$\left\langle \mathbf{u_N}\right\rangle^T=\left\langle u_1 \quad u_1' \quad u_2 \quad u_2'\right\rangle$, $\left\langle \boldsymbol{\theta}_\mathbf{N}\right\rangle^T=\left\langle \theta_1 \quad \theta_1' \quad \theta_2 \quad \theta_2'\right\rangle$ are the vectors of nodal displacements, $\left\langle \mathbf{u_{0N}}\right\rangle^T=\left\langle u_{01} \quad u_{01}' \quad u_{02} \quad u_{02}'\right\rangle$, $\left\langle \boldsymbol{\theta}_\mathbf{0N}\right\rangle^T=\left\langle \theta_{01} \quad \theta_{01}' \quad \theta_{02} \quad \theta_{02}'\right\rangle$ are the vector of nodal initial out-of-straightness, and $u_1, u_1', ..., \theta_2'$ are the nodal displacements. The moment distribution within the element is related to the nodal moments vectors $\mathbf{M^T}=\left\langle M_1 \quad M_2\right\rangle$ through linear interpolation, i.e.,

$$\lambda M(z)=\lambda\left\langle \mathbf{H}(z)\right\rangle_{1\times 2}^{T}\left\{\mathbf{M}\right\}_{2\times 1} \tag{3.14}$$

in which $\left\langle \mathbf{H(z)}\right\rangle_{1\times 2}^{T}=\left\langle (-1+z/L) \quad (z/L)\right\rangle$. From Eq. (3.13), by substituting into the energy expressions Eqs. (3.1)-(3.3), and omitting the strong axis bending terms as they are uncoupled from the lateral torsional response, one obtains

$$\begin{aligned}\pi=&\frac{1}{2}\left\langle \mathbf{u_N}\right\rangle^T\left[\mathbf{k_{e1}}\right]\left\{\mathbf{u_N}\right\}+\frac{1}{2}\left\langle \boldsymbol{\theta}_\mathbf{N}\right\rangle^T\left[\mathbf{k_{e2}}\right]\left\{\boldsymbol{\theta}_\mathbf{N}\right\}\\&+\lambda\left\langle \mathbf{u_N}\right\rangle^T\left[\mathbf{k_g}\right]\left\{\boldsymbol{\theta}_\mathbf{N}\right\}+\lambda\left\langle \mathbf{u_N}\right\rangle^T\left[\mathbf{k_g}\right]\left\{\boldsymbol{\theta}_\mathbf{0N}\right\}+\lambda\left\langle \mathbf{u_{0N}}\right\rangle^T\left[\mathbf{k_g}\right]\left\{\boldsymbol{\theta}_\mathbf{N}\right\}+\lambda\left\langle \mathbf{u_{0N}}\right\rangle^T\left[\mathbf{k_g}\right]\left\{\boldsymbol{\theta}_\mathbf{0N}\right\}\end{aligned} \tag{3.15}$$

in which $\left[\mathbf{k_{e1}}\right]=EI_y\int_0^L \mathbf{N_u^{T\prime\prime}N_u''}dz$, and $\left[\mathbf{k_{e2}}\right]=GJ\int_0^L \mathbf{N_\theta^{T\prime}N_\theta'}dz+EC_w\int_0^L \mathbf{N_\theta^{T\prime\prime}N_\theta''}dz$ are the elastic stiffness matrices pertaining to weak axis flexure and torsion/warping, respectively, and $\left[\mathbf{k_g}\right]=\lambda\int_0^L\left[-M_1(1-z/L)+M_2(z/L)\right]\mathbf{N_u^{\prime\prime T}N}_\theta dz$ is the geometric stiffness matrix and the entries of matrices $\left[\mathbf{k_{e1}}\right]$, $\left[\mathbf{k_{e2}}\right]$ and $\left[\mathbf{k_g}\right]$ are provided in Appendix 3-A. By evoking the stationarity condition and rearranging, one obtains

$$\left[\mathbf{k_e}\right]\left\{\mathbf{d}\right\}+\lambda\left[\mathbf{k_g}\right]\left\{\mathbf{d}\right\}=\lambda\left\{\mathbf{F}\left(\mathbf{d_0}\right)\right\} \tag{3.16}$$

in which

$$\left[\mathbf{k}_{\mathbf{e}}\right]=\begin{bmatrix}\mathbf{k}_{\mathbf{e1}} & \mathbf{0}\\ \mathbf{0} & \mathbf{k}_{\mathbf{e2}}\end{bmatrix},\qquad \left[\mathbf{k}_{\mathbf{g}}\right]=\begin{bmatrix}\mathbf{0} & \mathbf{k}_{\mathbf{g}}\\ \mathbf{k}_{\mathbf{g}} & \mathbf{0}\end{bmatrix},\qquad \left\{\mathbf{d}\right\}=\begin{Bmatrix}\mathbf{u}_{\mathbf{N}}\\ \boldsymbol{\theta}_{\mathbf{N}}\end{Bmatrix},\quad \left\{\mathbf{d}_{\mathbf{0}}\right\}=\begin{Bmatrix}\mathbf{u}_{\mathbf{0N}}\\ \boldsymbol{\theta}_{\mathbf{0N}}\end{Bmatrix},$$

where $\left[\mathbf{k}_{\mathbf{e}}\right]$ is the elastic stiffness matrix, and $\left\{\mathbf{d}\right\}$ is the nodal displacement vector. The right-hand side vector $\lambda\left\{\mathbf{F}\left(\mathbf{d}_{\mathbf{0}}\right)\right\}=-\lambda\left[\mathbf{k}_{\mathbf{g}}\right]\left\{\mathbf{d}_{\mathbf{0}}\right\}$ represents the external force vector induced by the initial out-of-straightness. For a perfectly straight beam, the nodal initial out-of-straightness vector $\left\{\mathbf{d}_{\mathbf{0}}\right\}$ vanishes and so does the right hand-side of Eq. (3.16) . The resulting equation reverts to the well-known eigenvalue problem

$$\left[\mathbf{k}_{\mathbf{e}}\right]\left\{\mathbf{d}\right\}+\lambda\left[\mathbf{k}_{\mathbf{g}}\right]\left\{\mathbf{d}\right\}=\left\{\mathbf{0}\right\} \tag{3.17}$$

which can be solved for the critical load level λ and corresponding buckling mode shape $\left\{\mathbf{d}\right\}$. This special case coincides the work by Barsoum and Ghallagher (1971). For a beam with IOS and IAT, the right hand side of Eq. (3.16) does not vanish and the solution of Eq. (3.16) provides a nonlinear relationship between the load factor λ and the nodal displacements $\left\{\mathbf{d}\right\}$.

3.5 Convergence study and verification for a perfectly straight beam

A convergence study is conducted by examining a 6m span simply supported beam with a W250X45 cross-section (Section dimensions and properties are: depth $d=266\,mm$, flange width $b=148\,mm$, flange thickness $t=13\,mm$, web thickness $w=7.6\,mm$, Saint-Venant torsional constant $J=261\times10^{3}\,mm^{4}$, weak axis moment of inertia $I_{y}=7.03\times10^{6}\,mm^{4}$ and warping constant $C_{w}=1.13\times10^{9}\,mm^{6}$) subjected to a) a concentrated transverse force acting at beam mid-span and b) uniform bending moments. The modulus of elasticity is $E=200,000\,MPa$ and the Poisson ratio is $\upsilon=0.3$. The beam is assumed to be perfectly straight. Thus, the right hand-side of Eq. (3.16) vanishes. The resulting eigenvalue problem is solved for the critical load. A mesh sensitivity analysis is conducted by modelling the problem using 2, 4, 8, and 16 elements. The results shown in Table 3.2 indicate that no more than 8 elements are needed to predict the critical load within four significant digits.

Table 3.2: convergence study on the critical load

Number of elements	Critical moments for case (a) (kNm)	M_a/M^*_{a-16}	Critical moment for case (b) (kNm)	M_b/M^*_{b-16}	Moment gradient (M_a/M_b)
2	137.66	1.005	101.14	1.005	1.361
4	137.00	1.001	100.70	1.000	1.360
8	136.91	1.000	100.67	1.000	1.360
16	136.91	1.000	100.67	1.000	1.360

* M_{a-16} = critical moment based on 16 elements in case (a), M_{b-16} = critical bending moments based on 16 elements in case (b)

The moment gradient obtained in the last column of Table 3.2 compares to $C_{CAN} = 4M_{\max}/\sqrt{M^2_{\max} + 4M^2_A + 7M^2_B + 4M^2_C} = 1.265$ based on the Canadian Standards (CAN/CSA S16-14) where M_A, M_B and M_C are the bending moments at the quarter-span, mid-span and three-quarter span points. The corresponding value in American Standards (ANSI/AISC 360-16) is $C_{AISC} = 12.5|M_{\max}|/\left(2.5|M_{\max}| + 3|M_A| + 4|M_B| + 3|M_C|\right) = 1.316$, that based on the Australian Standard (AS 4100-1998) is $C_{AUS} = 1.7M_{\max}/\sqrt{M^2_A + M^2_B + M^2_C} = 1.388$ and that based on the Eurocode Guide (EN 1993-1-1:2005) is $C_{EU} = 1.365$. For the case of uniform moments, the present solution predicts a critical moment M_{cr} of 100.7 kNm. This value nearly coincides with that based on the thin-walled B31OS element in ABAQUS of 99.5 kNm using 40 elements. Another comparison is done by modeling the problem using the shell element S4R in ABAQUS. The S4R element has 4 nodes with six degrees of freedom per node with reduced integration and hourglass control. The mesh used involves six elements for each flange, eight elements along the web height, and 180 elements along the span. The simply supported boundary conditions are imposed by restraining the vertical, horizontal displacement and the rotation about the longitudinal axis of both flanges and web at both ends. The critical moment obtained is 95.9 kNm which is 4.8% percent lower than that predicted by the present element. The slight difference is due to the fact that, unlike thin-walled beam elements, the shell solution captures shear deformation and distortional effects. The corresponding buckling mode is depicted in Figure 3.3. A comparison of the buckling modes shapes normalized with respect to the peak lateral displacement at the centroid

of the mid-span $\bar{u}_c\left(z = L/2\right)$ shows that the buckling mode shapes based on the present solution essentially coincide with those based on B31OS and S4R elements model in ABAQUS (Figure 3.4). Slight differences are observed in the angle of twist plots depicted in Figure 3.4 (b) where a difference of 1.16% is observed between the present solution and the B31OS solution and a 3.11% difference with the S4R model.

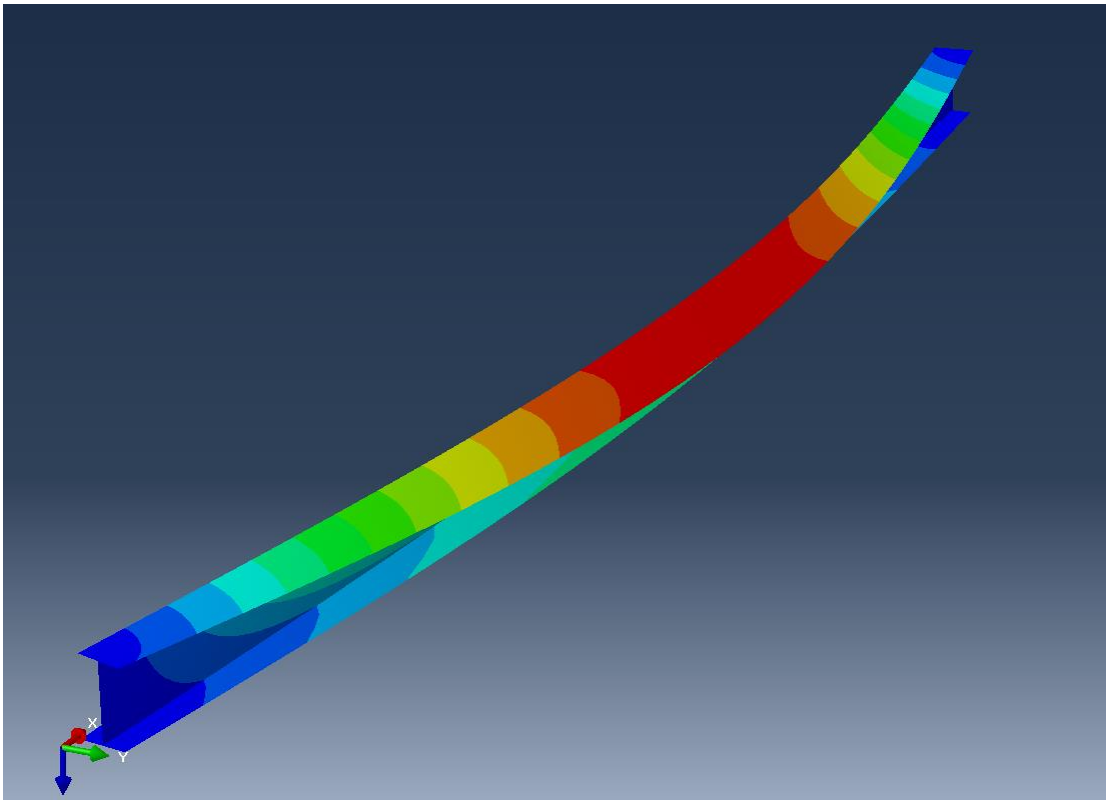

Figure 3.3 Buckling shape for a 6-m span beam with W250X45 section under uniform bending moments based on S4R model in ABAQUS

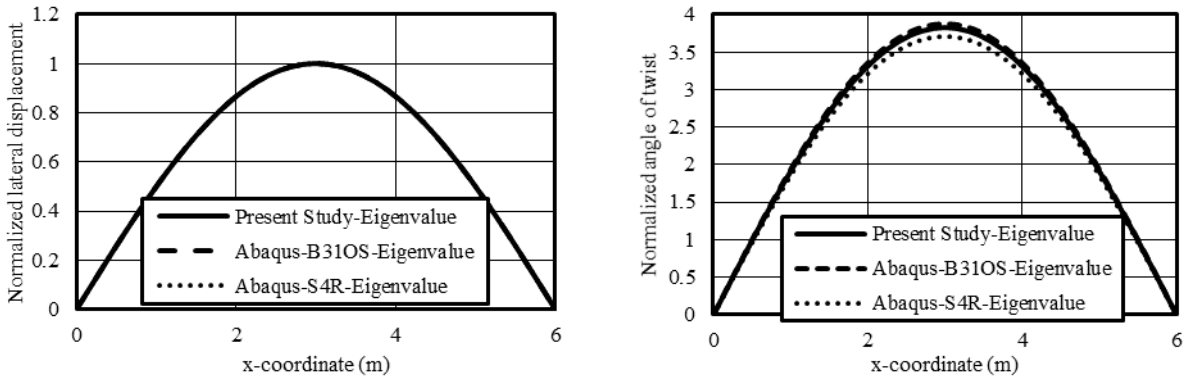

(a) (b)

Figure 3.4 First buckling mode for 6m straight beam based on a) present study, b) B31OS solution and c) S4R solution

3.6 Verification for a beam with initial geometric imperfections

3.6.1 Mesh sensitivity analysis

A beam with initial geometric imperfections, cross-section, span, and material properties identical to those described in section 3.5 is considered in this section. The IOS $u_0(z)$ and IAT $\theta_0(z)$ are assumed to follow the first buckling mode shape as obtained from the eigen-solution for the perfectly straight beam in Section 3.5. The amplitude of the peak IOS at mid-span of the compression flange is $u_{0-c}(L/2) = u_0(L/2) + (d/2)\theta_0(L/2)$, in which subscript c denotes the compression flange, subscript 0 denotes the initial out-of-straightness, and d is the total section height. The peak IOS $u_{0-c}(L/2)$ was set equal to $L/1000 = 6mm$. A mesh sensitivity analysis for the present element is conducted by analyzing the beam using 2, 4, 8 and 16 elements as illustrated in Figure 3.5. The lateral displacements at the centroid of the mid-span section against the the number of elements when the applied moment is $M = 90.1kNm$. The difference in lateral displacement at mid-span as predicted by the 8 and 16 elements is found negligible. Thus, 8 elements in the model are judged to be adequate to capture the displacement response for beams with initial out-of-straightness. In the following analyses, 40 elements are used in the present finite element solution to obtain smooth curves for the additional lateral displacement $u(z)$ and the angle of twist $\theta(z)$.

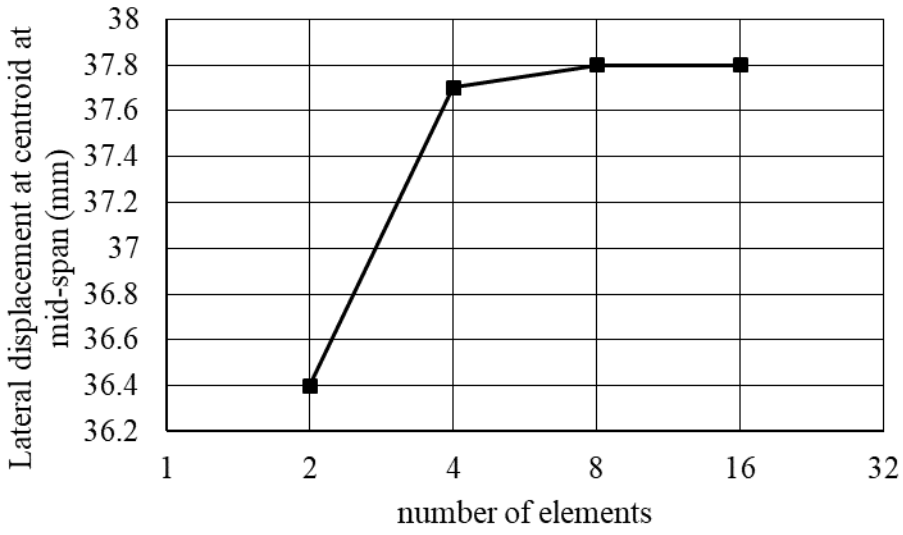

Figure 3.5 Lateral displacement at centroid at mid-span versus the number of elements used in the present finite element solution (applied moment = 90.1kNm)

3.6.2 Comparison with other solutions

The problem was solved using the present model and a nonlinear incremental load-deformation analysis based on the S4R element shell FEA (Figure 3.6). The specifics of the S4R mesh are identical to those of Section 3.5. Keyword NLGEOM in ABAQUS is adopted to evoke the geometric nonlinear feature. Under the present model, the beam is meshed into 40 elements. Figure 3.6 depicts the applied moments versus the peak total lateral displacement at compression flange mid-span as given by $\bar{u}_c(L/2) = u_0(L/2) + u(L/2) + (d/2)\left[\theta_0(L/2) + \theta(L/2)\right]$ where, as matter of convention, the bar on top of an argument displacement denotes the total out-of-straightness obtained by the summation of the initial out-of-straightness and the additional displacement. When the applied moments are comparatively low, the peak total lateral displacement predicted by the present finite element formulation is observed to coincide with that based on the ABAQUS model. The difference between the two models is observed to slightly grow with the loading level, but still agree within 2.2% within the range of deformations investigated.

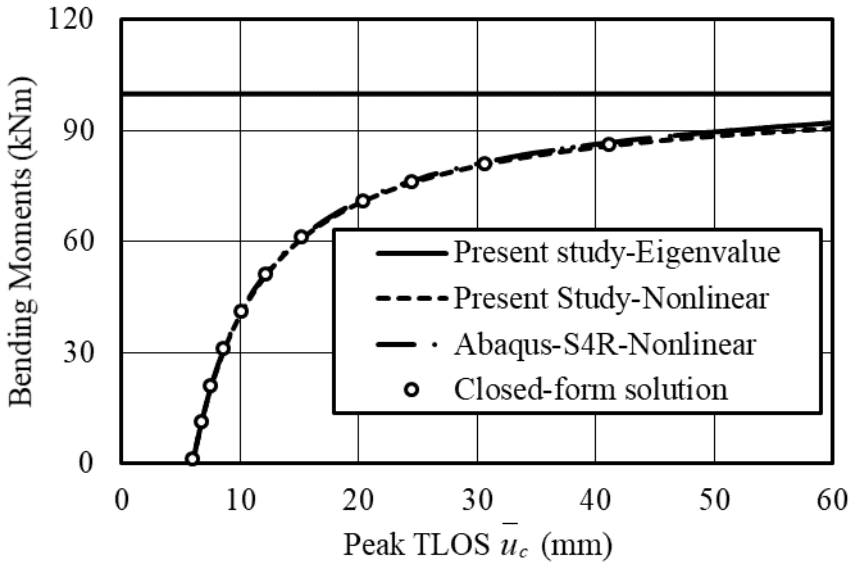

Figure 3.6 Bending moments versus total lateral displacement at the compression flange For W250x45 section

3.6.3 Verification and Comparisons

Four common cross-sections (Table 3.3) are examined using the present finite element solution and the B31OS element in ABAQUS to assess the validity of the present finite element solution. The B31OS element is a two-node linear element and has seven degrees of freedom (three translations, three rotations and a warping deformation) for each node. The B31OS model is discretized into 40 elements along the span. The initial out-of-straightness is modeled directly by input of the pre-calculated coordinates for the considered beam with initial out-of-straightness. Option NLGEOM in Abaqus is evoked to apply the load incrementally and generate the load-displacement relation in Figure 3.7.

Figure 3.7 shows that, for all four sections examined, the lateral displacement increases slowly with the applied moments within the range $M/M_{cr} \le 0.8$, but rises rapidly beyond this range. The present finite element solution predicts a moment-displacement relationship that asymptotically approaches the relation $M/M_{cr} = 1$, M_{cr} being the elastic critical moments as determined by the eigen-value solution of a perfectly straight beam.

The best agreement between the present finite element solution and B31OS model is obtained for the W250X28 section. When the additional lateral displacement at the compression fiber is $u_c = L/270$ the difference in M / M_{cr} predictions is 1.5% (Figure 3.7). This percentage difference

decreases to 1.3% when $u_c = L/180$, and 0.9% when $u_c = L/90$. The largest difference between the predictions of the present finite element and B31OS solutions is observed for the W250X58 section, where the difference in M / M_{cr} is found to be 9.7% when the additional lateral displacement at the extreme fiber is $u_c = L/270$. This difference is found to marginally increase to 10.2% and 10.5% when the displacements increases to $u_c = L/180$ and $u_c = L/90$, respectively.

Table 3.3 Section dimensions and geometric properties for the examined cross-sections

	d	b	t	w	I_x	I_y	C_w	J
	mm				mm^4 $\times 10^6$	mm^4 $\times 10^5$	mm^6 $\times 10^{10}$	mm^3 $\times 10^4$
W250X18	251	101	5.3	4.8	22.4	9.1	1.4	2.2
W250X28	260	102	10	6.8	40.0	17.8	2.8	9.7
W250X45	266	148	13	7.6	71.7	70.3	11.3	26.1
W250X58	252	203	13.5	8	87.3	188.0	26.8	40.9

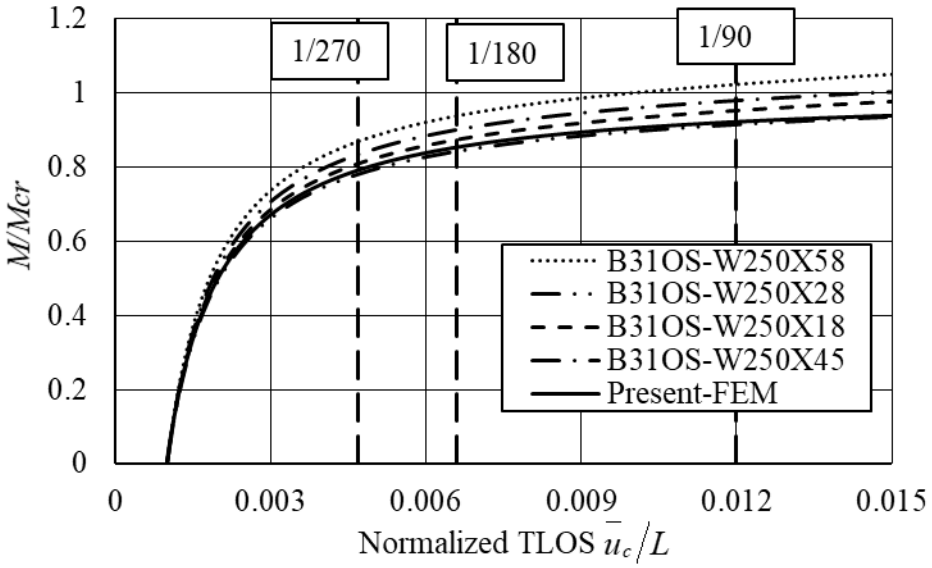

Figure 3.7 Moment-lateral displacement relations for W250X18, W250X28, W250X45 and W250X58 obtained from B31OS mode in ABAQUS

3.7 Effect of the IOS pattern on response for beams under uniform moments

In the absence of experimental measurements, previous studies (e.g., Kala and Melcher 2009 and Nguyen and Chan et al. 2013) have assumed the initial out of straightness to follow a sinusoidal

distribution. Other studies (Aguero et al. 2015 a,b) have postulated that initial geometric imperfections to follow the first buckling mode for a straight beam. The validity of such assumptions on the response need to be examined and is the scope of the following sub-sections.

3.7.1 Effect of IOS/IAT patterns

Consider a beam with a W250x45 under strong axis moment M that induces compression at the top flange (Figure 3.8). It is assumed that the initial geometric imperfections are fully characterized by the IOS $u_0(z)$ (defined at the section centroid) and the IAT $\theta_0(z)$ for the cross-section. The corresponding initial IOS at the compression flange is $u_{0-c}(z) = u_0(z) + (d/2)\theta_0(z)$ and that at the tension flange is $u_{0-t}(z) = u_0(z) - (d/2)\theta_0(z)$. It is assumed that both $u_0(z)$ and $\theta_0(z)$ are sinusoidal curves so that peak IOS $u_{0-p} = \max\left(u_{0-t}(L/2), u_{0-c}(L/2)\right)$ may take place either at the top flange under compression (Pattern a in Figure 3.8) or the bottom under tension (Pattern b in Figure 3.8b) of the mid-span section. The peak IOS is specified to take some value such as $u_{0-p} = L/1000$ while the IOS at the other flange u_{0-q} ranges from $-u_{0-p}$ to $+u_{0-p}$. Five IOS cases (1 through 5) are considered

$$\left(u_{0-p}, u_{0-q}\right) = (L/1000)\left[(1,1) \quad (1, 0.325) \quad (1,0) \quad (1,-1) \quad (0,1)\right]$$

where Case 1 corresponds to equal lateral IOS at both flanges (i.e., with no IAT), Case 2 corresponds to first mode shape of the beam where the bottom flange undergoes a lateral displacement equal to 32.5% of that of the top flange for the present problem, Case 3 corresponds to a top flange IOS with no IOS at bottom flange, Case 4 corresponds to two equal and opposite lateral displacements of both flanges, thus corresponding to the case with IAT but no IOS, and Case 5 corresponds to bottom flange IOS (with no IOS at top flange).

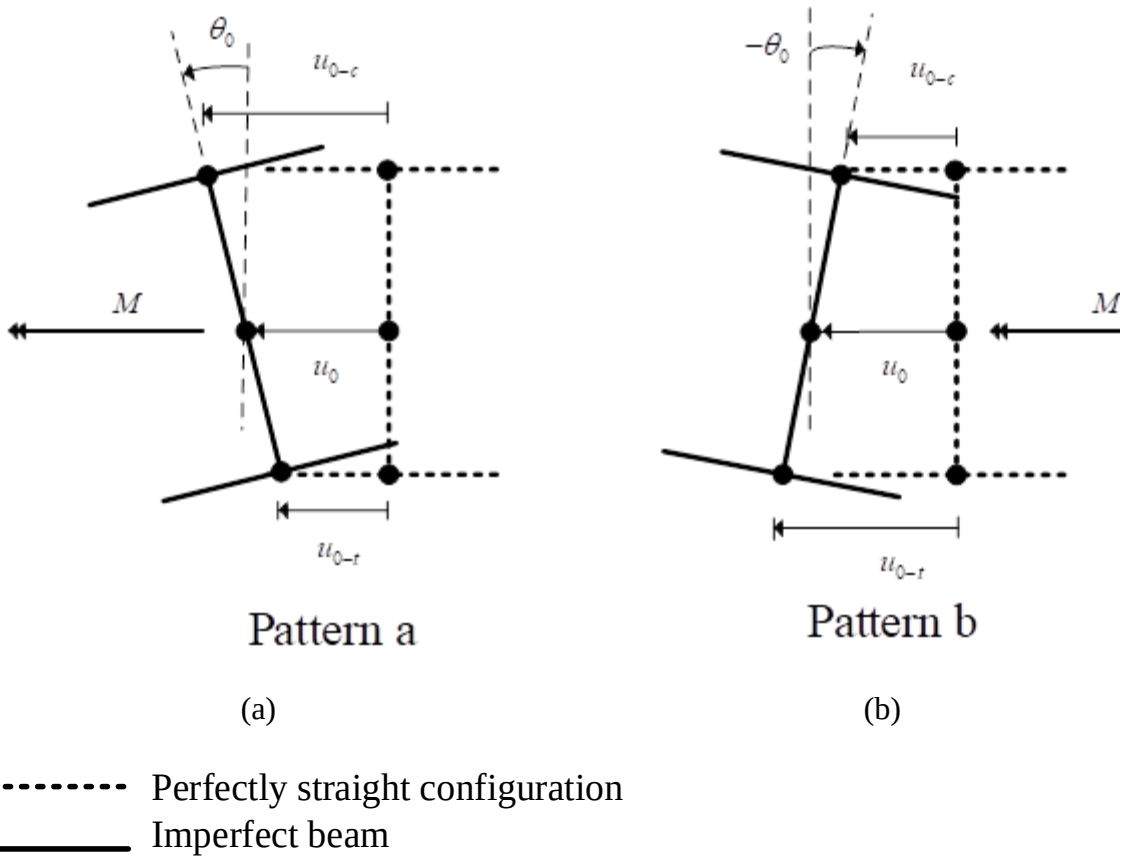

Figure 3.8 Illustration for the combination of IOS and IAT for (a) pattern a and (b) pattern b

Figure 3.9 (a) shows that a beam with a specified IOS a larger positive and a given load level, an increase in IAT $\theta_0(z)$ corresponds to a larger total lateral out-of-straightness (TLOS) displacement at the compression flange $\bar{u}_c$ (Case a in Figure 3.8 a). However, for the case where the IAT $\theta_0(z)$ is negative (Figure 3.8 b), a larger IAT magnitude results in a smaller TLOS displacement the compression flange since the cross-section rotates to the position of zero twist as the applied load is increased before it undergoes a positive angle of twist. This observation coincides with the characteristics of the closed form solution buckling solution where both $u(z)$ and $\theta(z)$ are positive.

Taking Case 1 $(u_{0-p}, u_{0-q}) = (L/1000)(1,0)$ which conforms to pattern (a) in Figure 3.8 (a) the load-displacement curves for the lateral displacement at the compression flange/angle of twist at mid-span are presented in the plot labelled as (1, 0) in Figure 3.8 (b). If the beam is installed upside down, the compression flange in case (a) becomes the tension flange in case (b) (i.e.

$\left(u_{0-p}, u_{0-q}\right) = \left(L/1000\right)\left(0,1\right)$), and the behavior of the load-displacement curve would differ as depicted in the plot labelled (0,1) in Figure 3.9. This suggests that the orientation of the section influences the load-displacement curves.

In the absence of specific experimental measurements for initial geometric imperfections, past studies on steel beams (Kala and Melcher 2009 and Nguyen and Chan et al. 2013) have been postulated to conform to the first buckling mode shape. Such an approach corresponds to $\left(L/1000\right)\left(1, 0.325\right)$ in the present study. The plots provided Figure 3.9(a), suggest that this approach leads to conservative estimates for the lateral displacements and the angle of twist for the cases $\left(u_{0-p}, u_{0-q}\right) = \left(L/1000\right)\left(0,1\right)$ and $\left(u_{0-p}, u_{0-q}\right) = \left(L/1000\right)\left(1,1\right)$ but corresponds to un-conservative estimates for cases $\left(u_{0-p}, u_{0-q}\right) = \left(L/1000\right)\left(1,0\right)$ and $\left(u_{0-p}, u_{0-q}\right) = \left(L/1000\right)\left(1,-1\right)$. However, it is observed that the difference between all five cases considered decreases as the applied moments decrease. For example, the ratio of moments for the two extreme cases $\left(u_{0-p}, u_{0-q}\right) = \left(L/1000\right)\left(0,1\right)$ and $\left(L/1000\right)\left(1,-1\right)$, is 25% when $\bar{u}_c = 30mm$ while the difference between the case $\left(u_{0-p}, u_{0-q}\right) = \left(L/1000\right)\left(1,1\right)$ and $\left(L/1000\right)\left(1, 0.325\right)$ is smaller than 6%. The corresponding difference in total angle of twist $\bar{\theta}$ for these two cases are found negligible when $\bar{\theta} \geq 0.15 rad$.

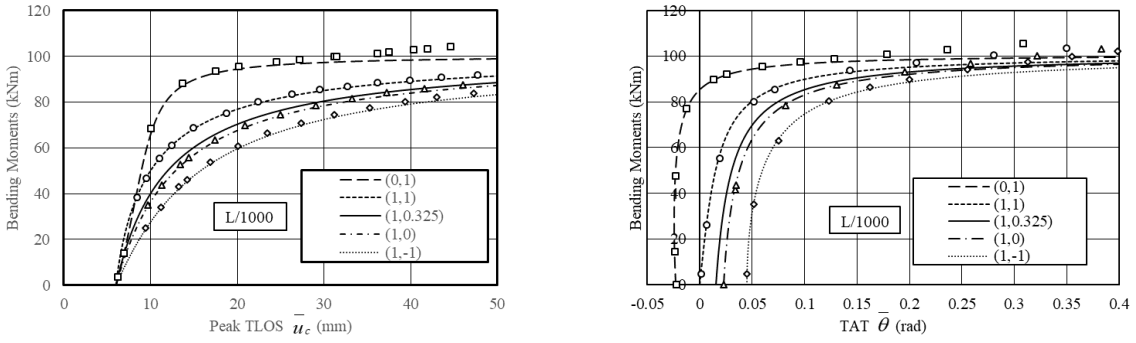

(a) (b)

Figure 3.9 Bending moments versus (a) peak total lateral out-of-straightness (TLOS) at section mid-height and (b) total angle of twist (TAT) for $\left(u_{0-p}, u_{0-q}\right)$ = (a) $\left(L/1000\right)\left(1,1\right)$, (b) $\left(L/1000\right)\left(1, 0.325\right)$, (c) $\left(L/1000\right)\left(1,0\right)$, (d) $\left(L/1000\right)\left(1,-1\right)$ and (f) $\left(L/1000\right)\left(0,1\right)$ (peak lateral displacement is $L/1000$ in all cases)

3.7.2 Contribution of higher modes

A perfectly straight beam corresponding to that investigated in the previous section is examined to obtain the first and third buckling modes by conducting an eigenvalue analysis. The extracted buckling modes are then normalized so that the peak lateral displacement for the corresponding mode at the top flange of mid-span section is equal to unity to reach the normalized buckling modes $\{\eta_1\}$ and $\{\eta_3\}$. A load-displacement analysis based on the present model is conducted based on an IOS pattern given by a linear combination $(L/1000)\left(\rho\{\eta_1\}+(1-\rho)\{\eta_3\}\right)=6mm\left(\rho\{\eta_1\}+(1-\rho)\{\eta_3\}\right)$. Six cases are considered for $\rho=1.0, 5/6, 4/6, 3/6, 2/6, 1/6$ where $\rho=1.0$ corresponds to the case where IOS follows only the first mode, and $\rho=5/6$ corresponds to the case where the magnitude of IOS due to the first mode is $5mm$ and that due to the third mode is $1mm$, etc. Plots for the bending moments versus the peak TLOS are provided in Figure 3.10. At a given bending moment level, the beam with the lower contribution of the first buckling mode is observed to undergo a smaller lateral displacement. The observation suggests that, for a given peak initial out-of-straightness $u_{0-c}(L/2)$, the first mode is consistently more detrimental and then the third mode and will thus be adopted in subsequent investigations.

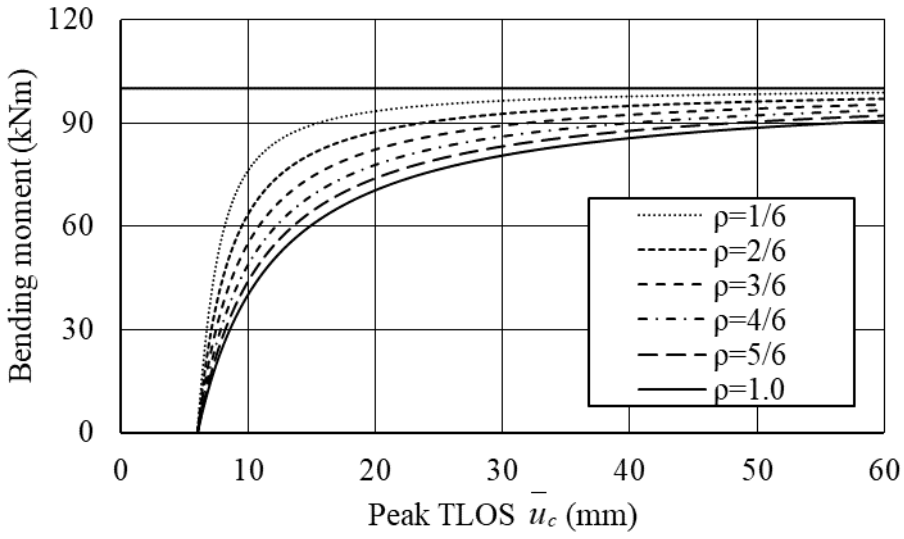

Figure 3.10 Bending moments versus the peak total lateral out-of-straightness (TLOS) for the first and third buckling modes superposition cases

3.8 Proposed design criteria for beams with initial geometric imperfections

As depicted in Figure 3.6, an eigenvalue solution provides a clear-cut value for the critical load/moments for an initially perfectly straight beam. Such an analysis does not incorporate the IOS-IAT effects. To the contrary, a nonlinear analysis accounts for IOS-IAT effects but provides no clear-cut value for critical load. To establish a design value, it is thus necessary to introduce failure criteria for design. Two types of failure criteria can be considered:

(1) A serviceability criterion can be postulated such that it limits the peak additional lateral displacement $u\left(L/2\right)+\left(d/2\right)\theta\left(L/2\right)$ under service loads to a threshold value such as $L/180$, $L/360$ etc. where the magnitude of such a threshold value depends on the type of application involved.

(2) A stress based criterion, where the normal stresses induced by the combined normal stresses induced by the strong axis moment M_x, weak axis moment M_y and bimoments B are not to exceed the yield strength of the material F_y, taken as 350MPa in subsequent runs, or a fraction thereof εF_y, to account for the presence of residual stresses such a criterion may take the form

$$\sigma\left(z\right)=+\frac{M_x\left(z\right)}{I_x}\frac{h}{2}-\frac{M_y\left(z\right)}{I_y}\frac{b}{2}+\frac{B\left(z\right)}{C_w}\frac{bd}{4}\le\varepsilon F_y \tag{3.18}$$

in which, ε is a fraction of the yield strength that accounts for the presence of residual stress. In ANSI- AISC 360-16 the fraction ε is taken as 0.7. The criterion in Eq. (3.18) is valid for Class 3 sections (i.e., non-compact in ANSI/AISC 360-16), and would yield conservative results for Class 1 or 2 section (compact sections). To obtained the normal stress at section z for the uniform bending moment case, Eq. (3.18) is expressed in terms of the applied moment M as (Figure 3.11)

$$\sigma\left(z\right)=+\frac{M\cos\theta\left(z\right)}{I_x}\frac{h}{2}-\frac{M\sin\theta\left(z\right)}{I_y}\frac{b}{2}+\frac{B\left(z\right)}{C_w}\frac{bd}{4} \tag{3.19}$$

in which, $B\left(z\right)$ is obtained by post-multiplying the elastic stiffness matrix $\left[\mathbf{k_e}\right]$ of the relevant element by the corresponding nodal displacements $\left\{\mathbf{d}_e\right\}$. When the angle of twist $\theta\left(z\right)$ in Eq. (3.19) is small, one obtains

$$\sigma(z) \approx +\frac{M}{I_x}\frac{h}{2} - \frac{M\theta(z)}{I_y}\frac{b}{2} + \frac{B(z)}{C_w}\frac{bd}{4} \tag{3.20}$$

The maximum compressive stress takes place at beam mid-span and is obtained by setting $z = L/2$.

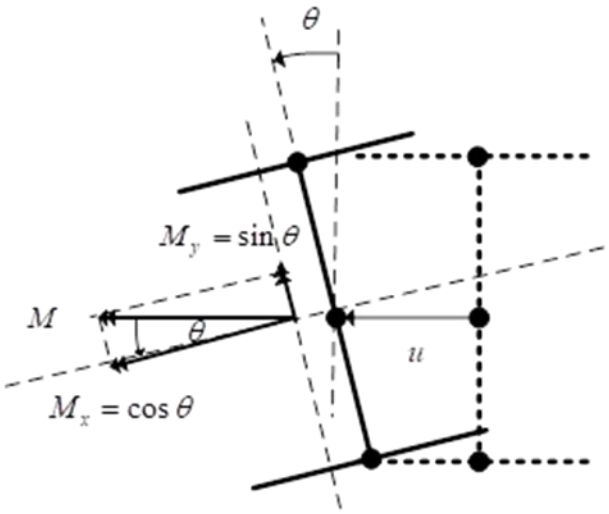

Figure 3.11 Geometric relationship for the projections of the applied moment on the bending axes

3.8.1 Verification of stresses

Consider a six-meter-span beam with W250X28 cross-section with IOS $L/1000 = 6mm$ based on IOS that follows the first mode. For a beam under uniform bending moments, the normal stresses have been computed using three different approaches as detailed in the following:

(1) In the present finite element solution, the internal forces (M_x, M_y and B) are obtained by post-multiplying the elastic stiffness matrix $[\mathbf{k_e}]$ of the relevant element by the corresponding nodal displacement $\{\mathbf{d_e}\}$ to recover the nodal force vector $\{\mathbf{f}\}_{8\times1} = [\mathbf{k_e}]_{8\times8}\{\mathbf{d_e}\}_{8\times1}$. The elements of nodal forcv vector $\{\mathbf{f}\}$ contain the internal forces M_x, M_y, B needed to compute the stresses from Eq. (3.18).

(2) For a simply supported beam under uniform moments $M(z) = M$, the bending moments are given from equilibrium, i.e., $M_x(z) = M\cos\theta(z)$, $M_y(z) = M\sin\theta(z)$ as illustrated in Figure

3.11. However, the bimoment $B(z)$ needs to be determined from the technique described in the previous section. The stresses are then computed from Eq. (3.19).

(3) For the verification, the stress output as obtained from a B31OS solution.

A comparison of the results is shown in Figure 3.12. All three solutions predict nearly coinciding normal stresses. Thus, the present FEM solution in conjunction with Eq. 3.18 will be used to compute the normal stresses in subsequent sections.

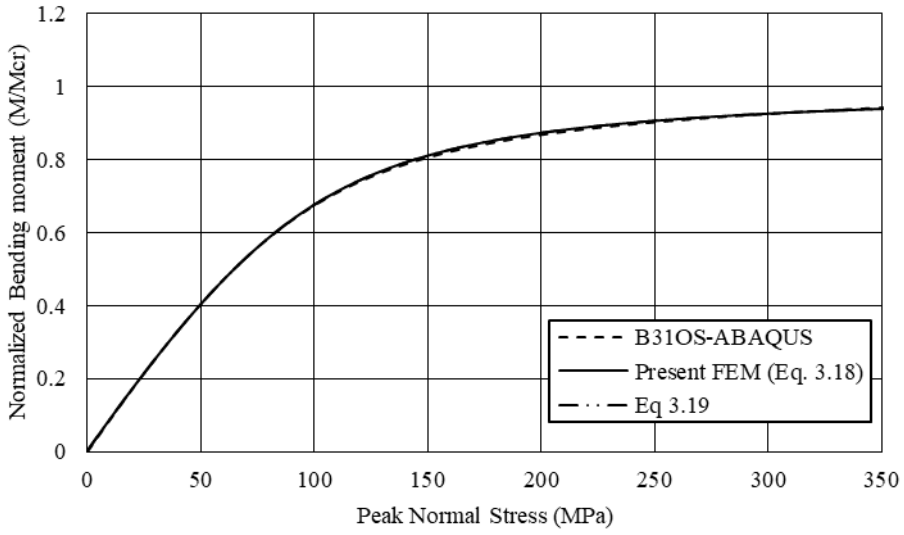

Figure 3.12 Comparison between normal stresses as determined by various techniques

3.8.2 Applying the displacement failure criterion-Illustrative Example

A simply supported beam with W250X45 cross-section has a 6m span and is subjected to uniform bending moments M . The beam is assumed to be initially non-straight and to follow the first buckling mode. Three IOS magnitudes are examined for the peak initial out-of-straightness at the top flange $u_{0-c} = L/600 = 10\,mm$ $u_{0-c} = L/800 = 7.5\,mm$ and $u_{0-c} = L/1000 = 6\,mm$. The relationships between the bending moments and corresponding total lateral displacement at the compression flange $\bar{u}_c(L/2) = u_0(L/2) + u(L/2) + (d/2)\left[\theta_0(L/2) + \theta(L/2)\right]$ are compared in Figure 3.13. All three cases exhibit an asymptotic behaviour towards the critical moment as predicted by the eigenvalue solution for a hypothetically perfectly straight beam with similar dimensions. For a given target total lateral displacement at the compression flange, an increase in IOS is observed to decrease the corresponding bending moments attained. For example, if a total

lateral displacement at the compression flange of $\bar{u}_c\left(L/2\right)=30\text{mm}$ is targeted, the cases where the total peak IOS are $L/600$, $L/800$ and $L/1000$, respectively correspond to 66.6%, 75.0%, and 80.0% of the critical moments M_{cr} of the perfectly straight beam (as determine by an eigenvalue solution). Also, depicted in Figure 3.13 are the bending moments corresponding to a additional peak lateral displacement $u_c = L/180$. Bending moment fractions of 0.77*Mcr*, 0.82*Mcr* and 0.85*Mcr* are attained respectively for peak IOS = $L/600$, $L/800$ and $L/1000$.

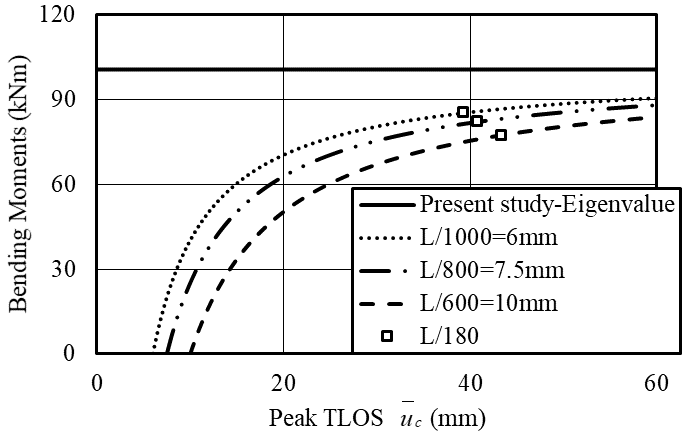

Figure 3.13 Bending moments versus total lateral displacement at compression flange midspan for various IOS a) $u_{c0}=L/1000=6mm$ **b)** $u_{c0}=L/800=7.5mm$ **and c)** $u_{c0}=L/600=10mm$

3.8.3 Illustrative example for applying stress failure criterion

A comparison between the stress predictions of ABAQUS-S4R and ABAQUS-B31OS solutions and those of the present study is provided in Figure 3.14 for the example defined in the previous section. For a specified target peak normal stress of 70% of the yield strength, the present solution is observed to slightly underestimate the peak bending moments compared to the ABAQUS S4R shell model predictions. The present model predicts that the beam with W250X45 cross-section attains 80.3% of the critical moments while the corresponding fraction of the W250X18 cross-section is 91.2%. The present solution predicts that the peak normal stress as determined from Eq. (3.18) attains the threshold yield stress of $0.7F_y=245MPa$ when the applied bending moment is 80.34 kNm (Figure 3.14 a). The corresponding prediction based on the S4R model is 83.9kNm, a 4.29% difference. In comparison, for the W250X18 section, Figure 3.14 (b) shows that the moments predicted by the present model is 10.0 kNm while the corresponding value based on the

ABAQUS model is 10.6 kNm, a 5.67% difference. For the W250X45 cross-section, the bending moment-normal stress relationship based on all three solutions are in close agreement (Fig. 3.13a). The plot based on the B31OS element is observed to be close to that based on the present FEM for small applied moments (i.e., $M \leq 60kNm$). Beyond this range, the response of the B31OS model slightly departs from the present solution and merges with the response of the S4R model. To the contrary, for the W250x18 beam, the difference between the applied moments from B31OS element and the present FEM is found to decrease as the normal stresses increase. For example, when $\sigma = 50MPa$, the difference between the two models is 14.1%. When the peak normal stresses at mid-span increase to $\sigma = 200MPa$, the corresponding difference is 3.4%.

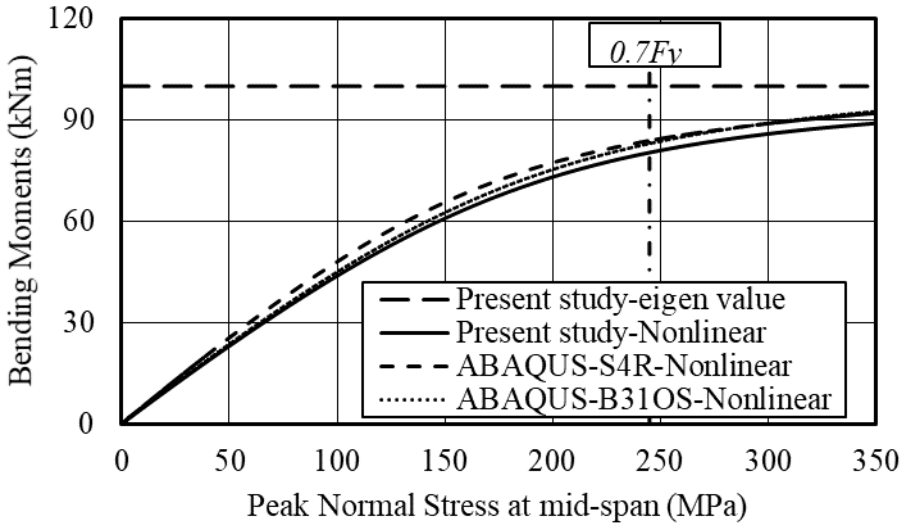

(a)

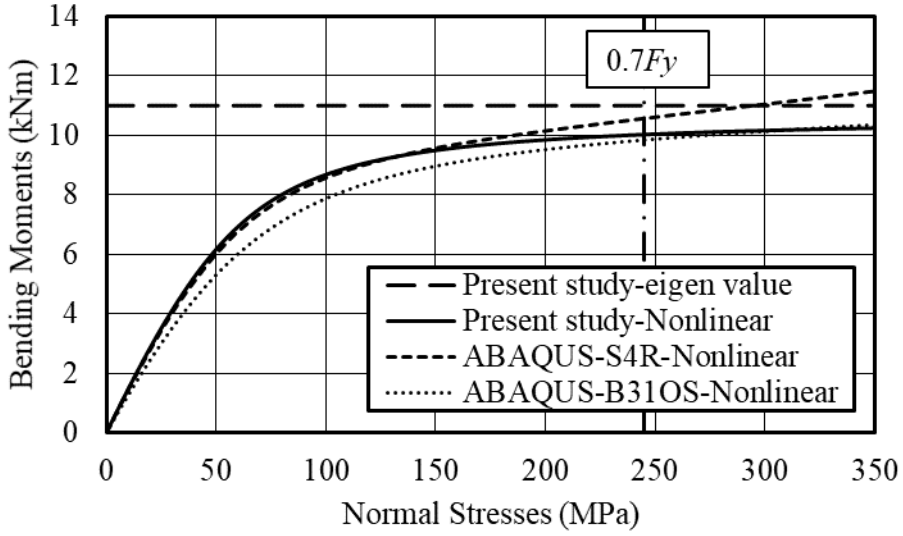

(b)

Figure 3.14 Peak normal stresses for 6m-span simply supported beams with a) W250X45 and b) W250X18

Stress contours

The stress contours for the longitudinal stresses in the compression flange of the W250X45 cross-section as predicted by the present model are illustrated in Figure 3.15 for applied strong axis moment levels of $M = 60$, 70 , 80, and 90kNm . The maximum stresses as given by Eq. (3.18)

are observed to occur at the flange tip of the mid-span section since the stress contributions of the strong axis bending, weak axis bending and bimoments attain peak values at these locations.

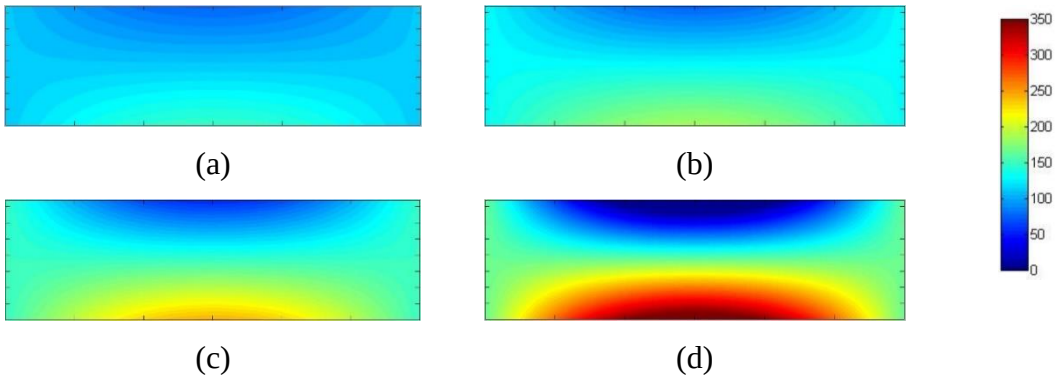

Figure 3.15 Stress contours predicted by the present solution for top flange under a) $M = 60.0$ kNm**, b)** $M = 70.0$ kNm**, c)** $M = 80.0$ kNm **and d)** $M = 90.0$ kNm **for simply supported beam with W250X45 cross-section (scaling factor for width=10x scaling factor for span)**

Contributions of moments and bimoments to stresses

The applied moment M is normalized with respect to the elastic critical moments M_{cr} as determined from the corresponding eigenvalue solution for the straight beam and the ratio M / M_{cr} is plotted against the normalized peak displacement at the compression flange $\overline{u_c}$ normalized with respect to the beam span (Figure 3.16).

The contribution of the internal forces to the normal stress (normalized by the yield strength) are illustrated in Figure 3.16 for the four cross-sections considered. Figure 3.16 (a, c, e and g), show that the normal stress due to the strong axis bending moments increases rapidly with the applied moments and reach a plateau when the normalized peak TLOS is around 0.01.

At a normalized peak lateral displacement ratio $\overline{u_c}/L = 0.01$, the stress level due to the strong axis bending is found to take the values $0.17F_y$, $0.25F_y$, $0.49F_y$ and $0.80F_y$ for W250X18, W250X28, W250X45 and W250X58, respectively. These stress ratios correspond with moment of inertia ratios of I_y/I_x = 0.041, 0.045, 0.098, and 0.215 respectively, suggesting that the attained strong axis moment stress ratio decreases as the ratio decreases.

In all cases, the normal stresses due to the weak axis bending moment and bimoment are found to linearly increase with the increase in the normalized peak TLOS $\overline{u_c}/L$. As a result, for low load

levels, the normal stresses are primarily due to strong axis bending. As the applied loads increase, the share of normal stresses due to weak axis bending and bimoments increase compared to that of the strong axis contribution which decreases with $\bar{u}_c/L$ as illustrated in Figure 3.16 (b, d, f, and h). At a normalized peak TLOS of 0.03, the percentage of the normal stress due to weak axis bending moment is around 50% of the total normal stress in all four cases.

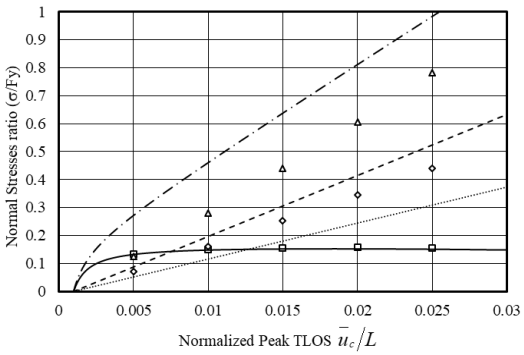
Normal Stresses ratio (σ/Fy)
Normalized Peak TLOS $\bar{u}_c/L$

(a)

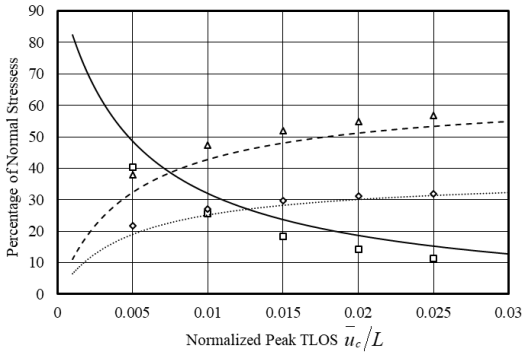
Percentage of Normal Stressess
Normalized Peak TLOS $\bar{u}_c/L$

(b)

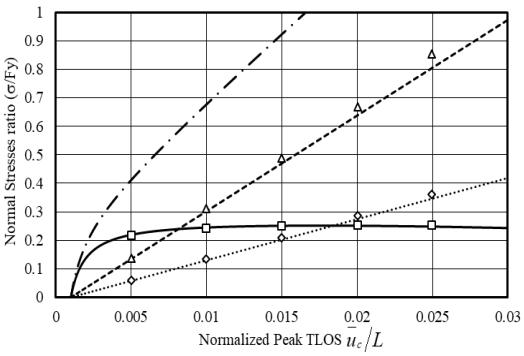
Normal Stresses ratio (σ/Fy)
Normalized Peak TLOS $\bar{u}_c/L$

(c)

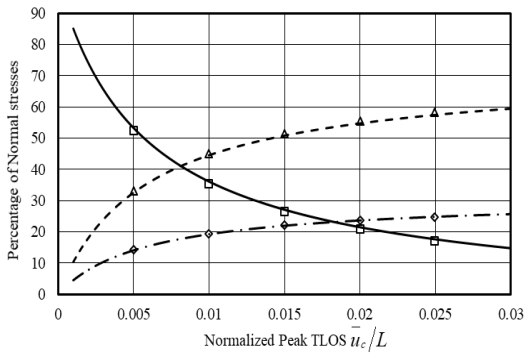
Percentage of Normal stresses
Normalized Peak TLOS $\bar{u}_c/L$

(d)

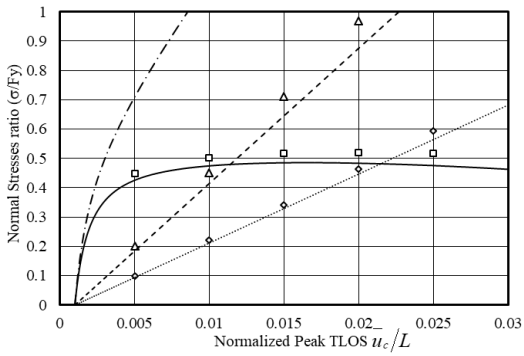
Normal Stresses ratio (σ/Fy)
Normalized Peak TLOS $\bar{u}_c/L$

(e)

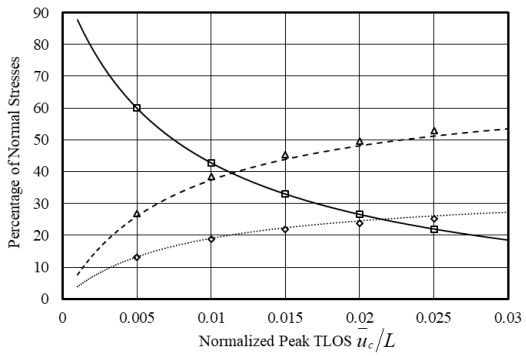
Percentage of Normal Stresses
Normalized Peak TLOS $\bar{u}_c/L$

(f)

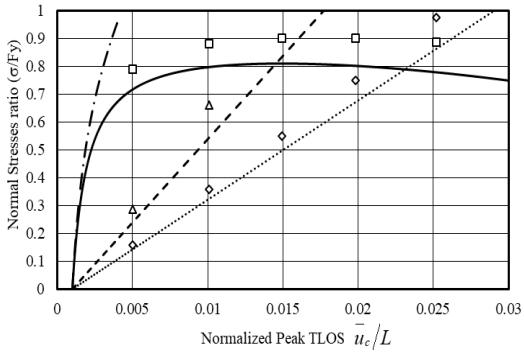
Normal Stresses ratio (σ/Fy)
Normalized Peak TLOS $\bar{u}_c/L$

(g)

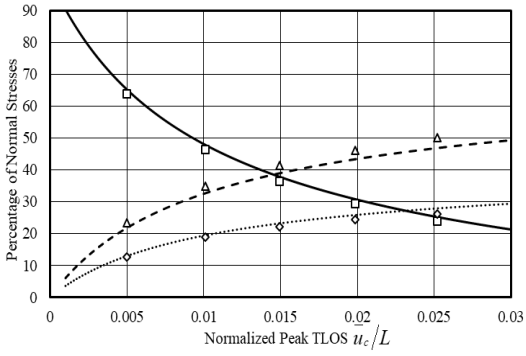
Percentage of Normal Stresses
Normalized Peak TLOS $\bar{u}_c/L$

(h)

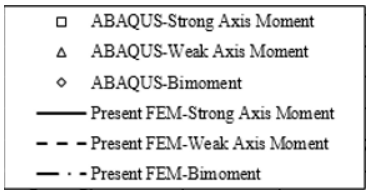

Figure 3.16 Normal stress ratio and percentage of normal stresses versus normalized peak displacement for W250X18 (a b), W250X28 (c and d), W250X45 (e and f) and W250X58 (g and h)

3.9 Parametric study

3.9.1 Effect of beam span on bending moment and normal stress ratios

To investigate the influence of beam span, four simply supported beams with a W250X45 cross-section with spans ranging from five to eight meters are investigated using the present solution. The imperfection pattern is assumed to follow the first mode (as discussed in Section 3.7.2) and the peak IOS is set to $u_{0-c} = L/1000$ in all cases, corresponding to values of a) 5*mm*, b) 6*mm*, c) 7*mm* and d) 8*mm*, respectively.

The relationship between the normalized peak TLOS $\bar{u}_c(L/2)/L$ and the normalized bending moments M/M_{cr} is depicted in in Figure 3.17 (a) for all spans examined. All four relationships are observed to perfectly coincide, indicating that the span has no effect on the normalized moment-displacement curves. Figure 3.17 (b) shows that for a given normalized peak total lateral out-of-straightness $\bar{u}_c/L$, the normal stresses ratio σ/F_y attained is found to decrease with the span, suggesting that longer span beams can sustain a larger normalized peak displacement compared to short span beams.

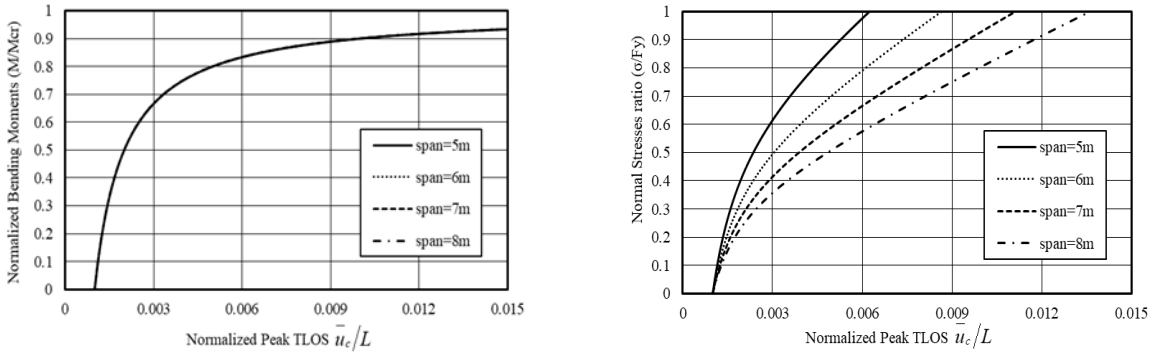

(a) (b)

Figure 3.17 (a) Normalized bending moments and (b) normalized normal stresses versus normalized peak total lateral out-of-straightness (TLOS) for W250X45 with span from 5 m to 8 m

3.9.2 Effect of section class on normalized bending moments and normal stress

Four simply supported beams with different section classes are examined. The W250x25 is taken as a reference case (Case 1 in Table 3.4). For a yield strength of 350MPa, the web meets class 1 requirements according to CAN-CSA S16 (2014). The web thickness is then reduced so that it becomes class 2 (Case 2), and then further reduced to become class 3 (Case 3) and class 4 (Case 4). The geometric parameters of the four sections are provided in Table 3.4. Figure 3.18 (a) shows identical bending moment versus normalized TLOS in all four cases while Figure 3.18 (b), shows a minor difference in stress ratios.

Table 3.4: Section properties for the four examined I-section class

	Total web depth (mm)	Web thickness (mm)	Flange breadth (mm)	Flange thickness (mm)
Class 1	**257**	**6.1**	**102**	**8.4**
Class 2	257	6.1	102	6.5
Class 3	257	6.1	102	5.0
Class 4	257	6.1	102	4.0

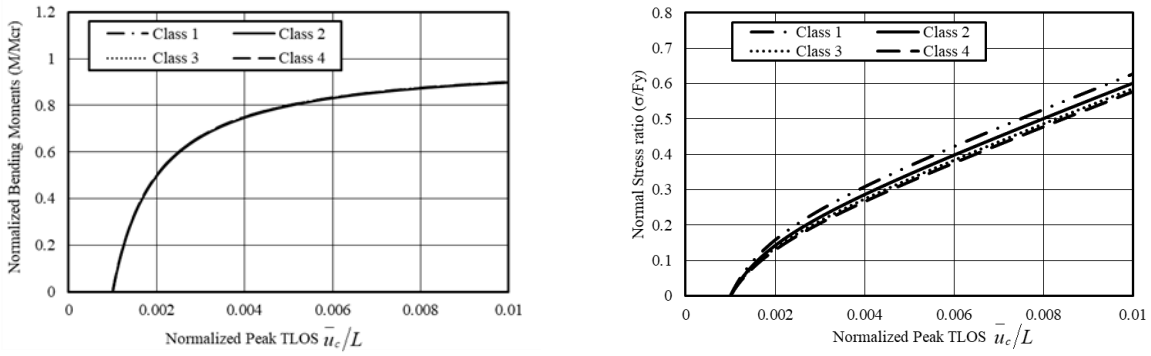

(a) (b)

Figure 3.18 (a) Normalized bending moments and (b) stress ratios versus normalized peak total lateral out-of-straightness (TLOS) for various classes

3.10 Summary and Conclusions

A thin-walled-beam finite element solution was developed for the lateral torsional response of steel beams with initial geometric imperfections. The validity of the solution was assessed by comparisons against Abaqus shell models (using S4R elements) and thin-walled elements (using

B31OS elements). Two design criteria were proposed based on threshold values for (1) the total lateral displacement and (2) the maximum normal stress. Illustrative examples were provided for applying each of the criteria. Patterns of the initial geometric imperfections were studied and a parametric study was performed to study the effect of spans and section class on the behavior of examined beams. The main findings of the study are summarized as follows:

1. The present finite element solution reliably predicts the load-displacement behavior for geometrically imperfect beams.

2. For a given peak initial lateral out-of-straightness, the most detrimental initial imperfection patterns were found to be associated with the highest initial angle of twist where the other flange has an equal and opposite lateral out-of-straightness.

3. When the initial imperfections are expressed as the summation of buckling modes, the most adverse geometric imperfection pattern is found to be associated with the first buckling mode.

3. For the displacement based design criterion, it is observed that only the magnitude of the initial imperfection affects the response of the beam. Thus, the LTB resistance of a beam is solely influenced by the magnitude of the initial imperfection u_{0-c} , and the threshold displacement chosen by the designer.

4. The stress ratios σ / F_y due to minor axis bending and warping are found to linearly increase with the normalized peak additional lateral displacement $\bar{u}_c / L$ while normal stress ratio σ / F_y due to major axis bending reaches a plateau value.

5. According the stress-based design criterion, for a given normalized peak TLOS $\bar{u}_c / L$ the stress ratio σ / F_y is found to decrease with the beam span.

6. The present model suggests that web thickness does not influence the normalized moment versus $\bar{u}_c / L$ response and to have a rather minor role in the stress ratio σ / F_y versus $\bar{u}_c / L$ response.

Appendix 3.A. Matrices in Finite Element Solution

This appendix provides the explicit expression for the matrices in the finite element solution. In Eq.(3.16), $[\mathbf{k}_e]$ and $[\mathbf{k}_g]$ shall be computed numerically as follows

Elastic stiffness matrix $[\mathbf{k}_e]$

$$
[\mathbf{k}_e] = \begin{bmatrix}
\frac{12EI_y}{L^3} & -\frac{6EI_y}{L^2} & 0 & 0 & 0 & \frac{12EI_y}{L^3} & -\frac{6EI_y}{L^2} & 0 & 0 & 0 & -\frac{6GJ}{5L} - \frac{12EC_w}{L^3} & \frac{GJ}{10} + \frac{6EC_w}{L^2} \\
-\frac{6EI_y}{L^2} & \frac{4EI_y}{L} & 0 & 0 & 0 & -\frac{6EI_y}{L^2} & \frac{2EI_y}{L} & 0 & 0 & 0 & \frac{GJ}{10} + \frac{6EC_w}{L^2} & -\frac{GJL}{30} + \frac{2EC_w}{L} \\
0 & 0 & \frac{6GJ}{5L} + \frac{12EC_w}{L^3} & \frac{GJ}{10} + \frac{6EC_w}{L^2} & 0 & 0 & 0 & -\frac{6GJ}{5L} - \frac{12EC_w}{L^3} & \frac{GJ}{10} + \frac{6EC_w}{L^2} & 0 & 0 & 0 \\
0 & 0 & \frac{GJ}{10} + \frac{6EC_w}{L^2} & \frac{2GJL}{15} + \frac{4EC_w}{L} & 0 & 0 & 0 & -\frac{GJ}{10} - \frac{6EC_w}{L^2} & -\frac{GJL}{30} + \frac{2EC_w}{L} & 0 & 0 & 0 \\
-\frac{12EI_y}{L^3} & \frac{6EI_y}{L^2} & 0 & 0 & 0 & \frac{12EI_y}{L^3} & -\frac{6EI_y}{L^2} & 0 & 0 & 0 & \frac{6GJ}{5L} + \frac{12EC_w}{L^3} & -\frac{GJ}{10} - \frac{6EC_w}{L^2} \\
-\frac{6EI_y}{L^2} & \frac{2EI_y}{L} & 0 & 0 & 0 & \frac{6EI_y}{L^2} & \frac{4EI_y}{L} & 0 & 0 & 0 & -\frac{GJ}{10} - \frac{6EC_w}{L^2} & \frac{2GJL}{15} + \frac{4EC_w}{L} \\
0 & 0 & -\frac{6GJ}{5L} - \frac{12EC_w}{L^3} & -\frac{GJ}{10} - \frac{6EC_w}{L^2} & 0 & 0 & 0 & \frac{6GJ}{5L} + \frac{12EC_w}{L^3} & -\frac{GJ}{10} - \frac{6EC_w}{L^2} & 0 & 0 & 0 \\
0 & 0 & \frac{GJ}{10} + \frac{6EC_w}{L^2} & -\frac{GJL}{30} + \frac{2EC_w}{L} & 0 & 0 & 0 & -\frac{GJ}{10} - \frac{6EC_w}{L^2} & \frac{2GJL}{15} + \frac{4EC_w}{L} & 0 & 0 & 0
\end{bmatrix}
$$

Geometric stiffness matrix $\left[\mathbf{k}_{\mathbf{g}}\right]$

$$
\left[\mathbf{k}_{\mathbf{g}}\right]=\begin{bmatrix}
0 & 0 & \frac{11M_1}{10L}-\frac{M_2}{10L} & \frac{M_1}{10} & 0 & -\frac{M_1}{10L}+\frac{11M_2}{10L} & -\frac{M_2}{10} \\
0 & 0 & \frac{M_2}{5}-\frac{9M_1}{10} & -\frac{M_1L}{10}+\frac{M_2L}{30} & 0 & -\frac{M_1}{10}-\frac{M_2}{5} & \frac{M_2L}{30} \\
0 & 0 & -\frac{11M_1}{10L}+\frac{M_2}{10L} & -\frac{M_1}{10} & 0 & \frac{M_1}{10L}-\frac{11M_2}{10L} & \frac{M_2}{10} \\
\frac{11M_1}{10L}-\frac{M_2}{10L} & \frac{M_2}{5}-\frac{9M_1}{10} & 0 & 0 & -\frac{M_1}{5}-\frac{M_2}{10} & 0 & 0 \\
\frac{M_1}{10} & -\frac{M_1L}{10}+\frac{M_2L}{30} & 0 & -\frac{M_2L}{30} & 0 & 0 & -\frac{M_2L}{30} \\
0 & 0 & -\frac{11M_1}{10L}+\frac{M_2}{10L} & \frac{M_1}{10} & 0 & \frac{M_1}{10L}-\frac{11M_2}{10L} & \frac{M_1}{5}-\frac{9M_2}{10} \\
0 & 0 & \frac{M_1}{5}-\frac{M_2}{10} & -\frac{M_2L}{30} & 0 & \frac{M_1}{5}-\frac{9M_2}{10} & -\frac{M_1L}{30}+\frac{M_2L}{10} \\
-\frac{11M_1}{10L}+\frac{M_2}{10L} & -\frac{M_1}{10}-\frac{M_2}{5} & 0 & 0 & \frac{M_1}{10L}-\frac{11M_2}{10L} & 0 & 0 \\
-\frac{M_2}{10} & \frac{M_1L}{30} & 0 & 0 & \frac{M_2}{10} & 0 & 0
\end{bmatrix}
$$

4. Parametric study for proposed design equations

4.1 Objectives

The present chapter complements the study in Chapter 3 by identifying the key parameters affecting the moment fraction attainable based on the displacement and stress criteria proposed in the previous chapter. The influential dimensionless parameters are first extracted from the closed form solution for an initially crooked beam under uniform moments. Next, the parameters identified are extended to investigate other loading cases.

4.2 Considered beams for the parametric study

A total of 21 cross-sections (Table 4.1) among common W150 to W310 sections in Part 6 of Handbook of Steel Construction 2016 are selected for the parametric study. The dimensions and section properties based on the idealized sections are provided in Table 4.1. In the calculation of section properties rounded fillets were omitted to compare the results of the present model to that of shell solution which does not model fillets. All spans were selected to lie within the range $L_{\min} \le L \le L_{\max}$, where the lower limit $L_{\min}$ by equating the equation for the elastic LTB to $0.67M_p$ (Eq. (4.1)) for class 1 and 2 sections which is based at the border of the elastic LTB buckling failure and inelastic LTB in the Canadian design standard (CAN/CSA S16-14) for beams under uniform bending moment (i.e. $C_{CAN} = 1$). For class 3 section, the plastic moment M_p in Eq. (4.1) shall be replaced by the yield moment M_Y.

$$L_{\min} = \frac{\pi\sqrt{2EI_yEC_w}}{-EI_yGJ + \sqrt{\left(EI_yGJ\right)^2 + 4E^2I_yC_w\left(0.67M_p\right)^2}} \tag{4.1}$$

The upper limit $L_{\max}$ is taken as the lesser of $2L_{\min}$ and 12m given that beams longer than 12m would require splicing and would thus normally avoided by designers.

Table 4.1 Dimensions and section properties for the considered cross-sections in the parametric study

	Section	d	b	t	w	span	A	Ix	Iy	J	Cw
		(mm)				(m)	mm^2 x10^3	mm^4 x10^6	mm^4 x10^6	mm^4 x10^4	mm^4 x10^9
1	W150x24	160	102	10.3	6.6	5.37	30.6	13.4	1.8	9.3	10.2
2	W200x42	205	166	11.8	7.2	8.74	53.1	40.9	9.0	22.2	84.0
3	W200x36	201	165	10.2	6.2	8.68	45.7	34.4	7.6	14.5	69.6
4	W150x18	153	102	7.1	5.8	5.37	22.9	9.2	1.3	3.7	6.7
5	W200x31	210	134	10.2	6.4	7.05	40.0	31.4	4.1	11.9	40.9
6	W250x45	266	148	13.0	7.6	7.79	57.2	71.1	7.0	26.1	113.0
7	W250x39	262	147	11.2	6.6	7.74	49.2	60.1	5.9	16.9	93.4
8	W200x27	207	133	8.4	5.8	7.00	33.9	25.8	3.3	7.1	32.5
9	W200x22	206	102	8.0	6.2	5.37	28.6	20.0	1.4	5.7	13.9
10	W150x14	150	100	5.5	4.3	5.26	17.3	6.9	0.9	1.7	4.8
11	W250x28	260	102	10.0	6.4	5.37	36.3	40.0	1.8	9.7	27.7
12	W150x13	148	100	4.9	4.3	5.26	16.1	6.1	0.8	1.4	4.2
13	W250x33	258	146	9.1	6.1	7.68	41.7	48.9	4.7	9.9	73.2
14	W310x45	313	166	11.2	6.6	8.74	56.9	99.2	8.6	19.1	195.0
15	W200x19	203	102	6.5	5.8	5.37	24.8	16.6	1.2	3.6	11.1
16	W200x21	203	133	6.4	5	7.00	27.0	19.8	2.5	3.6	24.3
17	W250x25	257	102	8.4	6.1	5.37	32.3	34.2	1.5	6.5	23.0
18	W310x33	313	102	10.8	6.6	5.37	41.8	65.0	1.9	12.2	43.8
19	W310x39	310	165	9.7	5.8	8.68	49.4	85.1	7.3	12.6	164.0
20	W250x24	253	145	6.4	5	7.63	31.1	34.7	3.3	4.0	49.5
21	W310x31	306	164	7.4	5	8.63	39.3	65.4	5.4	6.1	121.0

4.3 Moment ratios based on threshold displacement criterion

4.3.1 Formulation

Chapter 3 formulated expressions for the additional lateral displacement $u(z)$ and the angle of twist $\theta(z)$ for a beam under uniform moments M with a general initial out-of-straightness pattern of the form

$$\left\langle u_0(z) \quad \theta_0(z) \right\rangle^T = \sum_{m=1}^{n} \phi_m \left\langle 1 \quad \left(\frac{\pi^2 E I_y}{M_{crm} L^2} \right) \right\rangle \sin \frac{m\pi z}{L} \tag{4.2}$$

in which $M_{crm} = \lambda_m M = m\pi/L\sqrt{EI_y GJ + \left(m\pi E/L\right)^2 C_w I_y}$ is the critical moment corresponding to buckling mode m . The corresponding response as characterized by the additional displacements $u(z)$ and $\theta(z)$ was found to take the form

$$u(z) = \frac{M}{EI_y}\sum_{m=1}^{n}\phi_m \frac{EI_y M + \left(\frac{\pi^2 EI_y}{M_{crm}L^2}\right)EI_y EC_w\left(\frac{m\pi}{L}\right)^2 + \left(\frac{\pi^2 EI_y}{M_{crm}L^2}\right)EI_y GJ}{EC_w EI_y\left(\frac{m\pi}{L}\right)^4 + EI_y GJ\left(\frac{m\pi}{L}\right)^2 - M^2}\sin\left(\frac{m\pi z}{L}\right) \tag{4.3}$$

$$\theta(z) = \sum_{m=1}^{n}\phi_m \frac{\frac{M^2}{EI_y}\left(\frac{\pi^2 EI_y}{M_{crm}L^2}\right) + M\left(\frac{m\pi}{L}\right)^2}{EC_w\left(\frac{m\pi}{L}\right)^4 + GJ\left(\frac{m\pi}{L}\right)^2 - \frac{M^2}{EI_y}}\sin\left(\frac{m\pi z}{L}\right) \tag{4.4}$$

Consider the special case where the initial imperfections follow the first mode. By setting $\phi_1 \neq 0$ and $\phi_2 = \phi_3 = ...\phi_i.. = 0$ in (4.2) and setting $z = L/2$ to recover the peak lateral IOS $u_{0-c}(L/2)$ at the compression flange located at a height $d/2$, one obtains

$$u_{0-c}(L/2) = u_0(L/2) + (d/2)\theta_0(L/2) = \phi_1\left(1 + (d/2)\frac{\pi^2 EI_y}{M_{cr}L^2}\right) \tag{4.5}$$

in which $M_{cr} = M_{cr1} = (\pi/L)\sqrt{EI_y GJ + \left(\pi E/L\right)^2 C_w I_y}$. If the peak lateral IOS is not to exceed a threshold value L/γ_i , the amplitude ϕ_1 associated with the an initial imperfection following the first buckling mode is obtained by equating $u_{0-c}(L/2)$ to L/γ, yielding

$$\phi_1 = \frac{L}{\gamma_i\left(1 + (d/2)\frac{\pi^2 EI_y}{M_{cr}L^2}\right)} \tag{4.6}$$

Under applied moments M , the corresponding additional peak lateral displacement $u_c(L/2)$ takes place also in the compression flange of the mid-span section and is obtained from (4.3) and (4.4) as

$$u_c\left(L/2\right)=u\left(L/2\right)+\left(d/2\right)\theta\left(L/2\right)=\phi_1\frac{M}{M_{cr}-M}\left(1+\frac{d}{2}\frac{\pi^2 EI_y}{M_{cr}L^2}\right) \tag{4.7}$$

From Eq. (4.6) by substituting into Eq. (4.7), one obtains

$$u_c\left(L/2\right)=\frac{L\left(M/M_{cr}\right)}{\gamma_i\left(1-M/M_{cr}\right)} \tag{4.8}$$

By adding the initial out-of-straightness $u_{0-c}=L/\gamma_i$ to both sides of Eq. (4.8), the total lateral out-of-straightness at mid-span section $u_{ct}\left(L/2\right)$ of the compression flange is obtained as

$$\bar{u}_c\left(L/2\right)=u_c\left(L/2\right)+u_{0-c}\left(L/2\right)=\frac{L}{\gamma_i}\left[\frac{1}{1-M/M_{cr}}\right] \tag{4.9}$$

Solving Eq. (4.9) for M/M_{cr} one obtains $M/M_{cr}=1-\left[L/\bar{u}_c\left(L/2\right)\gamma_i\right]$. If the total lateral out-of-straightness $\bar{u}_c\left(L/2\right)$ is not to exceed the specified threshold value $\bar{u}_c\left(L/2\right)=L/\gamma+L/\gamma_i$, the magnitude of the corresponding moment M_{γ,γ_i} is given by

$$\frac{M_{\gamma,\gamma_i}}{M_{cr}}=1-\frac{\gamma}{\gamma+\gamma_i} \tag{4.10}$$

In the absence of other information, typical threshold values for initial out-of-straightness γ_i can be taken consistent with allowable camber and sweep limits for beams provided in Part 6 of the Handbook of Steel Construction (2016) and plumbness limits for column as provided in Clause 29.3.3 of CAN-CSA-S16 (2014) and could be in the order of $\gamma_i=1000,\ 1500,\ \ldots$ etc. Also, in the absence of additional application-specific information for beams, typical threshold values of γ could be in the range 180-360 in a manner consistent with displacement thresholds specified in informative Appendix D of CSA/CAN S16-14.

The moment ratios $M_{\gamma,\gamma_i}/M_{cr}$ as computed from Eq. (4.10) are provided in Table 4.2. For comparison, the critical moments $M_{cr}\left(FEA\right)$ were obtained based on the present eigenvalue analysis to characterize the critical moment for the hypothetical case of a perfectly straight beam.

Also, the moment $M\left(FEA\right)$ corresponding to the threshold $\bar{u}_c\left(L/2\right)=L/\gamma+L/\gamma_i$ is obtained based on the finite element formulation developed in Chapter 3. Threshold initial out-of-straightness values of $\gamma_i=1000$, 1500, 2000 are taken and a threshold for the additional displacement of $\gamma=180$ is assumed. The results in Table 4.2 show that both approaches lead to essentially identical results. A plot of the results is provided in Figure 4.1where the moment M_{γ,γ_i} (as obtained from the present FEM) corresponding to a peak additional lateral displacement at the compression flange $u_c=L/180$ is normalized by the critical moment M_{cr} for a perfectly straight beam is plotted against the ratio of the yield moment to the critical moment ratio M_Y/M_{cr} which can be regarded as a measure of beam slenderness (for a given section M_Y/M_{cr} increases as the span increases). In a manner consistent with the predictions of Eq. (4.10), the moment resistance ratio $M_{\gamma,\gamma_i}/M_{cr}$ is found to be independent of the beam slenderness and solely dependent upon the IOS magnitude selected. For a selected threshold lateral displacement $\gamma=180$, the ratios $M_{\gamma,\gamma_i}/M_{cr}$ are found to decease as the initial out of straightness increase (i.e., as γ_i increases).

Table 4.2 Moment resistance ratios between the present finite element solution and the prediction of Eq. (4.10)

Section	Span	Critical moment based on FEA (kNm)	Critical moment based on CSA (kNm)	Displacement based moment resistance fraction (FEM)			Moment resistance fraction based on Eq. (4.10)			Percentage difference		
	(m)	(kNm)	(kNm)	L/1000	L/1500	L/2000	L/1000	L/1500	L/2000	L/1000	L/1500	L/2000
W150x24	5.37	31.4	31.4	0.847	0.898	0.924	0.848	0.893	0.917	0.12%	0.56%	0.76%
W200x42	8.74	66.9	67.0	0.847	0.898	0.924	0.848	0.893	0.917	0.12%	0.56%	0.76%
W200x36	8.68	51.0	51.0	0.847	0.898	0.923	0.848	0.893	0.917	0.12%	0.56%	0.65%
W150x18	5.37	17.0	17.0	0.847	0.898	0.924	0.848	0.893	0.917	0.12%	0.56%	0.76%
W200x31	7.05	41.9	41.9	0.847	0.898	0.924	0.848	0.893	0.917	0.12%	0.56%	0.76%
W250x45	7.79	73.7	73.7	0.847	0.898	0.924	0.848	0.893	0.917	0.12%	0.56%	0.76%
W250x39	7.74	56.1	56.1	0.847	0.899	0.924	0.848	0.893	0.917	0.12%	0.67%	0.76%
W200x27	7.00	30.1	30.1	0.847	0.898	0.924	0.848	0.893	0.917	0.12%	0.56%	0.76%
W200x22	5.37	22.7	22.7	0.847	0.898	0.924	0.848	0.893	0.917	0.12%	0.56%	0.76%
W150x14	5.26	10.4	10.4	0.848	0.898	0.923	0.848	0.893	0.917	0.00%	0.56%	0.65%
W250x28	5.37	33.7	33.7	0.847	0.898	0.924	0.848	0.893	0.917	0.12%	0.56%	0.76%
W150x13	5.26	8.9	8.9	0.847	0.898	0.924	0.848	0.893	0.917	0.12%	0.56%	0.76%
W250x33	7.68	39.9	39.8	0.847	0.898	0.924	0.848	0.893	0.917	0.12%	0.56%	0.76%
W310x45	8.74	66.1	66.1	0.847	0.898	0.924	0.848	0.893	0.917	0.12%	0.56%	0.76%
W200x19	5.37	16.7	16.7	0.847	0.898	0.923	0.848	0.893	0.917	0.12%	0.56%	0.65%
W200x21	7.00	19.4	19.4	0.849	0.898	0.923	0.848	0.893	0.917	0.12%	0.56%	0.65%
W250x25	5.37	33.7	25.9	0.846	0.899	0.924	0.848	0.893	0.917	0.24%	0.67%	0.76%
W310x33	5.37	40.4	40.4	0.847	0.898	0.923	0.848	0.893	0.917	0.12%	0.56%	0.65%
W310x39	8.68	51.6	51.6	0.847	0.898	0.924	0.848	0.893	0.917	0.12%	0.56%	0.76%
W250x24	7.63	22.9	22.9	0.846	0.898	0.923	0.848	0.893	0.917	0.24%	0.56%	0.65%
W310x31	8.63	33.8	33.8	0.847	0.898	0.924	0.848	0.893	0.917	0.12%	0.56%	0.76%

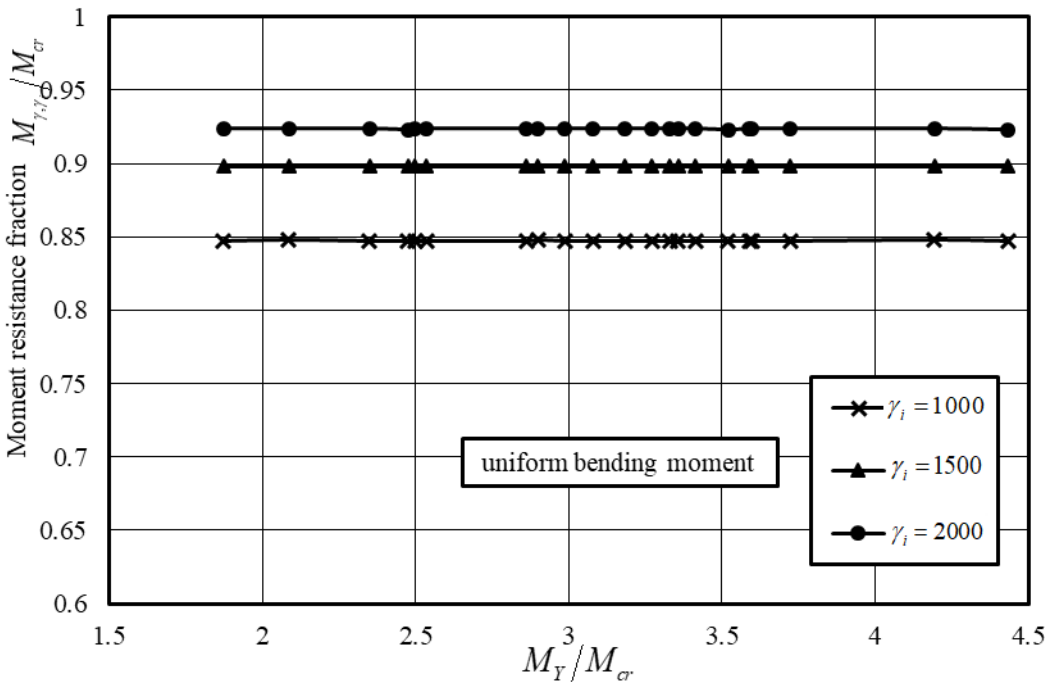

Figure 4.1 Moment resistance ratio based on displacement criterion for 21 common cross-sections under uniform bending moment

4.3.2 Extension of the approach to other loading cases

While the FEM findings of the past section were evident given the closed form expression in Eq. (4.10), it is not possible to obtain a similar closed form solutions of cases of non-uniform moments. Thus, the present section aims at investigating whether similar findings can numerically be obtained for other loading conditions. Two cases are considered; uniformly distributed loading and mid-span point loading. As depicted in Figure 4.2 a, b, it turns out that the moment resistance ratio $M_{\gamma,\gamma_i} / M_{cr}$ obtained is also (1) independent of the slenderness $M_{\gamma,\gamma_i} / M_{cr}$, (2) solely dependent on the initial out of straightness γ_i , and (3) its value can be accurately predicted by Eq. 4.10. It is emphasized that while Eq. (4.10) was developed for the case of uniform moments, the FEA results suggest that it remains equally valid for uniformly distributed and mid-span point loading.

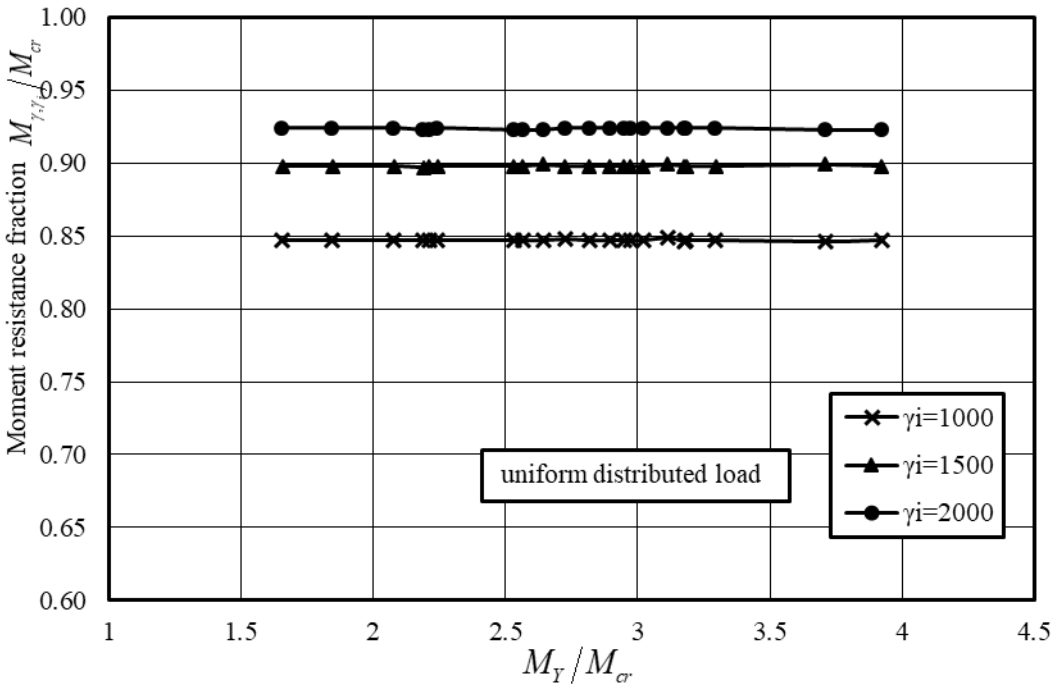

(a)

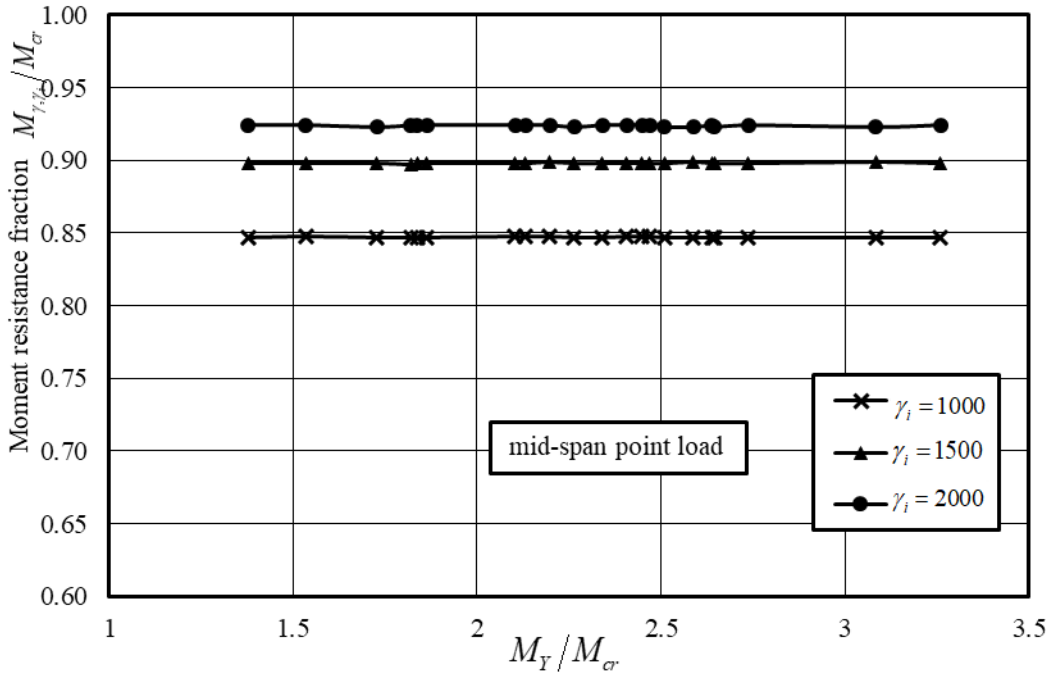

(b)

Figure 4.2 Moment resistance ratio based on displacement criterion for considered sections under (a) uniform distributed load and (b) point load at mid-span with three scenarios for out-of-straightness

4.3.3 Effect of span

To investigate the effect of the span on the moment resistance ratio attained based on the displacement criterion, a beam is considered with a W200X36 cross-section under uniform bending moment with spans varying from 6 to 10m which correspond to $L/b = 36.4$ to $L/b = 60.6$ (Figure 4.3). As in previous sections, three initial out-of-straightness scenarios are considered $\gamma_i = 1000,\ 1500,\ 2000$. For a given out-of-straightness, the moment resistance ratio is found to be independent of the slenderness L/b.

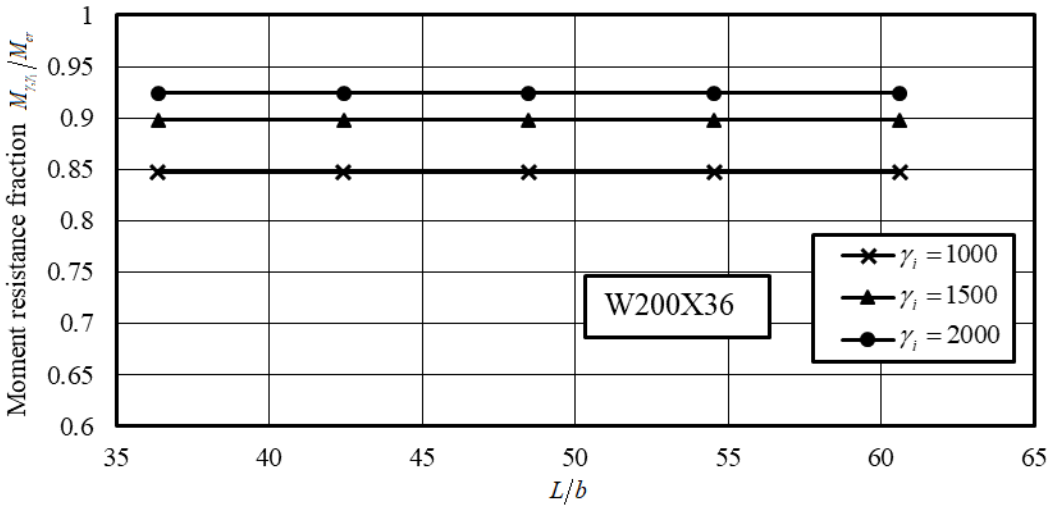

Figure 4.3 moment resistance ratio for W200X36 cross-section with varying spans

4.3.4 Nominal moment resistance based on displacement criterion

In the previous section, it was observed that the only parameter influencing the moment resistance ratio $M_{\gamma,\gamma_i} / M_{cr}$ is the ratio of the initial out-of-straightness coefficient and the displacement target value γ_i/γ. When the displacement target value is set to $L/180$, the moment resistance ratios are always found to be 0.847, 0.898 and 0.924 for $\gamma_i = L/1000, L/1500$ and $L/2000$ for examined beams, respectively. Thus, if the effect of out-of-straightness is to be incorporated into the solution, an out-of-straightness reduction factor can be applied to the critical moment M_{cr}. The value of the reduction factor is 0.847, 0.898 and 0.924 for $\gamma_i = L/1000, L/1500$ and $L/2000$ respectively. For example, the nominal design moment M_n accounting for initial out of straightness is given by

$M_n = 0.847M_{cr}$ when $\gamma_i = L/1000$. The reduction factor is applicable for uniform moments, uniformly distributed loading, or mid-pan point loading.

Figure 4.4 (a) depicts the nominal moment normalized with respect to the plastic moment versus the span (presented using the dimensionless slenderness M_Y/M_{cr}) for beam with a W150X14 cross-section for three out-of-straightness scenarios ($\gamma_i = 1000, 1500, 2000$) in addition to the case of zero out-of-straightness $\gamma_i = \infty$ as extracted from the eigen-solution. The results indicate that the nominal resistance ranges from 84.7% of the critical moment for $\gamma_i = 2000$ to 92.4% for $\gamma_i = 1000$.

Strictly speaking, the above findings are limited to the elastic range of the response as no attempts were made to model the effect of plasticity nor to account for residual stresses. One recalls that for a perfectly straight beam of a Class 1 or 2 cross-section, CAN-CSA-S16 (2014) stipulates that when $M_{cr} < 0.67M_p$, the nominal resistance is governed by the inelastic lateral torsional buckling resistance as given by $M_n = 1.15M_p\left[1 - 0.28M_p/M_{cr}\right]$ where the elastic critical moment expressions for M_{cr} as provided in the present standard do not account for initial-out-of-straightness effects. The present study provides a basis to account for such effects by simply replacing M_{cr} by M_{γ,γ_1} so that $M_{\gamma,\gamma_1} < 0.67M_p$, the nominal resistance would be governed by inelastic lateral torsional buckling as given by the modified equation $M_{n\gamma,\gamma_i} = 1.15M_p\left[1 - 0.28M_p/M_{\gamma,\gamma_i}\right]$. It is clear that the proposed equation reverts to the present standard equation for the case of no initial out-of-straightness $\gamma \to \infty$ where $M_{\gamma,\gamma_i} \to M_{cr}$. The resulting plots are presented in Fig. 4.4b for the case γ_i . The validity of proposed modified equation would have to be verified by conducting a finite element analysis that incorporates such effects and is outside the scope of the present study.

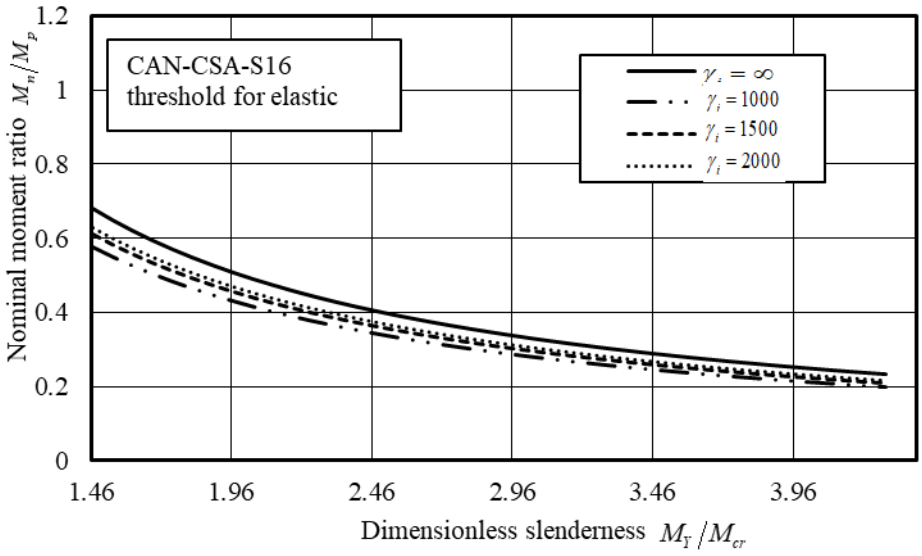

(a)

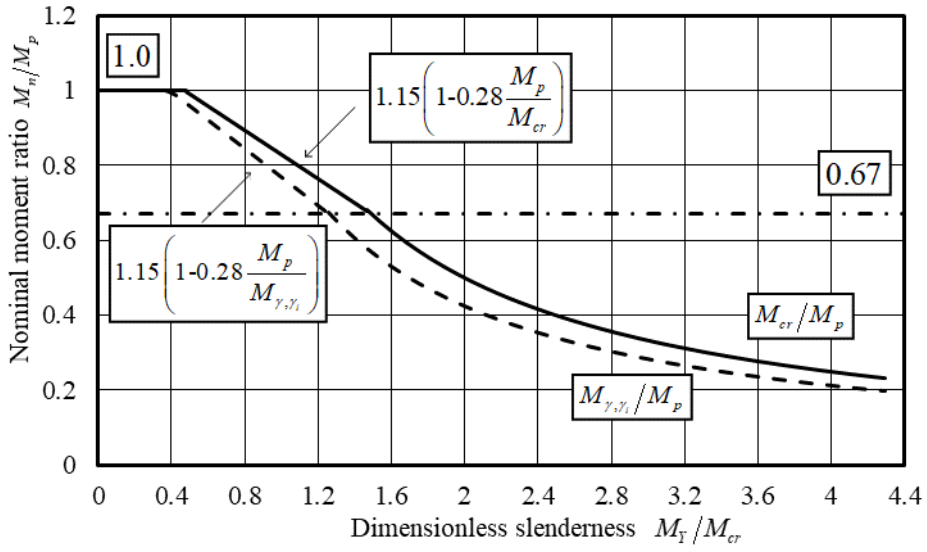

(b)

Figure 4.4 Normalized nominal moment resistance for W150x14 section ($\gamma = L/180$) (a) Elastic range for various out-of-straightness values ($\gamma_i = 1000, 1500, 2000, \infty$) and (b) total range for the case $\gamma_i = 1000$

4.4 Moment ratio based on the threshold stress criterion

4.4.1 Formulation

For a wide flange beam subjected to biaxial bending and warping, the normal stresses $\sigma(x, y, z, \omega)$ at a point with coordinates (x, y, ω) of a section z is given by

$$\sigma(x,y,z,\omega)=\frac{M_x(z)}{I_x}y+\frac{M_y(z)}{I_y}x+\frac{B(z)}{C_w}\omega \tag{4.11}$$

The peak stresses $\sigma_{\max}(z)$ take place at the corner points of the section where the point coordinates have maximal values, i.e., $(x,y,\omega)=(x_{\max},y_{\max},\omega_{\max})=[b/2,d/2,bd/4]$. By defining the section moduli $S_x=I_x/y_{\max}$, $S_y=I_y/x_{\max}$, and $S_w=C_w/\omega_{\max}$, one has

$$\sigma_{\max}(z)=\frac{M_x(z)}{S_x}+\frac{M_y(z)}{S_y}+\frac{B(z)}{S_w} \tag{4.12}$$

Noting that $M_y(z)=-EIu''(z)$ and $B(z)=-EC_w\theta''$, the magnitude of maximum stress in the section is can be expressed as

$$\sigma_{\max}(z)=\frac{M(z)}{S_x}+\frac{EI_y\left|u(z)''\right|}{S_y}+\frac{EC_\omega\left|\theta(z)''\right|}{S_w} \tag{4.13}$$

From Eqs. (4.3) and (4.4), by differentiating $u(z)$ and $\theta(z)$, and substituting into (4.13) one obtains

$$\begin{aligned}\sigma_{\max}(z)&=\frac{M}{S_x}+E\phi_1\left(|x_{\max}|\left(\frac{\pi}{L}\right)^2\frac{M}{M_{cr}-M}\sin\left(\frac{\pi z}{L}\right)+|\omega_{\max}|\left(\frac{\pi}{L}\right)^2\left(\frac{\pi^2EI_y}{M_{cr}L^2}\right)\frac{M}{M_{cr}-M}\sin\left(\frac{\pi z}{L}\right)\right)\\&=\frac{M}{S_x}+\frac{M}{M_{cr}-M}E\phi_1\left(\frac{\pi}{L}\right)^2\left[\frac{b}{2}+\frac{bd}{4}\left(\frac{\pi^2EI_y}{M_{cr}L^2}\right)\right]\sin\left(\frac{\pi z}{L}\right)\end{aligned} \tag{4.14}$$

The peak normal stress takes place at mid-span where $z=L/2$ and is given by

$$\sigma_{\max}=\sigma_{\max}(L/2)=\frac{M}{S_x}+\frac{M}{M_{cr}-M}E\phi_1\left(\frac{\pi}{L}\right)^2\left[\frac{b}{2}+\frac{bd}{4}\left(\frac{\pi^2EI_y}{M_{cr}L^2}\right)\right] \tag{4.15}$$

From Eq. (4.15), by substituting into Eq. (4.5), one obtains

$$\sigma_{\max}(L/2)=\frac{M}{S_x}+\left(\frac{M}{M_{cr}-M}\right)\frac{\pi^2Eb}{2\gamma_iL} \tag{4.16}$$

The peak stress is set to a specified threshold fraction ε of the yield stress, i.e., $\sigma = \varepsilon F_y$. Typically, design standards assume the residual stresses around $0.3F_y - 0.33F_y$. Thus, the condition $\sigma_{\max} < 0.7F_y$ or $\sigma_{\max} < 0.67F_y$ must be satisfied for the material to remain in the elastic range and the typical values for the threshold stress fraction are $\varepsilon = 0.67, 0.7$. By equating $\sigma_{\max}(L/2)$ as obtained from (4.16) to the threshold value εF_y , one obtains

$$\varepsilon F_y = \frac{M}{S_x} + \left(\frac{M}{M_{cr} - M} \right) \frac{\pi^2 Eb}{2\gamma_i L} \tag{4.17}$$

Rearranging, one has

$$M^2 - \left(M_{cr} + \frac{\pi^2 EbS_x}{2\gamma_i L} + \varepsilon F_y S_x \right) M + \varepsilon F_y S_x M_{cr} = 0 \tag{4.18}$$

Solving Eq. (4.18) for the moment M , one obtains

$$M = \frac{1}{2}\left(M_{cr} + \frac{\pi^2 EbS_x}{2\gamma_i L} + \varepsilon F_y S_x \right) \pm \frac{1}{2}\sqrt{\left(M_{cr} + \frac{\pi^2 EbS_x}{2\gamma_i L} + \varepsilon F_y S_x \right)^2 - 4\varepsilon S_x F_y M_{cr}} \tag{4.19}$$

Dividing both sides by M_{cr} one recovers the moment ratio $M_{\gamma,\varepsilon}/M_{cr}$ attainable based on the threshold stress εF_y

$$\frac{M_{\gamma_i,\varepsilon}}{M_{cr}} = \frac{1}{2}\left(1 + \frac{\pi^2}{2\gamma_i}\left(\frac{Eb}{F_y L} \right)\left(\frac{M_Y}{M_{cr}} \right) + \varepsilon \frac{M_Y}{M_{cr}} \right) \pm \frac{1}{2}\sqrt{\left(1 + \frac{\pi^2}{2\gamma_i}\left(\frac{Eb}{F_y L} \right)\left(\frac{M_Y}{M_{cr}} \right) + \varepsilon \frac{M_Y}{M_{cr}} \right)^2 - 4\varepsilon \frac{M_Y}{M_{cr}}} \tag{4.20}$$

Equation 1.16 indicates that the moment ratio attainable depends on the four dimensionless parameters γ_i , ε , $Eb/F_y L$ and M_Y/M_{cr} where one recalls that $M_Y = S_x F_y$, $M_{cr} = \pi/L\sqrt{EI_y GJ + (\pi E/L)^2 C_w I_y}$ and ratio M_Y/M_{cr} will be adopted in subsequent sections to provide a dimensionless measure of the section slenderness.

4.4.2 Comparison and Verification

The comparison for the moment ratios $M_{\gamma_i,\varepsilon}/M_{cr}$ as predicted by Eq. (4.20) and those based on the present FEM (Table 4.3) are found to be nearly identical, with a maximum difference of 0.7%. Equation (4.20) indicates that the moment ratio $M_{\gamma_i,\varepsilon}/M_{cr}$ depends on seven parameters $\gamma_i, \varepsilon, M_Y/M_{cr}, L/d, d/b, b/t, d/w$. In the following sections, the effects of each of the seven parameters are assessed by varying each parameter at a time while keeping the other six constants. An idealized (i.e., with no fillets) W200x36 with ($d/b, b/t, d/w$=1.22, 16.18, 32.4) cross-section with a stress fraction $\varepsilon = 0.70$ and an out-of-straightness coefficient $\gamma_i = 1000$ is used as a reference case when assessing the geometric dimensionless parameters $d/b, b/t, d/w$.

Table 4.3 Percentage difference in predicted moment resistance ratio based on FEA critical moment and CSA critical moment approach for Beams under uniform bending moment ($Eb/F_yL = 11.54$, $\varepsilon = 0.70$ and $\omega_2 = 1.0$)

Section	Span	Critical moment based on FEA (kNm)	Critical moment based on CSA (kNm)	Yield to critical moment ratio based on FEA	FEA moment (kNm) for imperfection			Moment resistance fraction*			Moment resistance fraction based on Mcr-CSA** (ω2=1.00)			Percentage difference***		
	(m)	(kNm)	(kNm)	M_Y/M_{cr}	L/1000	L/1500	L/2000	L/1000	L/1500	L/2000	L/1000	L/1500	L/2000	L/1000	L/1500	L/2000
W150x24	5.37	31.4	31.4	1.9	26.0	27.3	28.0	0.828	0.869	0.893	0.829	0.869	0.893	0.0%	0.1%	0.1%
W200x42	8.74	66.9	67.0	2.1	56.7	59.3	60.8	0.847	0.886	0.909	0.846	0.886	0.908	-0.1%	-0.1%	0.0%
W200x36	8.68	51.0	51.0	2.3	44.0	45.9	47.0	0.863	0.900	0.921	0.862	0.899	0.920	-0.2%	-0.1%	-0.1%
W150x18	5.37	17.0	17.0	2.5	14.7	15.3	15.7	0.868	0.904	0.925	0.867	0.904	0.924	-0.1%	0.0%	0.0%
W200x31	7.05	41.9	41.9	2.5	36.4	37.9	38.8	0.869	0.905	0.925	0.868	0.904	0.925	-0.1%	-0.1%	0.0%
W250x45	7.79	73.7	73.7	2.5	64.2	66.8	68.3	0.870	0.906	0.926	0.870	0.906	0.926	-0.1%	0.0%	0.0%
W250x39	7.74	56.1	56.1	2.9	49.4	51.3	52.4	0.881	0.915	0.934	0.880	0.914	0.933	-0.1%	0.0%	0.0%
W200x27	7.00	30.1	30.1	2.9	26.5	27.5	28.1	0.882	0.916	0.935	0.881	0.915	0.934	-0.2%	-0.1%	-0.1%
W200x22	5.37	22.7	22.7	3.0	20.1	20.8	21.3	0.884	0.917	0.936	0.883	0.917	0.935	0.0%	0.0%	0.0%
W150x14	5.26	10.4	10.4	3.1	9.2	9.6	9.8	0.886	0.919	0.937	0.885	0.918	0.937	-0.1%	-0.1%	-0.1%
W250x28	5.37	33.7	33.7	3.2	30.0	31.1	31.7	0.888	0.920	0.938	0.887	0.920	0.938	0.0%	0.0%	0.0%
W150x13	5.26	8.9	8.9	3.3	7.9	8.2	8.3	0.890	0.922	0.940	0.889	0.921	0.939	-0.1%	-0.1%	-0.1%
W250x33	7.68	39.9	39.8	3.3	35.5	36.8	37.5	0.891	0.923	0.940	0.890	0.922	0.940	-0.1%	-0.1%	0.0%
W310x45	8.74	66.1	66.1	3.4	58.9	61.0	62.1	0.891	0.923	0.940	0.890	0.923	0.940	-0.1%	-0.1%	0.0%
W200x19	5.37	16.7	16.7	3.4	14.9	15.4	15.7	0.892	0.924	0.941	0.891	0.923	0.941	-0.1%	0.0%	0.0%
W200x21	7.00	19.4	19.4	3.5	17.3	17.9	18.3	0.894	0.925	0.942	0.893	0.924	0.942	-0.1%	-0.1%	-0.1%
W250x25	5.37	33.7	25.9	3.6	29.9	31.1	31.7	0.887	0.920	0.938	0.894	0.925	0.942	0.7%	0.5%	0.5%
W310x33	5.37	40.4	40.4	3.6	36.1	37.4	38.0	0.894	0.926	0.943	0.894	0.925	0.942	0.0%	0.0%	0.0%
W310x39	8.68	51.6	51.6	3.7	46.3	47.9	48.7	0.896	0.927	0.944	0.896	0.927	0.943	-0.1%	0.0%	0.0%
W250x24	7.63	22.9	22.9	4.2	20.6	21.3	21.7	0.901	0.931	0.947	0.901	0.930	0.946	-0.1%	-0.1%	0.0%
W310x31	8.63	33.8	33.8	4.4	30.5	31.5	32.1	0.903	0.932	0.948	0.903	0.932	0.948	-0.1%	0.0%	0.0%
												Min		-0.2%	-0.1%	-0.1%
												Max		0.7%	0.5%	0.5%
												Mean		0.0%	0.0%	0.0%
												Stan Deviation		0.0018	0.00133	0.00112

4.4.3 Effect of slenderness

The ratio $M_{\gamma_i,\varepsilon}/M_{cr}$ for the sections in Table 4.1 is determined based on solution (Eq. 4.20) for a yield stress fraction of $\varepsilon = 0.70$. Three scenarios are considered for the out-of-straightness coefficient; $\gamma_i = 1000, 1500, 2000$. Figure 4.5 (a) shows that an increase in the slenderness M_Y/M_{cr} corresponds to an increase in the moment resistance ratio $M_{\gamma_i,\varepsilon}/M_{cr}$. For example, when $\gamma_i = 1000$, a beam with a slenderness $M_Y/M_{cr} = 4.06$ attains a moment resistance ratio of 0.894 and when M_Y/M_{cr} reduces to 1.75, the moment resistance ratio drops to 0.808. Also shown is a beam with a relatively low IOS (e.g., $\gamma_i = 2000$) is able to attain a relatively high moment resistance ratio compared to a beam with higher IOS (e.g., $\gamma_i = 1000$). For example, for a slenderness $M_Y/M_{cr} = 2.36$, the moment resistance ratio attained is 0.916 when $\gamma_i = 2000$ but drops to 0.856 when $\gamma_i = 1000$.

The sections are reconsidered under three specified yield stress fraction scenarios $\varepsilon = 0.67, 0.70$ and 0.75, while maintaining constant the out-of-straightness coefficient $\gamma_i = 1000$. Figure 4.5 b shows that, for a given slenderness M_Y/M_{cr}, an increase in the specified yield stress fraction ε is associated with an increase the moment resistance ratio $M_{\gamma_i,\varepsilon}/M_{cr}$. For instance, when $M_Y/M_{cr} = 2.78$, the moment resistance ratio is 0.863 at $\varepsilon = 0.67$ and increases to 0.872 at $\varepsilon = 0.70$ and further increases to 0.884 when $\varepsilon = 0.75$. The difference between the attained moment resistance ratios based on different specified yield stress fractions ε is small for low slenderness values and becomes negligible for larger slenderness. For example, when the slenderness is $M_Y/M_{cr} = 1.75$, the difference in moment resistance ratios corresponding to $\varepsilon = 0.67$ and $\varepsilon = 0.75$ is 0.037 and drops to 0.009 when the slenderness increases to $M_Y/M_{cr} = 4.06$.

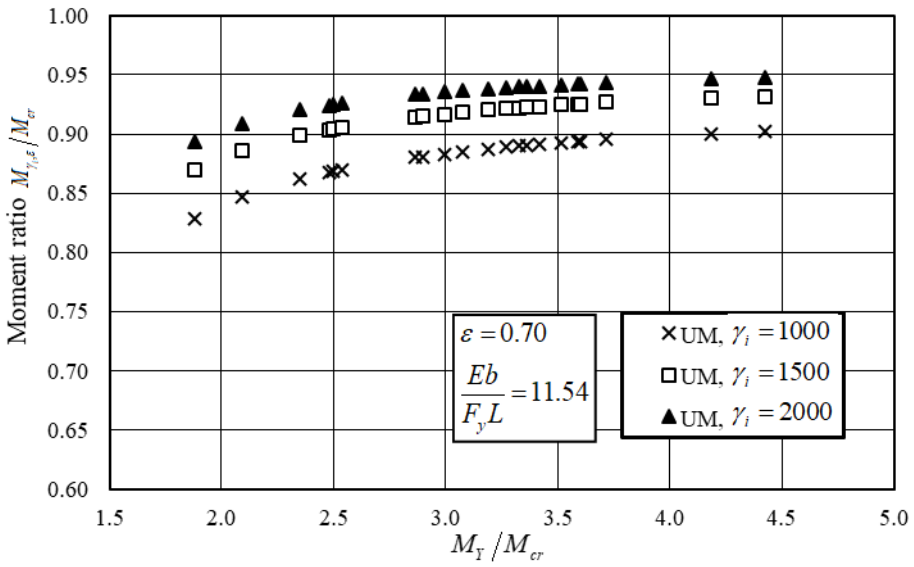

(a)

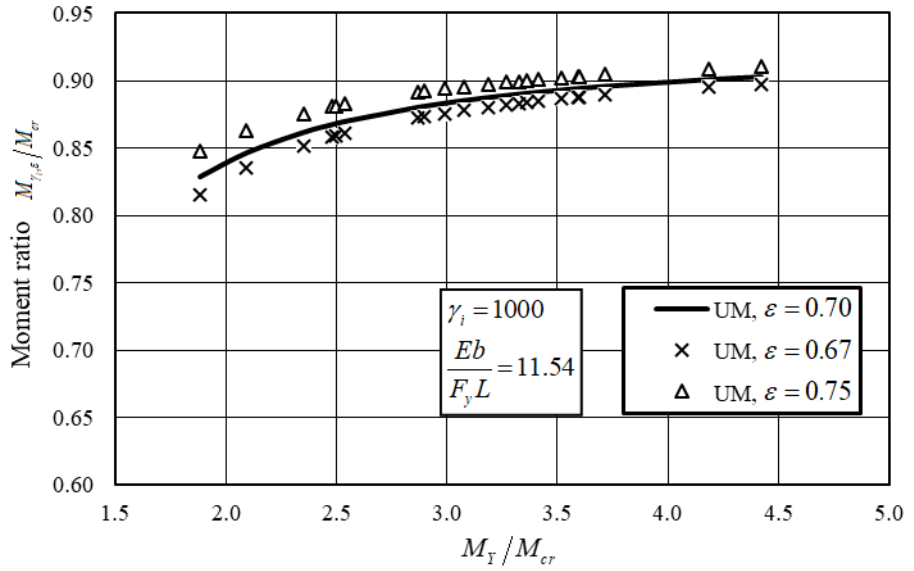

(b)

Figure 4.5 Effect of yield to buckling moment ratio M_Y/M_{cr} on the moment resistance ratio for (a) various out-of-straightness coefficient γ_i and (b) various yield stress fractions ε

4.4.4 Effect of initial out-of-straightness and yield stress fraction

To assess the effect of out-of-straightness coefficient γ_i and yield stress fraction ε on the moment resistance ratio $M_{\gamma_i,\varepsilon}/M_{cr}$, two sets of analyses are conducted on a beam with W200X36 cross-

section. In the first series, the yield stress fraction is kept constant at $\varepsilon = 0.7$ while the initial out-of-straightness coefficient γ_i is varied from 1000 to 2000 (Figure 4.6 a). In the second series, the out-of-straightness coefficient is kept constant at $\gamma_i = 1000$ while the yield stress fraction ε is varied from 0.67 to 1.0 (Figure 4.6 b).

In both series, the beam slenderness L/b is varied and the moment resistance ratio $M_{\gamma_i,\varepsilon}/M_{cr}$ is predicted in Eq. (4.20). Figure 4.6 a, b shows that the moment resistance ratio increases with slenderness. For example, for the case $\gamma_i = 1000$, $\varepsilon = 0.70$, when $L/b = 33.3$ the moment resistance ratio attained is 0.691. When the slenderness increases to $L/b = 66.7$, the moment resistance ratio $M_{\gamma_i,\varepsilon}/M_{cr}$ is found to increase to 0.905. Figure 4.6 (a) shows that a large out-of-straightness coefficient γ corresponds to a low IOS, which corresponds to a comparatively high moment resistance ratio. For example, for a slenderness $L/b = 45.5$, the moment resistance ratio attained is 0.890 when $\gamma_i = 2000$ and drops to 0.821 when $\gamma_i = 1000$. As expected, in Figure 4.6(b), where $\gamma_i = 1000$ is kept constant, the moment resistance ratio attained is found to increase with the yield stress fraction. For instance, when $L/b = 51.52$ the moment resistance ratio is 0.846 at $\varepsilon = 0.67$, increases to 0.856 when, $\varepsilon = 0.70$ and further increases to 0.916 when $\varepsilon = 1.00$.

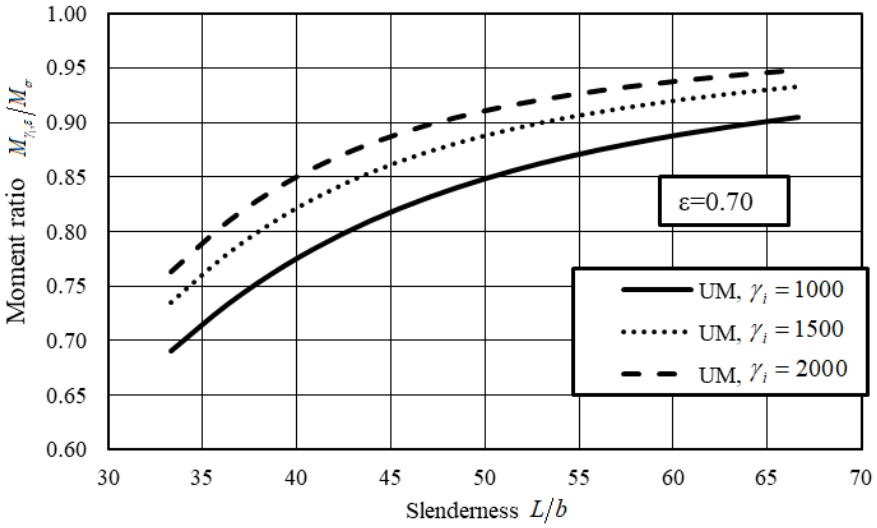

(a)

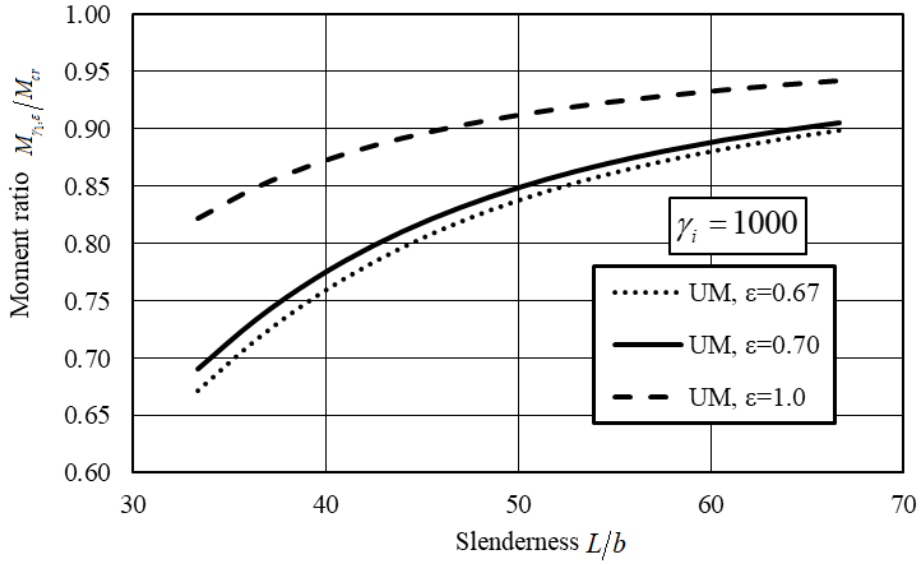

(b)

Figure 4.6 effect of slenderness on Moment resistance ratios of W200x36 for (a) various out-of-straightness coefficient γ_i and (b) various yield stress fraction ε on the moment resistance ratio – All beams are under uniform moments

4.4.5 Effect of slenderness

Five common cross-sections are investigated; 1) W150X18, 2) W200X36, 3) W250X45, 4) W250X58 and 5) W310X60 to assess the effect of slenderness L/b on the moment resistance ratios $M_{\gamma_i,\varepsilon}/M_{cr}$ attained. In all cases, the slenderness L/b is varied while keeping constant parameters

$\varepsilon = 0.70$ and $\gamma_i = 1000$. The results in Figure 4.7 show slight differences in the moment resistance ratios attained for all five sections for short spans and become negligible for large slenderness. For example, for a slenderness $L/b = 35$, the difference between the highest and lowest moment resistance ratio is 0.057. This difference drops to 0.016 when the slenderness increases to about 59.

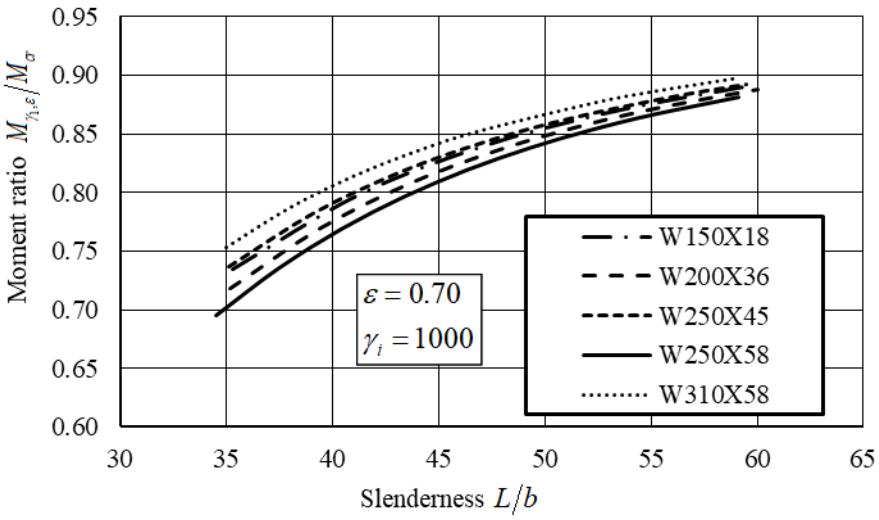

Figure 4.7 Effect of the span to flange width ratio on moment resistance ratio for beams under uniform moment for various beam cross-sections

4.4.6 Effect of cross-section parameters

For a beam with a given cross-section and loading pattern, the critical moments depend on the beam span L, section depth d, flange width b, flange thickness t and web thickness w or, in a dimensionless form, one has $M_{\gamma_i,\varepsilon}/M_{cr} = f\left(d/b, b/t, d/w, L/b\right)$. A study is thus conducted to investigate the effects of the dimensionless parameters on moment resistance ratio $M_{\gamma_1,\varepsilon}/M_{cr}$ by varying one of parameters d/b, b/t and d/w at a time while keeping the other two parameters constant. An idealized W200X36 cross-section is adopted as the reference case (geometric parameters are $d_r = 201mm$, $b_r = 165mm$, $t_r = 10.2mm$, $w_r = 6.2mm$, and the corresponding dimensionless parameters are $\left(d/b\right)_r = 1.22$, $\left(d/w\right)_r = 32.4$ and $\left(b/t\right)_r = 16.2$). All dimensionless parameters were varied from 0.8 to 1.2 of the reference case value (i.e., d/b =0.8-

$1.2\left(d/b\right)_r$, $d/w = 0.8\text{-}1.2\left(d/w\right)_r$ and $b/t = 0.8\text{-}1.2\left(b/t\right)_r$). When assessing the effect of d/b, the web thickness is changed proportionally with the section depth to maintain a constant ratio d/w (Appendix 4.A). Figure 4.8 provides plots for the moment resistance ratio $M_{\gamma_1,\varepsilon}/M_{cr}$ versus the slenderness L/d . A family of plots is depicted for d/t values ranging from 16.4 to 24.6 in Figure 4.8 (a). The moment resistance ratio is found to increase with the slenderness L/b. For a given slenderness, a relatively thick flange (i.e. with low b/t) leads to a lower moment resistance ratio $M_{\gamma_1,\varepsilon}/M_{cr}$. The difference in moment resistance ratio is found to be relatively large for comparatively short span beams (e.g., $L/b = 42.0$) and reduces for longer spans (e.g., $L/b = 58.0$). Figure 4.8 b is provides a series of plots for the moment resistance ratio $M_{\gamma_1,\varepsilon}/M_{cr}$ as a function of the slenderness L/b for $\gamma_i = 1000$, $\varepsilon = 0.70$, $d/w = 32.4$ and $b/t = 16.2$. Five plots are provided for various d/b ratios ranging from 0.97 to 1.46. The moment resistance ratio is observed to increase with the slenderness. At a given slenderness, a comparatively deeper section (i.e., d/b is large) corresponds to a higher moment resistance ratio. The difference in moment resistance ratio is observed to be large for relatively short span beams (e.g., $L/b = 38.0$) and decreases for larger spans (e.g., $L/b = 53.0$).

The plots in Figure 4.8 c illustrate the effect of web slenderness d/w on the moment resistance ratio. Web slenderness was varied from 27.0 to 40.5 while keeping constant $\varepsilon = 0.70, \gamma_i = 1000, d/w = 32.4, b/t = 16.2$. The moment resistance ratio is found to be nearly independent from the web slenderness d/w For example, when $L/b = 37.0$, the moment resistance ratio is 0.747 for $d/w = 40.5$ and marginally changes to 0.744 for $d/w = 27.0$.

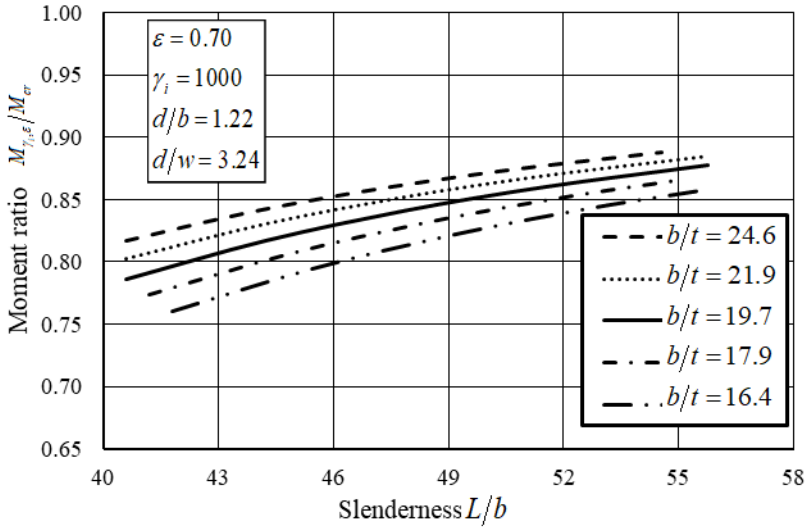
1.00
0.95
0.90
0.85
0.80
0.75
0.70
0.65
Moment ratio $M_{\gamma_i,\varepsilon}/M_{cr}$
$\varepsilon = 0.70$
$\gamma_i = 1000$
$d/b = 1.22$
$d/w = 3.24$
$b/t = 24.6$
$b/t = 21.9$
$b/t = 19.7$
$b/t = 17.9$
$b/t = 16.4$
40
43
46
49
52
55
58
Slenderness L/b

(a)

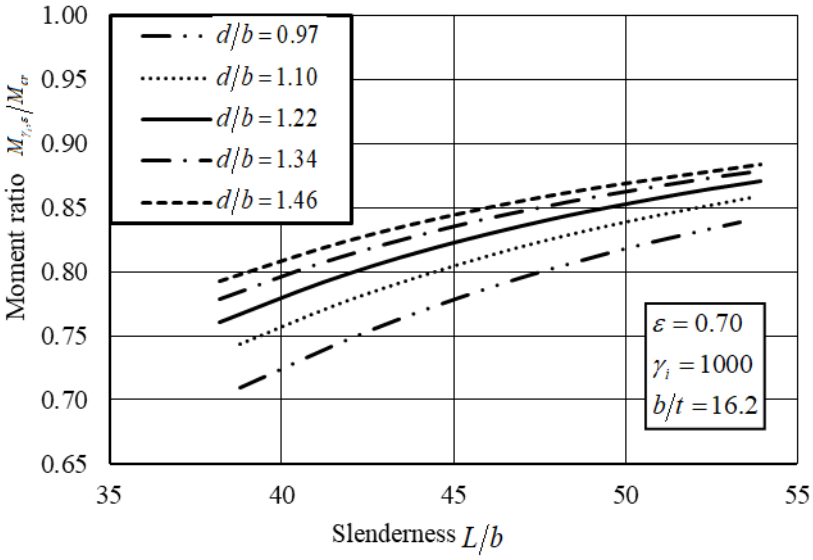
1.00
0.95
0.90
0.85
0.80
0.75
0.70
0.65
Moment ratio $M_{\gamma_i,\varepsilon}/M_{cr}$
$d/b = 0.97$
$d/b = 1.10$
$d/b = 1.22$
$d/b = 1.34$
$d/b = 1.46$
$\varepsilon = 0.70$
$\gamma_i = 1000$
$b/t = 16.2$
35
40
45
50
55
Slenderness L/b

(b)

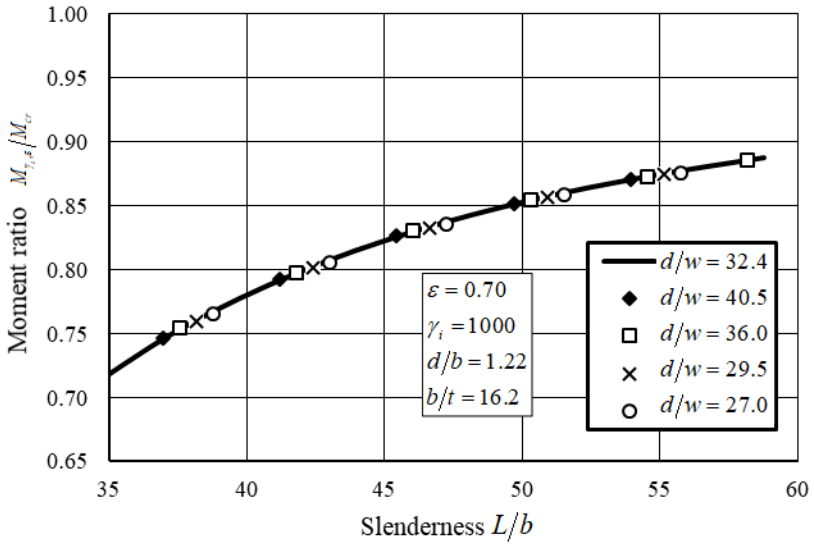

(c)

Figure 4.8 . Effects of (a) flange thickness (b) section depth and (c) web thickness on moment resistance ratio for W200x36 under uniform bending

4.4.7 Moment resistance ratios for other loading cases

Figure 4.9 a provides a comparison of the attained moment ratios $M_{\gamma_i,\varepsilon}/M_{cr}$ for the beams defined in Table 4.1 for three loading cases; 1) uniform bending moments (UM), 2) Mid-span point load (PL) and 3) uniformly distributed load (UDL). The moment resistance ratios attained for the uniform bending moment case are computed based on Eq.(4.20), while those for the cases of point load (PL) and uniformly distributed loads (UDL) are determined from the present finite element analysis.

A family of plots (Figure 4.9 a) is provided for the moment resistance ratio $M_{\gamma_i,\varepsilon}/M_{cr}$ as a function of the slenderness M_Y/M_{cr} for a yield stress fraction $\varepsilon = 0.70$ and IOS coefficients $\gamma_i = 1000, 1500, 2000$. The moment resistance ratio $M_{\gamma_i,\varepsilon}/M_{cr}$ is found to increase with the slenderness M_Y/M_{cr} and with the out-of-straightness coefficient γ_i (i.e., decreases with the degree of out-of-straightness of the beam). For a given beam and an out-of-straightness coefficient, the moment resistance ratio attained is lowest for the point load (PL) case, followed by the uniformly loaded case (UDL) and is largest the case of uniform moment (UM). As a general observation, the predicted moment resistance ratios for the three loading cases considered are observed to differ largely for relatively low slenderness M_Y/M_{cr} but the difference decreases as

slenderness increases. For example, when the initial out of straightness coefficient is $\gamma_i = 1000$, the difference between the point load case (PL) and the uniformly distributed case (UDL) is 7.4% when the slenderness is $M_Y / M_{cr} = 1.38$ and difference decreases to 26% when the slenderness increases to $M_Y / M_{cr} = 3.26$.

In Figure 4.9b, where $\gamma_i = 1000$ is kept constant and yield stress fractions were varied, i.e., $\varepsilon = 0.67, 0.70, 0.75$, it is found that an increase in the specified yield stress fraction corresponds to a higher moment resistance ratio at a given slenderness M_Y / M_{cr} .

Figure 4.9 c depicts for the moment resistance ratio attained $M_{\gamma_i,\varepsilon} / M_{cr}$ as a function of the slenderness L/b for a specified yield fraction $\varepsilon = 0.70$ and out-of-straightness coefficients $\gamma_i = 1000, 1500, 2000$ for a beam with a W200X36 cross-section with varying spans for the loading cases UM, UDL, and PL. The moment resistance ratio $M_{\gamma_i,\varepsilon} / M_{cr}$ is found to increase with the slenderness L/b . Increasing the out-of-straightness coefficient attains a high moment resistance ratio $M_{\gamma_i,\varepsilon} / M_{cr}$. The difference in the attained moment resistance ratios $M_{\gamma_i,\varepsilon} / M_{cr}$ between the different loading cases is observed to slightly decrease with the slenderness L/b . For example, when the initial out of straightens coefficient is $\gamma_i = 1000$ and the slenderness is $L/b = 43.0$, the difference in moment resistance ratio between the PL and UDL cases is 7.1%. The difference decreases to 5.7% when slenderness increases to 55.2.

A family of plots (Figure 4.9 d) is provided for the moment resistance ratio with the slenderness for an initial-out of straightens coefficient $\gamma_i = 1000$ or specified yield stress fractions of $\varepsilon = 0.67, 0.70, 0.75$. Again, it is found that moment resistance ratio increases with the slenderness. Also, a higher specified yield stress fraction corresponds to a higher moment resistance ratio at a given slenderness.

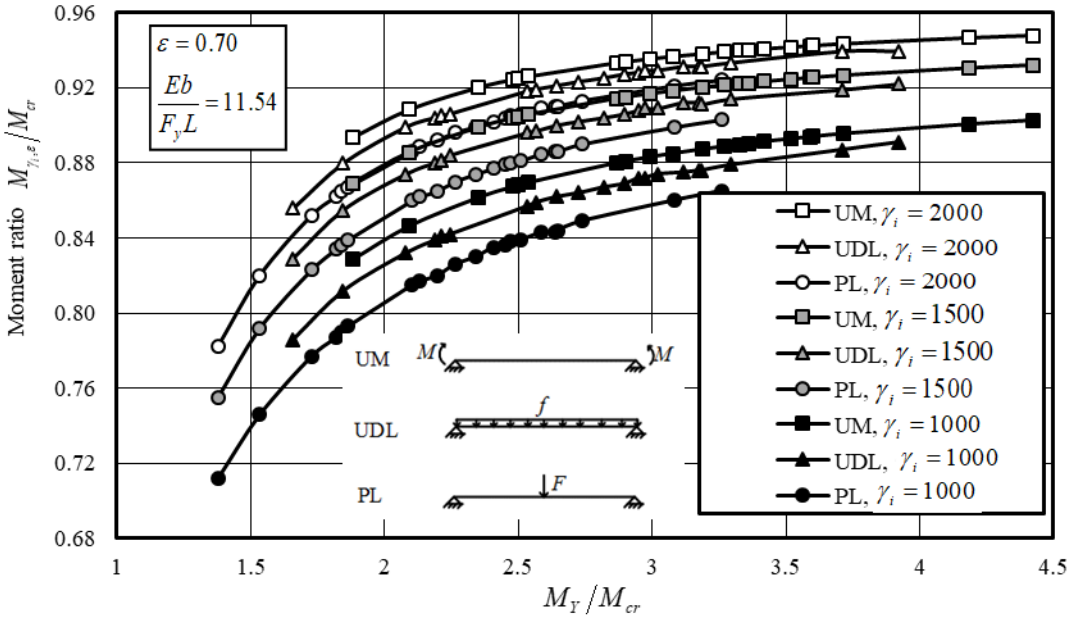
$\varepsilon = 0.70$
$\frac{Eb}{F_y L} = 11.54$
UM
UDL
PL
M
f
F
UM, $\gamma_i = 2000$
UDL, $\gamma_i = 2000$
PL, $\gamma_i = 2000$
UM, $\gamma_i = 1500$
UDL, $\gamma_i = 1500$
PL, $\gamma_i = 1500$
UM, $\gamma_i = 1000$
UDL, $\gamma_i = 1000$
PL, $\gamma_i = 1000$
Moment ratio $M_{\gamma_i,\varepsilon}/M_{cr}$
M_Y/M_{cr}
0.96
0.92
0.88
0.84
0.80
0.76
0.72
0.68
1
1.5
2
2.5
3
3.5
4
4.5

(a)

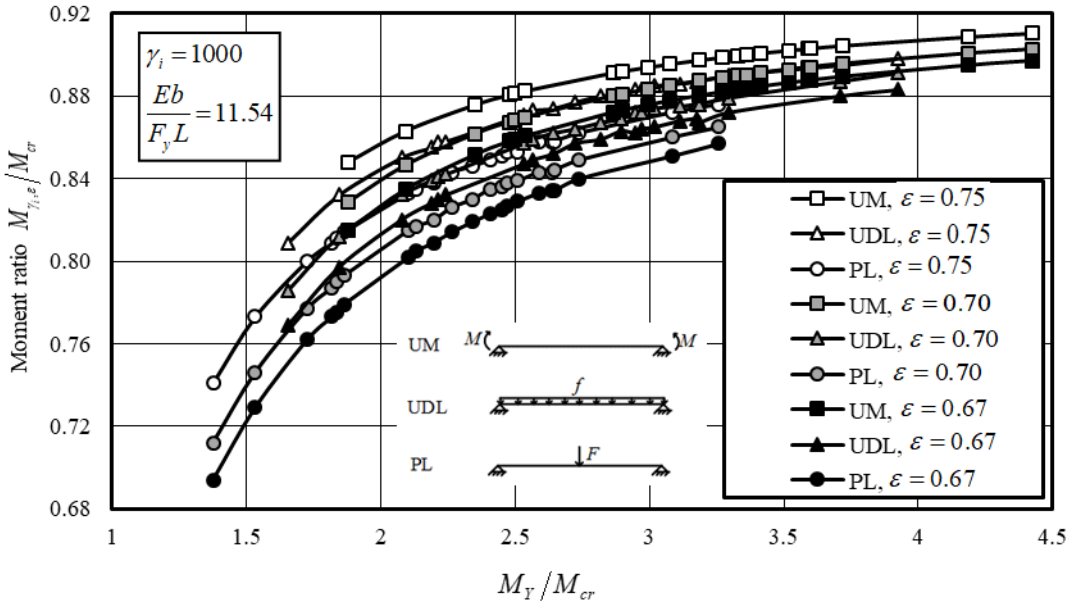
$\gamma_i = 1000$
$\frac{Eb}{F_y L} = 11.54$
UM
UDL
PL
M
f
F
UM, $\varepsilon = 0.75$
UDL, $\varepsilon = 0.75$
PL, $\varepsilon = 0.75$
UM, $\varepsilon = 0.70$
UDL, $\varepsilon = 0.70$
PL, $\varepsilon = 0.70$
UM, $\varepsilon = 0.67$
UDL, $\varepsilon = 0.67$
PL, $\varepsilon = 0.67$
Moment ratio $M_{\gamma_i,\varepsilon}/M_{cr}$
M_Y/M_{cr}
0.92
0.88
0.84
0.80
0.76
0.72
0.68
1
1.5
2
2.5
3
3.5
4
4.5

(b)

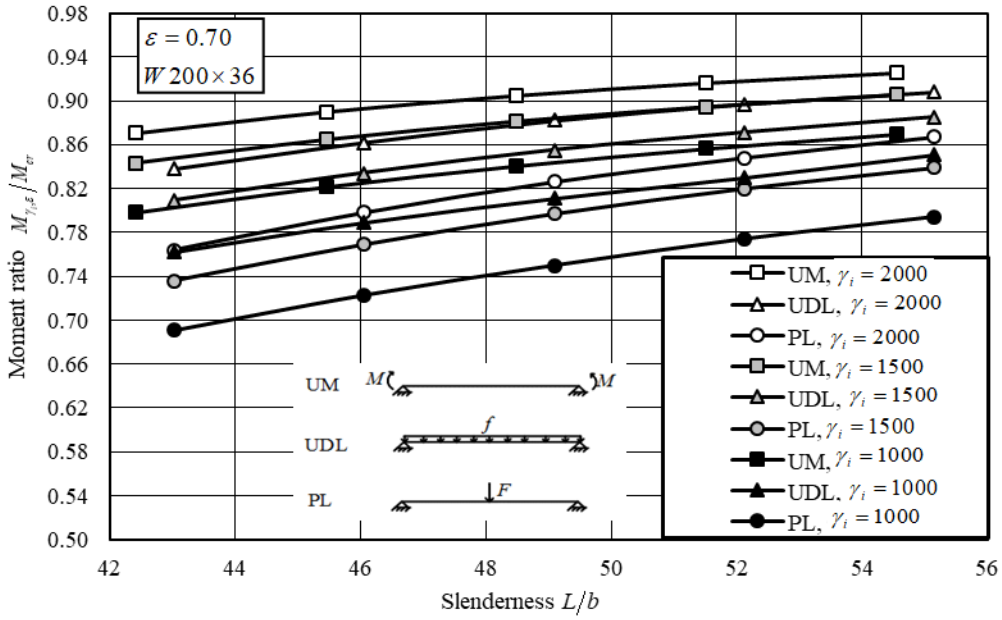

(c)

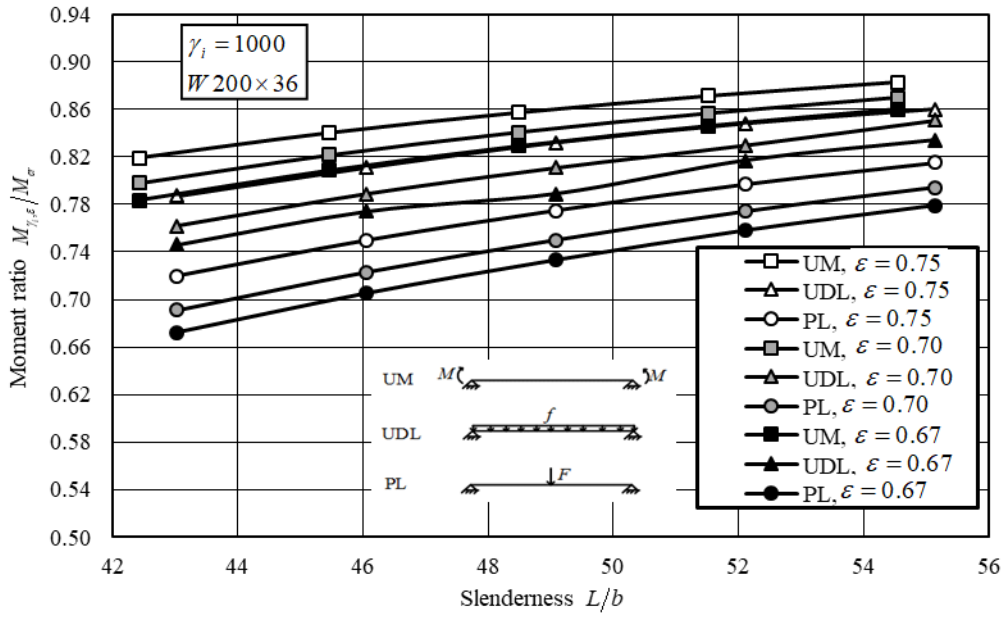

(d)

Figure 4.9 Moment resistance ratio for considered sections under uniform moment, point load at mid-span and UDL for (a) out-of-straightness γ_i = 1000, 1500 and 2000, (b) yield stress fraction ε = 0.67, 0.70 and 0.75. Moment resistance ratio for W200X36 for (c) out-of-straightness coefficients γ_i = 1000, 1500 and 2000, (d) yield stress fractions ε = 0.67, 0.70 and 0.75

4.4.8 Extension of the analytical solution to other loading cases

The trends of the three loading cases considered observed in Figure 4.9 but are offset given that the critical moments differ due to the moment gradient effect. This observation suggests a possible modification of Eq. (4.20) by replacing the uniform critical moment M_{crm} by $\omega_2 M_{crm}$, in which ω_2 is a moment gradient factor. Thus, a modified form of Eq. (4.20) is proposed in the following

$$\frac{M_{\gamma_i,\varepsilon}}{\omega_2 M_{crm}} \approx \frac{1}{2}\left(1+\frac{\pi^2}{2\gamma_i}\left(\frac{Eb}{F_y L}\right)\left(\frac{M_Y}{\omega_2 M_{crm}}\right)+\varepsilon\frac{M_Y}{\omega_2 M_{crm}}\right) \pm \frac{1}{2}\sqrt{\left(1+\frac{\pi^2}{2\gamma_i}\left(\frac{Eb}{F_y L}\right)\left(\frac{M_Y}{\omega_2 M_{crm}}\right)+\varepsilon\frac{M_Y}{\omega_2 M_{crm}}\right)^2 - 4\varepsilon\frac{M_Y}{\omega_2 M_{crm}}} \tag{4.21}$$

For the point load case (PL), the moment gradient factor based on FEA can be computed by dividing the critical moment for a perfectly straight beam as predicted by the present eigenvalue model, by that for the case of uniform moment, leading to $\omega_2(FEM) =$ 1.36. This value is close to that provided by American Standards (ANSI/AISN 360-10), Australian Standards (AS 4100-1998) and Eurocode Guide (EN 1993-1-1:2005) as discussed in (Hassan and Mohareb 2015), but slightly higher than that based the Canadian standards (CAN/CSA S16-14) is $\omega_2(CSA) = 1.265$. Thus, the predictions of Eq. (4.21), based on moment gradients $\omega_2 = \omega_2(CSA) = 1.265$ and $\omega_2(FEA) = 1.360$ will be compared to FEM results will be investigated.

For the uniform distributed load case (UDL), the moment gradient factor computed by the present FEM is $\omega_2(FEM) = 1.13$, which is identical to that provided in Canadian standards (CAN/CSA S16-14) and Eurocode Guide (EN 1993-1-1:2005) and closed to $\omega_2(AS) = 1.17$ in the Australian Standards (AS 4100-1998) and $\omega_2(AISC) = 1.14$ in American Standards (ANSI/AISN 360-10). Thus, the moment gradient $\omega_2 = \omega_2(CSA) = 1.13$ is adopted in Eq. (4.21) when predicting the moment ratio $M_{\gamma_i,\varepsilon}/M_{cr}$ for the UDL case.

The beams described in Table 4.1 are re-examined the cased of point load at mid-span (PL) and uniform distributed load (UDL). The specified yield stress fraction $\varepsilon = 0.70$ is kept constant in all runs while the out-of-straightness coefficient γ_i is taken as 1000, 1500, and 2000. The moment resistance ratios $M_{\gamma_i,\varepsilon}/M_{cr}$ as predicted the present finite element solution and those predicted

by Eq. (4.21) under the two loading cases are summarized in Table 4.4 to Table 4.6 for PL with $\omega_2 = 1.265$, PL with $\omega_2 = 1.36$, and UDL with $\omega_2 = 1.13$, respectively. Also provided is the percentage difference in moment resistance ratios as predicted on the present finite element solution and those based on Eq. (4.21) is calculated to evaluate the accuracy of the predictions of Eq. (4.21).

For the point load (PL) case, Table 4.4 indicates that proposed Eq. (4.21) with $\omega_2 = \omega_2(CSA) = 1.265$ yield moment ratio predictions $M_{\gamma_i,\varepsilon}/M_{cr}$ deviate from FEM predictions with percentage differences ranging from 1.9% to 8.4% with an mean difference of 4.1%. Improved moment ratio predictions are attained by adopting the more accurate moment gradient $\omega_2 = \omega_2(FEM) = 1.36$ in conjunction with Eq. (4.21) where the percentage difference between both solutions range from 0.5% to 2.7% with a mean difference of 1.8%.

For the UDL case, Table 4.6 presents the prediction by Eq. (4.21) with $\omega_2 = \omega_2(CSA) = 1.13$ and by the present FEM. The percentage difference is found to range from 0.5% to 2.1% with an average of 1.0%.

Also, it is found that the percentage difference decreases with the increase of the initial out-of-straightness γ_i . For example, the maximum percentage difference for $\gamma_i = 1000$ is found as 2.1%. The corresponding value is 1.5% for the case with $\gamma_i = 2000$. Beams with comparatively larger M_Y/M_{cr} attain a lower percentage difference. For instance, for W150X24 of which the slenderness is $M_Y/M_{cr} = 1.7$, the percentage difference is 2.1% for $\gamma_i = 1000$. On the contrary, for W310X31 with $M_Y/M_{cr} = 3.9$, the percentage difference is 0.8%.

Table 4.4 Percentage difference in predicted moment resistance ratio based on FEA critical moment and CSA critical moment approach f or Beams under point load at mid-span ($Eb/F_yL = 11.54$, $\varepsilon = 0.70$ and $\omega_2 = 1.265$)

Section	Span	Critical moment based on FEA	Critical moment based on CSA	Yield to critical moment ratio based on FEA	FEA moment (kNm) for imperfection			Moment resistance fraction*			Moment resistance fraction based on Mcr-CSA** (ω2=1.265)			Percentage difference***		
	(m)	(kNm)	(kNm)	M_Y/M_{cr}	L/1000	L/1500	L/2000	L/1000	L/1500	L/2000	L/1000	L/1500	L/2000	L/1000	L/1500	L/2000
W150x24	5.37	42.5	39.7	1.4	30.3	32.1	33.3	0.712	0.755	0.782	0.771	0.812	0.837	8.4%	7.5%	7.0%
W200x42	8.74	90.8	84.7	1.5	67.7	71.9	74.4	0.746	0.792	0.820	0.801	0.842	0.868	7.4%	6.3%	5.8%
W200x36	8.68	69.3	64.5	1.7	53.8	57.0	59.0	0.777	0.823	0.852	0.827	0.867	0.892	6.4%	5.4%	4.6%
W150x18	5.37	23.0	21.5	1.8	18.1	19.2	19.9	0.787	0.834	0.862	0.836	0.876	0.900	6.2%	5.1%	4.4%
W200x31	7.05	56.9	53.0	1.8	45.0	47.6	49.2	0.790	0.836	0.865	0.838	0.878	0.901	6.0%	5.0%	4.2%
W250x45	7.79	100.1	93.3	1.9	79.4	84.0	86.8	0.793	0.839	0.867	0.840	0.880	0.903	5.9%	4.9%	4.2%
W250x39	7.74	76.2	71.0	2.1	62.1	65.6	67.5	0.815	0.860	0.886	0.857	0.895	0.917	5.2%	4.1%	3.5%
W200x27	7.00	40.9	38.0	2.1	33.4	35.2	36.3	0.817	0.862	0.889	0.859	0.896	0.918	5.1%	4.0%	3.3%
W200x22	5.37	30.9	28.7	2.2	25.3	26.7	27.5	0.820	0.865	0.892	0.862	0.900	0.921	5.2%	4.0%	3.2%
W150x14	5.26	14.2	13.2	2.3	11.7	12.3	12.7	0.826	0.870	0.896	0.865	0.902	0.923	4.8%	3.7%	3.0%
W250x28	5.37	45.8	42.7	2.3	38.1	40.1	41.2	0.830	0.874	0.899	0.869	0.905	0.925	4.7%	3.6%	2.9%
W150x13	5.26	12.1	11.2	2.4	10.1	10.6	10.9	0.835	0.877	0.902	0.871	0.907	0.927	4.4%	3.4%	2.8%
W250x33	7.68	54.2	50.4	2.4	45.3	47.7	49.0	0.836	0.879	0.904	0.873	0.908	0.928	4.4%	3.4%	2.7%
W310x45	8.74	89.8	83.6	2.5	75.3	79.0	81.3	0.838	0.880	0.905	0.874	0.909	0.929	4.3%	3.3%	2.6%
W200x19	5.37	22.7	21.1	2.5	19.1	20.0	20.6	0.839	0.881	0.906	0.875	0.910	0.930	4.3%	3.3%	2.6%
W200x21	7.00	26.4	24.5	2.6	22.2	23.4	24.0	0.843	0.885	0.909	0.878	0.912	0.932	4.1%	3.1%	2.5%
W250x25	5.37	35.3	32.8	2.6	29.7	31.2	32.1	0.843	0.886	0.910	0.879	0.914	0.933	4.3%	3.1%	2.5%
W310x33	5.37	54.9	51.1	2.6	46.3	48.6	49.9	0.844	0.886	0.910	0.879	0.914	0.933	4.2%	3.1%	2.5%
W310x39	8.68	70.3	65.3	2.7	59.7	62.6	64.2	0.849	0.890	0.913	0.882	0.916	0.934	3.9%	2.9%	2.4%
W250x24	7.63	31.2	28.9	3.1	26.8	28.0	28.7	0.860	0.899	0.921	0.889	0.922	0.940	3.4%	2.5%	2.0%
W310x31	8.63	46.0	42.8	3.3	39.8	41.6	42.5	0.865	0.903	0.924	0.893	0.924	0.941	3.2%	2.4%	1.9%
												Min		3.2%	2.4%	1.9%
												Max		8.4%	7.5%	7.0%
												Mean		5.0%	4.0%	3.4%
												Stan Deviation		0.01256	0.01249	0.01242

Table 4.5 Percentage difference in predicted moment resistance ratio based on FEA critical moment and CSA critical moment approach f or Beams under point load at mid-span ($Eb/F_yL = 11.54$, $\varepsilon = 0.70$ and $\omega_2 = 1.36$)

Section	Span	Critical moment based on FEA	Critical moment based on CSA	Yield to critical moment ratio based on FEA	FEA moment (kNm) for imperfection			Moment resistance fraction*			Moment resistance fraction based on Mcr-CSA** (ω2=1.36)			Percentage difference***		
	(m)	(kNm)	(kNm)	M_y/M_{cr}	L/1000	L/1500	L/2000	L/1000	L/1500	L/2000	L/1000	L/1500	L/2000	L/1000	L/1500	L/2000
W150x24	5.37	42.5	39.7	1.4	30.3	32.1	33.3	0.712	0.755	0.782	0.726	0.763	0.786	2.0%	1.1%	0.5%
W200x42	8.74	90.8	84.7	1.5	67.7	71.9	74.4	0.746	0.792	0.820	0.763	0.803	0.828	2.2%	1.4%	1.0%
W200x36	8.68	69.3	64.5	1.7	53.8	57.0	59.0	0.777	0.823	0.852	0.795	0.837	0.863	2.4%	1.8%	1.3%
W150x18	5.37	23.0	21.5	1.8	18.1	19.2	19.9	0.787	0.834	0.862	0.808	0.850	0.875	2.6%	1.9%	1.5%
W200x31	7.05	56.9	53.0	1.8	45.0	47.6	49.2	0.790	0.836	0.865	0.810	0.852	0.877	2.5%	1.9%	1.4%
W250x45	7.79	100.1	93.3	1.9	79.4	84.0	86.8	0.793	0.839	0.867	0.813	0.855	0.880	2.5%	1.9%	1.5%
W250x39	7.74	76.2	71.0	2.1	62.1	65.6	67.5	0.815	0.860	0.886	0.835	0.876	0.900	2.5%	1.8%	1.6%
W200x27	7.00	40.9	38.0	2.1	33.4	35.2	36.3	0.817	0.862	0.889	0.837	0.878	0.902	2.5%	1.8%	1.4%
W200x22	5.37	30.9	28.7	2.2	25.3	26.7	27.5	0.820	0.865	0.892	0.842	0.882	0.905	2.7%	2.0%	1.5%
W150x14	5.26	14.2	13.2	2.3	11.7	12.3	12.7	0.826	0.870	0.896	0.846	0.886	0.909	2.4%	1.8%	1.4%
W250x28	5.37	45.8	42.7	2.3	38.1	40.1	41.2	0.830	0.874	0.899	0.851	0.890	0.912	2.5%	1.8%	1.5%
W150x13	5.26	12.1	11.2	2.4	10.1	10.6	10.9	0.835	0.877	0.902	0.854	0.893	0.915	2.3%	1.8%	1.4%
W250x33	7.68	54.2	50.4	2.4	45.3	47.7	49.0	0.836	0.879	0.904	0.856	0.894	0.916	2.4%	1.8%	1.4%
W310x45	8.74	89.8	83.6	2.5	75.3	79.0	81.3	0.838	0.880	0.905	0.857	0.895	0.917	2.3%	1.7%	1.3%
W200x19	5.37	22.7	21.1	2.5	19.1	20.0	20.6	0.839	0.881	0.906	0.859	0.897	0.919	2.4%	1.8%	1.4%
W200x21	7.00	26.4	24.5	2.6	22.2	23.4	24.0	0.843	0.885	0.909	0.862	0.900	0.921	2.3%	1.7%	1.3%
W250x25	5.37	35.3	32.8	2.6	29.7	31.2	32.1	0.843	0.886	0.910	0.864	0.901	0.922	2.5%	1.7%	1.4%
W310x33	5.37	54.9	51.1	2.6	46.3	48.6	49.9	0.844	0.886	0.910	0.864	0.902	0.923	2.4%	1.8%	1.4%
W310x39	8.68	70.3	65.3	2.7	59.7	62.6	64.2	0.849	0.890	0.913	0.867	0.904	0.925	2.2%	1.6%	1.3%
W250x24	7.63	31.2	28.9	3.1	26.8	28.0	28.7	0.860	0.899	0.921	0.877	0.912	0.932	2.0%	1.5%	1.2%
W310x31	8.63	46.0	42.8	3.3	39.8	41.6	42.5	0.865	0.903	0.924	0.881	0.915	0.934	1.9%	1.4%	1.1%
												Min		1.9%	1.1%	0.5%
												Max		2.7%	2.0%	1.6%
												Mean		2.4%	1.7%	1.3%
												Stan Deviation		0.00205	0.00206	0.00222

Table 4.6 Percentage difference in predicted moment resistance ratio based on FEA critical moment and CSA critical moment approach for Beams under uniform distributed load ($Eb/F_yL = 11.54$, $\varepsilon = 0.70$ and $\omega_2 = 1.13$)

Section	Span	Critical moment based on FEA	Critical moment based on CSA	Yield to critical moment ratio based on FEA	FEA moment (kNm) for imperfection			Moment resistance fraction*			Moment resistance fraction based on Mcr-CSA** (ω2=1.13)			Percentage difference***		
	(m)	(kNm)	(kNm)	M_Y/M_{cr}	L/1000	L/1500	L/2000	L/1000	L/1500	L/2000	L/1000	L/1500	L/2000	L/1000	L/1500	L/2000
W150x24	5.37	35.5	35.5	1.7	27.9	29.4	30.4	0.786	0.829	0.856	0.802	0.844	0.869	2.1%	1.8%	1.5%
W200x42	8.74	75.6	75.7	1.8	61.4	64.6	66.5	0.812	0.855	0.880	0.826	0.867	0.891	1.7%	1.4%	1.2%
W200x36	8.68	57.7	57.6	2.1	48.0	50.4	51.9	0.832	0.874	0.899	0.846	0.885	0.908	1.6%	1.2%	1.0%
W150x18	5.37	19.2	19.2	2.2	16.1	16.9	17.4	0.839	0.880	0.904	0.853	0.892	0.914	1.7%	1.3%	1.1%
W200x31	7.05	47.4	47.3	2.2	39.9	41.8	42.9	0.841	0.881	0.905	0.854	0.893	0.915	1.6%	1.3%	1.1%
W250x45	7.79	83.4	83.3	2.2	70.2	73.7	75.6	0.842	0.884	0.906	0.856	0.894	0.916	1.7%	1.2%	1.1%
W250x39	7.74	63.5	63.4	2.5	54.4	56.9	58.3	0.857	0.896	0.918	0.870	0.906	0.926	1.5%	1.1%	0.9%
W200x27	7.00	34.0	34.0	2.6	29.2	30.5	31.2	0.859	0.897	0.919	0.871	0.907	0.927	1.4%	1.1%	0.8%
W200x22	5.37	25.7	25.7	2.6	22.2	23.1	23.7	0.862	0.900	0.921	0.874	0.909	0.929	1.3%	1.0%	0.8%
W150x14	5.26	11.8	11.8	2.7	10.2	10.6	10.9	0.864	0.902	0.923	0.876	0.911	0.930	1.4%	1.0%	0.8%
W250x28	5.37	38.2	38.1	2.8	33.1	34.5	35.3	0.867	0.904	0.925	0.879	0.913	0.932	1.4%	1.0%	0.8%
W150x13	5.26	10.0	10.0	2.9	8.7	9.1	9.3	0.869	0.906	0.927	0.881	0.915	0.934	1.4%	1.0%	0.7%
W250x33	7.68	45.2	45.0	2.9	39.4	41.0	41.9	0.872	0.908	0.928	0.882	0.916	0.935	1.1%	0.9%	0.7%
W310x45	8.74	74.8	74.7	3.0	65.2	68.0	69.5	0.872	0.909	0.929	0.883	0.916	0.935	1.2%	0.8%	0.6%
W200x19	5.37	18.9	18.9	3.0	16.5	17.2	17.6	0.874	0.909	0.929	0.884	0.917	0.936	1.1%	0.9%	0.7%
W200x21	7.00	22.0	21.9	3.1	19.3	20.1	20.5	0.875	0.912	0.931	0.886	0.919	0.937	1.2%	0.8%	0.7%
W250x25	5.37	29.4	29.3	3.2	25.8	26.8	27.4	0.876	0.912	0.931	0.887	0.920	0.938	1.3%	0.9%	0.7%
W310x33	5.37	45.7	45.6	3.2	40.0	41.6	42.5	0.876	0.911	0.931	0.887	0.920	0.938	1.3%	1.0%	0.8%
W310x39	8.68	58.6	58.3	3.3	51.5	53.6	54.7	0.879	0.914	0.933	0.889	0.922	0.939	1.2%	0.8%	0.7%
W250x24	7.63	26.0	25.8	3.7	23.1	23.9	24.4	0.887	0.919	0.939	0.895	0.926	0.943	0.9%	0.8%	0.5%
W310x31	8.63	38.4	38.2	3.9	34.2	35.4	36.1	0.891	0.922	0.939	0.898	0.928	0.945	0.8%	0.7%	0.6%
												Min		0.8%	0.7%	0.5%
												Max		2.1%	1.8%	1.5%
												Mean		1.4%	1.0%	0.8%
												Stan Deviation		0.00286	0.00246	0.00235

* Moment resistance ratio = M_{FEA}/M_{cr-FEA} ; ** Moment resistance ratio based on M_{cr-CSA} is computed in Eq.

*** Percentage difference = $\left[\left(M/M_{cr-CSA}\right)_{appx}-\left(M_{FEA}/M_{cr-FEA}\right)\right]/\left(M_{FEA}/M_{cr-FEA}\right)$

4.4.9 Nominal moment resistance based on stress criterion

The solution provided by Eq. (4.21) accounts for the initial-out-of-straightness effect and should replace the eigenvalue solution in the elastic buckling range. For medium span beams, inelastic lateral torsional buckling will likely take place. For instance when, for a perfectly straight beam with a class 3 cross-section with $M_{cr}/M_p > 0.67$, the Canadian standards assume that inelastic lateral torsional buckling takes place and one needs to account for the effects of plasticity and residual stresses, using the equation $M_n = 1.15M_Y\left(1-0.28M_Y/M_{cr}\right)$ with a ceiling value of $M_n = M_Y$ which corresponds to pure yielding. An extension of the concept was proposed for the displacement criterion under section 4.3.4.

In the present section, we adopt an alternative approach to account for plasticity and residual stresses in the inelastic lateral torsional buckling range in a manner consistent with the column resistance equations in CAN-CSA-S16 (2014), where the nominal resistance of a column C_n takes the form $C_n = AF_y\left(1+\tau^{2\chi}\right)^{-1/\chi}$, AF_y being the yield strength of the column, τ being the column slenderness, and $n = 1.34$ is a constant that it intended to match the outcome of the inelastic analysis and/or tests. An analogous equation is postulated here whereby the inelastic moment is assumed to be obtained by $M_n = S_xF_y\left(1+\mu^{\kappa}\right)^{-1/\kappa}$ where $M_Y = S_xF_y$ is the yield moment, $\mu = M_Y/M_{cr}$ is the slenderness ratio, and constant κ is to be obtained by matching the predictions of the present FEA analysis. In a manner similar to the column equation, the proposed equation approaches the yield moment $M_Y = S_xF_y$ as the slenderness approaches zero ($\mu \to 0$). Constant κ can be obtained by matching the attained moment ratios M_n/M_Y based on the FEM predictions within the elastic range. However, it is cautioned that the extrapolation of the curve predictions beyond the elastic domain is not recommended without conducting verifying the predictions of the equation against inelastic analysis results that accounts for the effects of plasticity and residual stresses, in addition to initial-of-straightness. As an illustration, a simply supported beam with a W150x14 cross-section is considered with variable spans (Section class is 3 based on yield strength of $F = 350MPa$). The moment ratio M_n/M_Y as predicted by the FEM is provided for a yield stress fraction $\varepsilon = 0.7$ and initial out-of-straightness coefficients of $\gamma_i = 1000, 1500, 2000$.

Given the FEA predictions for the nominal ratio M_n/M_Y and the corresponding slenderness M_Y/M_{cr} , an equation of the form $M_n = S_x F_y \left(1+\mu^{\kappa}\right)^{-1/\kappa}$ is fitted to the results, where the coefficient κ is obtained by minimizing the differences between the equation and the FEA predictions. The values $\kappa =$ 1.36, 1.63 and 1.80 were obtained for $\gamma_i = 1000, 1500, 2000$, respectively and percentage difference between the proposed equation and FEM were no larger than 2.41%, 2.42% and 2.13% respectively. The corresponding plots are depicted in Figure 4.10 for comparison. As discussed, since the present finite element solution does not account the effects of plasticity and the residual stress, equation $M_n = S_x F_y \left(1+\mu^{\kappa}\right)^{-1/\kappa}$ is currently limited in the range of the elastic LTB. The validity of this proposed equation for the range of the inelastic LTB should be verified by performing a finite element analysis incorporating these effects.

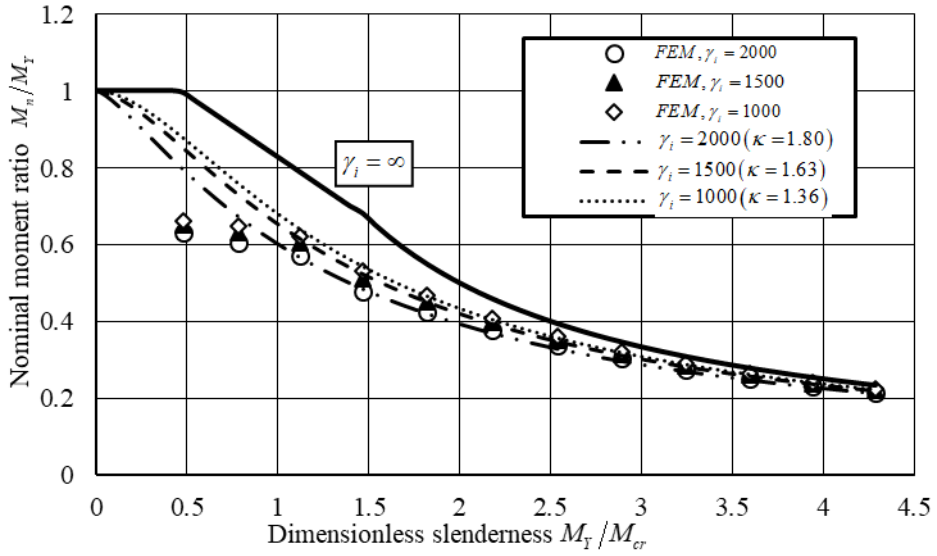

Figure 4.10 Proposed design curves based on stress target value $0.7F_y$ for $\gamma_i = L/1000, L/1500$ and $L/2000$ (W150X14)

4.5 Summary and Conclusions

Closed form expressions were developed for moment ratio predictions under displacement and stress based criteria for the case of uniform moments. The validity of the expressions was demonstrated by comparison with the finite element solution developed in Chapter 3. The closed form expressions provided the dimensionless parameters influencing the moment ratios and the effects of each parameter was systematically investigated by varying one parameter at a time while

maintaining constant all other parameters. The closed form solutions for the moment ratio were modified to extend their use to other loadings cases involving mid-span point loading uniformly distributed loading. The accuracy of the modified equations was demonstrated by comparison against numerical results based on the FEM solution developed in Chapter 3. Design curves incorporating the effect of IOS in the elastic range were proposed by modifying the current design equations in CAN/CSA S16-14 based on the parametric study results. The main findings of the study are summarized as follows:

1. The predicted moment ratio based on the yield criterion solely depends on the ratio between the IOS coefficient and the displacement threshold value. Thus, it is independent of the slenderness, cross-section dimensions, and the loading conditions considered.

2. The closed form solution for the moment ratio predicted by the stress based criterion for beams under uniform moments were found to be extendable to other loading cases considered (UDL and PL) by adopting appropriate moment gradient factors.

3. Based on the stress criterion, the predicted moment ratio $M_{\gamma_i,\varepsilon} / M_{cr}$ was shown to increase with the IOS coefficient, yield stress fraction, yield-to-critical moment ratio, span-to-section-depth ratio, flange-width-to-depth ratio and depth-to-flange-thickness ratio.

Appendix 4.A

Table 4.A.1 Cross-section geometry and properties for the parametric study on d/b

	d	b	t	w	Ix	Sx	Zx	Iy	Sy	J	Cw
d/b	(mm)				mm^4 $\times 10^7$	mm^3 $\times 10^5$	mm^3 $\times 10^5$	mm^4 $\times 10^6$	mm^3 $\times 10^4$	mm^4 $\times 10^5$	mm^6 $\times 10^{10}$
0.97	160.8	165	10.2	4.96	2.03	2.52	2.78	7.64	9.26	1.18	4.94
1.1	180.9	165	10.2	5.58	2.65	2.93	3.25	7.64	9.26	1.22	6.36
1.22	201.0	165	10.2	6.2	3.37	3.35	3.72	7.64	9.26	1.26	7.71
1.34	221.1	165	10.2	6.82	4.21	3.8	4.24	7.64	9.26	1.33	9.33
1.46	241.2	165	10.2	7.44	5.16	4.28	4.76	7.64	9.26	1.42	11.1

5. Estimating critical moments for perfectly straight beams from the lateral torsional response of initially crooked beams

5.1 Introduction

Chapters 3 developed an FEM solution that characterizes the nonlinear moment-lateral displacement relationship for a beam with a given IOS and IAT pattern subjected to transverse loads. The obtained relationships did not exhibit a distinct plateau corresponding to the critical moment of a perfectly straight beam but approached the critical moment asymptotically from below. When conducting experimental results beams with IOS and IAT, two questions arise: (a) Can the nonlinear moment-lateral displacement obtained be used to predict the critical moment for a perfectly straight beam? and (b) Can the nonlinear moment-lateral displacement be used to characterize the magnitude of initial imperfections of the beam. The original work of Southwell (1931) provided a basis to answer similar questions for simply supported columns with initial crookedness. The present chapter aims to extend the findings of Southwell for beams with IOS and IAT by developing a closed form solution for the nonlinear response of beams with IOS and IAT under uniform moments and developing Southwell-like solutions. Since closed form solutions cannot be developed for the cases involving variable moments, the FEM solution developed in chapter 3 used then to produce nonlinear moment-lateral displacement relations for various IOS-IAT scenarios, and the applicability of the Southwell-like solution is used to estimate the critical moments. Comparisons are then performed with the critical moments obtained from the eigen-value solutions. The numeric results suggest that the extended Southwell technique remains valid for case of non-uniform moments.

5.2 Theoretical Background

5.2.1 Overview of the Southwell plot technique for column buckling

Consider a simply supported column with an initial out-of- straightness $y_0(z)$ an elastic flexural stiffness EI subjected to an axial load P. The equilibrium condition can be shown (e.g., Southwell 1931), to take the form

$$EI\left(y'' - y_0''\right) + Py = 0 \tag{5.1}$$

in which, $y(z)$ is the transverse deflection. By expressing the transverse deflection $y(z)$ and initial out-of-straightness $y_0(z)$ as Fourier series, one obtains

$$y(z)=\sum_{m=1}^{\infty} w_m \sin\left(\frac{m\pi z}{L}\right)$$
$$y_0(z)=\sum_{m=1}^{\infty} \bar{w}_m \sin\left(\frac{m\pi z}{L}\right) \qquad (5.2)a,b$$

in which, w_m and $\overline{w_m}$ are the magnitudes of the transverse deflection and initial transverse out-of-straightness corresponding to mode m. From Eqs. (5.2) by substituting into Eq. (5.1), one obtains

$$\frac{w_m}{\bar{w}_m}=\frac{1}{1-P/P_m}, \qquad m=1,2... \qquad (5.3)$$

where P_m is the mth critical load obtained from the eigenvalue solution for equilibrium equation or a corresponding perfectly straight column. By setting $z=L/2$ into Eq. 5.2a, the additional deflection δ at mid-span is obtained as

$$\delta=y(L/2)-y_0(L/2)=\sum_{m=1}^{\infty} w_m \sin\left(\frac{m\pi}{2}\right)-\sum_{m=1}^{\infty} \bar{w}_m \sin\left(\frac{m\pi z}{L}\right)=w_1-\bar{w}_1-\left(w_3-\bar{w}_3\right)+w_5-\bar{w}_5... \qquad (5.4)$$

From Eq, (5.3) by substituting into Eq. (5.4). one obtains

$$\delta=\frac{\bar{w}_1}{P_1/P-1}-\frac{\bar{w}_3}{P_3/P-1}+\frac{\bar{w}_5}{P_5/P-1}... \qquad (5.5)$$

As $P\to P_1$, the first term of Eq. (5.5) gains dominance and the contributions of subsequent terms become comparatively negligible and one obtains

$$\delta=\frac{\bar{w}_1}{P_1/P-1} \qquad (5.6)$$

Eq. (5.6) can be rearranged as

$$\left(\frac{\delta}{P}\right)=\frac{1}{P_1}(\delta)+\frac{\bar{w}_1}{P_1} \qquad (5.7)$$

The above equation suggests that as the applied load P approaches the first critical load P_1, the relationship between $Y = \delta/P$ and $X = \delta$ becomes linear, and the slope $dY/dX = 1/P_1$ provides a basis to estimate the critical load P_1 . The intersection of the linear relationship with the $Y = \delta/P$ axis is $\bar{w}_1/P_1$ and provides an estimate of the initial out-of-straightness amplitude $\bar{w}_1$ corresponding to the first Fourier term.

5.2.2 Extension to lateral torsional buckling of beams under uniform moments

This section extends the Southwell plot technique, to beams with initial out-of-straightness (IOS) and initial angle of twist (IAT) lateral torsional buckling. A close form solution is attainable only for the case of uniform moments. Thus, a prismatic beam with initial out-of-straightness $u_0(z)$ and initial angle of twist $\theta_0(z)$ under uniform moment M is considered. As discussed in Section 4.3.1, the initial out-of-straightness $u_0(z)$ and initial angle of twist $\theta_0(z)$ can be expressed as

$$\left\langle u_0(z) \quad \theta_0(z) \right\rangle^T = \sum_{m=1}^{\infty} \phi_m \left\langle 1.0 \qquad \left(\frac{\pi^2 EI_y}{M_{crm} L^2} \right) \right\rangle \sin \frac{m\pi z}{L} \tag{5.8}$$

where ϕ_m is the contribution of the *mth* eigen mode to the IOS and IAT $\left\langle u_0(z) \quad \theta_0(z) \right\rangle^T$. The corresponding contribution of the *mth* eigen mode to the initial out-of-straightness of the compression flange has been shown to be

$$u_{0-c,m}(z) = u_m(z) + (d/2)\theta(z) = \phi_m \left[1 + (d/2) \left(\frac{\pi^2 EI_y}{M_{crm} L^2} \right) \right] \sin(m\pi z/L)$$

The corresponding additional lateral displacement $u_c(z)$ was found to be

$$u_c(z) = \sum_{m=1}^{\infty} u_{c,m}(z) = \sum_{m=1}^{\infty} \frac{1}{M_{crm}/M - 1} u_{0-c,m}(z) \tag{5.9}$$

where $u_{c,m}(z)$ is the additional lateral displacement corresponding to mode m and is given by

$$u_{c,m}(z) = \frac{1}{M_{crm}/M - 1} u_{0-c,m}(z) \qquad , m = 1, 2... \tag{5.10}$$

As $M \to M_{cr1}$, the first term of Eq. (5.9) gains dominance and the contributions of subsequent terms become comparatively negligible and one obtains

$$u_c(z) = \frac{1}{M_{cr1}/M - 1} u_{0-c}(z) \tag{5.11}$$

By re-arranging Eq.(5.10), one obtains

$$\left[\frac{u_c(z)}{M}\right] = \frac{1}{M_{cr1}}\left[u_c(z)\right] + \frac{u_{0-c}(z)}{M_{cr1}} \tag{5.12}$$

Equation (5.12) is linear between $Y = \left[u_c(z)/M\right]$ and $X = u_c(z)$ in a manner similar to Eq. (5.7) and the slope $dY/dX = (1/M_{cr1})$ of the $u_c(z)/M$ - $u_c(z)$ plot provides a basis to estimate the first critical moment M_{cr1} . Also, the intersection of the linear relationship with the $Y = u_c(z)/M$ axis is $u_{0-c}(z)/M_{cr1}$ which provides an estimate of the initial out-of-straightness amplitude associated with the first buckling mode.

5.3 Extension of the Southwell plot technique to beams with non-uniform moments

Since the findings of the previous section are confined to the case of beams under uniform moments, it is of interest to determine whether similar patterns can be observed for the more general case of non-uniform moments. Unlike the case of uniform moments, a closed form solution is unattainable under non-uniform moments. As such, the problem will be investigated numerically based on the FEM developed in Chapter 3.

A 7.80m span beam with a W250X45 cross-section is subjected to mid-span point load. Two cases for the initial out-of-straightness are examined. In Case 1, the initial out-of-straightness is assumed to be sum of the first, third and fifth modes, with equal amplitudes $(\phi_1, \phi_3, \phi_5) = L/3000(1,1,1) = 2.6(1,1,1)\,mm$. In Case 2, the initial out-of-straightness is assumed to exclusively follow the first mode with amplitudes $(\phi_1, \phi_3, \phi_5) = (L/3000, 0, 0) = (2.6, 0, 0)\,mm$ .The critical moments for the perfectly straight beam as obtained from the eigenvalue analysis is 100.3 kNm which corresponds to a load of 51.4kN. Using

the present FEM analysis, the load is ramped from 0.1kN to 51.4kN with a 0.01kN increments to obtain the non-linear load-lateral displacement relationship. The additional lateral displacement at the compression flange is examined at mid-span point $u_c = u_c\left(L/2\right)$. The analysis under Section 5.2.2 is postulated to hold true for the case of non-uniform moment and the validity of the assumption will be examined by comparing the buckling moment predictions of the developments of Section 5.2.2 to those based on the eigenvalue analysis. Thus, the critical moment M_{cr} is obtained from the inverse of the slope of $Y = \left[u_c/M\right]$ versus $X = u_c$ plot and the intercept of the relationship with $Y = u_c/M$ axis is assumed to be equal to u_{0-c}/M_{cr1} .Figure 5.1 presents the u_c/M - u_c relationship for the two IOS patterns considered.

The u_c/M - u_c relations for both IOS patterns are observed to slightly deviate for low values for the displacement u_c. Initially, the difference between both curves is 9.5% at an applied moment of $M = 0.2\,kNm$. As the applied moments increase, both relations approach one another, and when the applied moments $M = 66.0\,kNm$, the difference between both displacements reduces to 2.7%. This case corresponds to the right-most point in Figure 5.1. When the applied moment further increases to $M = 87.8\,kNm$, the corresponding percentage difference decreases further to 0.9% (not shown on Figure 5.1).

When conducting a lateral torsional buckling experiment on a beam with IOS, the loading is ramped up and the corresponding lateral displacement is recorded. Thus, the quantities $\left(M, u_c\right)_k$ would be known for multiple points $k = 1, 2....k_{max}$ along the loading path. The data collected is then used to determine $Y_k = \left[u_c/M\right]_k$ versus $X_k = \left[u_c\right]_k$. The computed $\left(X_k, Y_k\right)$ data within a given test range r can then be used to conduct a linear regression analysis of the form $Y_k = A_r X_k + B_r$, where the regression coefficients A_r, B_r depend on the regression range r and are related to the critical moment and initial IOS through the relations

$$A_r = \left(\frac{1}{M_{cr1}}\right)_r,\ B_r = \left(\frac{u_{0-c}}{M_{cr1}}\right)_r \tag{5.13}$$

It is evident that the accuracy of the predictions of M_{cr1} and u_{0-c} depends on the selected regression range. In order to characterize the effect of regression range r on the predictions of M_{cr1} and u_{0-c}, five ranges for applied moments are selected to conduct the regression analysis. These are 0.2-19.5, 19.7-39.0, 39.2-58.5, 58.7-78.0, and 78.2-100.3 kNm. The critical moment predictions and the IOS magnitude predictions are provided in Table 5.1. Column (7) indicates that the ratio of critical moment predicted based on the regression to that based on the eigenvalue prediction to range from 9.2% (for the lowest loading range considered of 0.2-19.5 kNm) down to 0.00% (for the highest loading range considered of 78.2- 100.3 kNm).

For the IOS scenario corresponding to case 2, given that the higher mode amplitudes were chose to vanish, it is observed that excellent predictions of the critical moments are obtained irrespective of the range of loading used for the regression. For a regression range of 0.20-19.5 and 78.2-100.3kNm, the predicted critical moment was 100.3 kNm, which coincide to that corresponding to that based on an eigenvalue analysis within four significant digits.

In summary, the previous findings suggest that proposed extension of the Southwell plot technique can be reliably used to predict the critical moments for a perfectly straight beam. For a beam with general IOS pattern involving higher mode contributions, the accuracy of predictions of the proposed method tends to quickly improve with the increase of the load range chosen for regression. For the hypothetical case where the IOS imperfection is assumed to follow solely the first mode, fast convergence towards the critical moment is observed and the use of data at low range of loading is found to reliably predict the critical moment for a perfectly straight beam.

Table 5.1 The predicted critical moment and magnitude of the IOS based on the considered range for the applied moment

Range #	Range	Regression coefficient		Predicted critical moment	Predicted IOS associated with the first mode	Percentage difference	
						for predicted moments*	for predicted IOS associated with first mode**
		A_r	B_r	$(M_{cr1})_p$	$(u_{0-c})_p$	$\frac{(M_{cr1})_p-(M_{cr1})_{EV}}{(M_{cr1})_{EV}}$	$\frac{(u_{0-c})_p-(u_{0-c})_{EX}}{(u_{0-c})_{EX}}$
(1)	(2)	(3)	(4)	(5)	(6)	(7)	(8)
	kNm	$1/kNm$	$1/kN$	*kNm*	*mm*	%	%
1	0.2-19.5	0.0214	4.57E-05	91.1	2.14	9.2	18
2	19.7-39.0	0.0205	4.63E-05	95.2	2.26	5.1	13
3	39.2-58.5	0.0199	4.72E-05	97.9	2.37	2.4	8.8
4	58.7-78.0	0.0196	4.83E-05	99.5	2.47	0.8	5.0
5	78.2-100.3	0.0194	5.00E-05	100.3	2.57	0.0	1.2

*$(M_{cr1})_{EV}$ critical moment as determined from eigenvalue analysis

**$(u_{0-c})_{EX}$ initial imperfection associated with first mode =*L/3000*=2.6mm

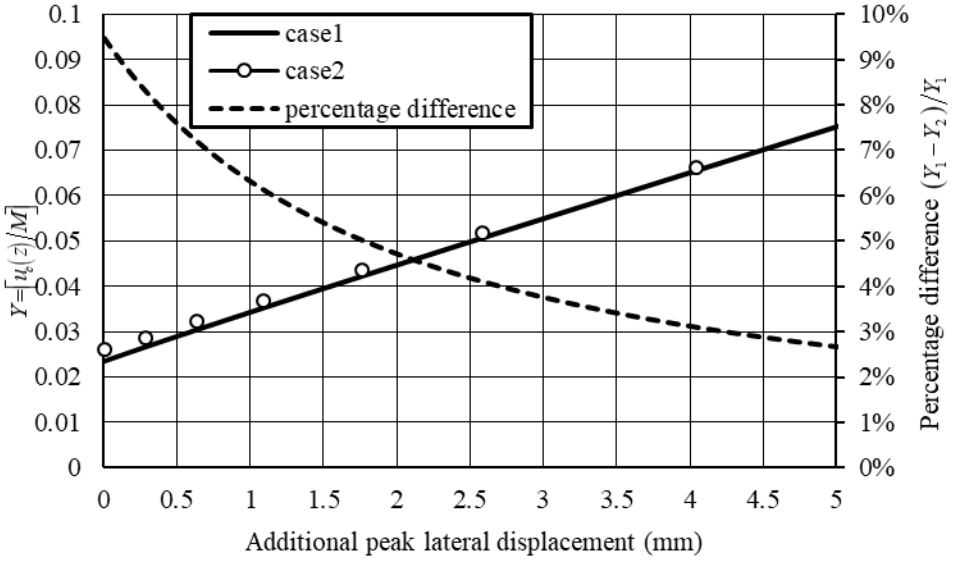

Figure 5.1 Relation between the additional peak lateral displacement to the applied load ratio and the additional peak lateral displacement (Southwell plot)

5.4 Extension of the technique to other displacements

The analysis in Section 5.3 adopted the mid-span lateral displacement at the compression flange and the corresponding critical moments to characterize the critical moment for a hypothetically perfectly straight beam and estimate the out-of-straightness. The mid-span displacement was adopted in a manner analogous to the technique advocated by Southwell (1931) to determine the buckling strength of columns based on the observed mid-span displacements. The present section

aims at assessing whether the findings remain valid if the lateral displacement is measured at other locations within the beam, or if the angle of twist is measured (instead the top flange displacement). The beam defined in section 5.3 is re-considered, with the IOS pattern of Case 2 with $(\phi_1, \phi_3, \phi_5) = L/3000(1,0,0)$. Four alternative displacements are investigated (1) additional mid-span lateral displacement at the centroid $u(L/2)$, (2) additional mid-span angle of twist $\theta(L/2)$, (3) additional centroid lateral displacement at quarter span $u(L/4)$. The additional mid-span lateral displacement at the compression flange $u_c(L/2)$, which was adopted in Section 5.4, is provided for comparison. Given the Southwell plot takes the form $Y_k = A_r X_k + B_r$, similar Southwell plots were assumed to hold true for each of the considered displacements, i.e.,

$$\left[\frac{u(L/2)}{M}\right] = \left[\frac{1}{M_{cr1}}\right]_{u(L/2)} \left[u(L/2)\right] + \left[\frac{u_0(L/2)}{M_{cr1}}\right]_{u(L/2)}$$
$$\left[\frac{\theta(L/2)}{M}\right] = \left[\frac{1}{M_{cr1}}\right]_{\theta(L/2)} \left[\theta(L/2)\right] + \left[\frac{\theta_0(L/2)}{M_{cr1}}\right]_{\theta(L/2)}$$
$$\left[\frac{u(L/4)}{M}\right] = \left[\frac{1}{M_{cr1}}\right]_{u(L/4)} \left[u(L/4)\right] + \left[\frac{u_0(L/4)}{M_{cr1}}\right]_{u(L/4)} \qquad (5.14)\text{a-d}$$
$$\left[\frac{u_c(L/2)}{M}\right] = \left[\frac{1}{M_{cr1}}\right]_{u_c(L/2)} \left[u_c(L/2)\right] + \left[\frac{u_{0-c}(L/2)}{M_{cr1}}\right]_{u_c(L/2)}$$

Since the examined IOS pattern is solely based on the first buckling mode, the data in the range 0.2-19.5 kNm is used for regression in all four cases. The corresponding modified Southwell plots are provided in Figure 5.2a-d and the predicted moments and the magnitude of the IOS associated with mode 1 are provided in Table 5.2. For all four displacements considered, the predicted critical moments were found to match those based on the eigenvalue analysis within four significant digits. Also, the predicted value for the initial imperfection at the considered location (Column 3) is found identical to the exact input initial imperfection (Column 4). The results indicate that the modified Southwell plot technique can be applied to *any* lateral displacement (or angle of twist), irrespective of its location, to reliably predict the critical moment and the initial imperfection associated with the first mode.

Table 5.2 Predicted critical moment and the magnitude of the IOS based on the considered displacement

Displacement	Predicted moment (kNm)	Predicted IOS	IOS exact value $(IOS)_{EX}$	Percentage difference	
				for predicted moments $\frac{(M_{cr1})_p - (M_{cr1})_{EV}}{(M_{cr1})_{EV}}$	for predicted IOS associated with first mode $\frac{(IOS)_p - (IOS)_{EX}}{(IOS)_{EX}}$
(1)	(2)	(3)	(4)	(5)	(6)
$u(L/2)$	100.3	1.82mm	1.82mm [a]	0	0
$\theta(L/2)$	100.3	0.0058rad	0.0058rad [b]	0	0
$u(L/4)$	100.3	1.20mm	1.20mm [c]	0	0
$u_c(L/2)$	100.3	2.59mm	2.60mm [d]	0	0.4%

[a] based on $\dfrac{L/3000}{1+\left(\pi^2 EI_y h/2M_{cr1}L^2\right)}\sin(\pi z/L), z = L/2$

[b] based on $\dfrac{L/3000}{h/2 + M_{cr1}L^2/\pi^2 EI_y}\sin(\pi z/L), z = L/2$

[c] based on $\dfrac{L/3000}{1+\pi^2 EI_y h/2M_{cr1}L^2}\sin(\pi z/L), z = L/4$

[d] based on $(L/3000)\sin(\pi z/L), z = L/2$

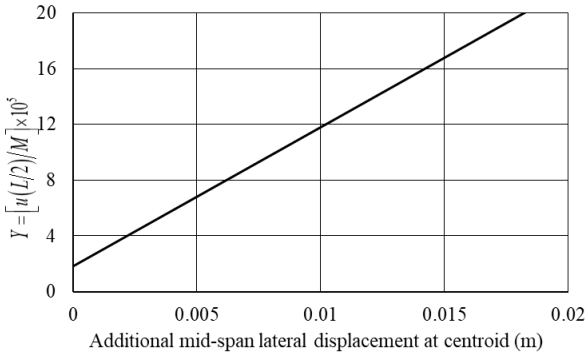

(a)

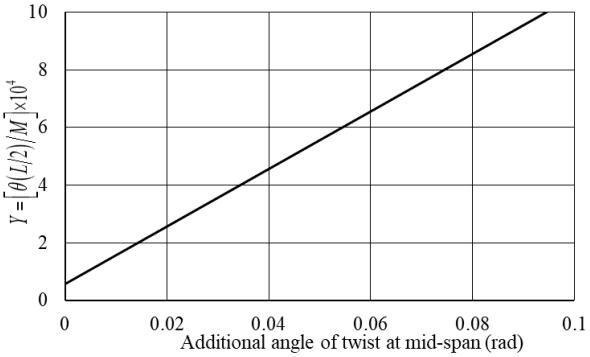

(b)

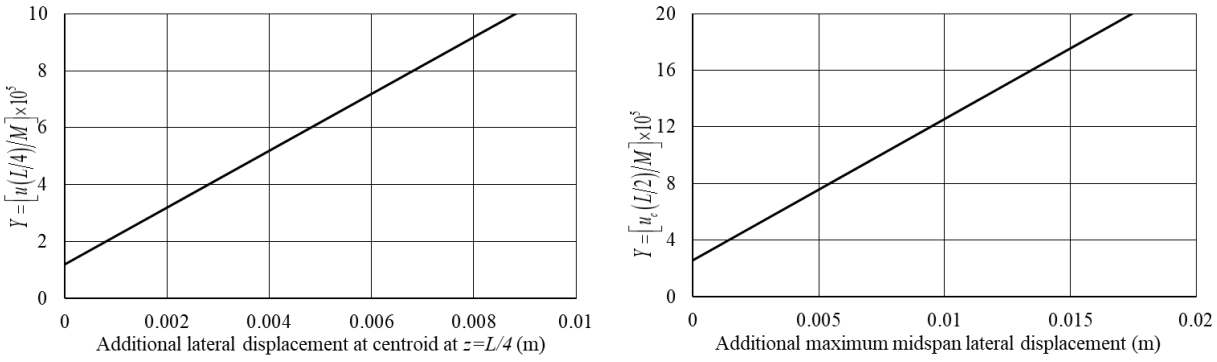

(c) (d)

Figure 5.2 Southwell plot based on four types of displacement (a) lateral displacement at the centroid at mid-span $u(L/2)$, (b) angle of twist about the centroid at mid-span $\theta(L/2)$, (c) lateral displacement at centroid at location $u(L/4)$ and (d) lateral displacement at the extreme fibre at mid-span $u_c(L/2)$

5.5 Prediction of the IOS magnitude

Sections 5.3 and 5.4 have shown that the Southwell plot are able to predict for the IOS magnitude associated with the first mode.

The 7.80m -span beam with a W250X45 cross-section defined in the previous under a mid-span point load is reconsidered is in this section. Four initial out-of-straightness scenarios are examined as a linear combination of modes1, 3, and 5. $(\phi_1,\phi_3,\phi_5)=L/1000(1,0,0)$ for case 1, $(\phi_1,\phi_3,\phi_5)=L/3000(1,1,1)$ for case 2, $(\phi_1,\phi_3,\phi_5)=L/1000(1,1,1)$ for case 3, and $(\phi_1,\phi_3,\phi_5)=L/3000,(3,1,1)$ for case 4. The corresponding mode contributions are provided in Columns 3 to 5 of TableTable 5.3. The moment resistance fractions $M_{\gamma,\gamma_1}/M_{cr}$ corresponding to the target displacements $L/360$, $L/270$, $L/180$ are provided in Columns 8 to 10, where the moment M_{γ,γ_1} is that predicted based on the FEM model developed in Chapter 3 and M_{cr} is predicted by an eigen value analysis. Columns 11 of Table 5.3 show the predictions of the critical moments for a hypothetical perfectly straight beam and various IOS measures based on three variations of the Southwell plot technique, based on the mid-span values of (1) additional lateral displacement at the compression flange, (2) additional lateral displacement at the centroid and (3) additional angle of twist.

In all three cases, the results show that the Southwell plot accurately predicts the IOS associated with the first buckling mode, as the percentage difference between the estimated IOS and the input IOS nearly vanishes.

For cases where the IOS is based on a linear combination of multiple buckling modes (Cases 2-4), the Southwell plot technique is found to predict IOS magnitude associated to the first buckling mode (Column 15-17), rather than the total IOS amplitude. For example, in Cases 2-4, the predicted displacement at the compression flange mid-span are 7.78, 2.59, and 7.79mm, which respectively nearly match the first mode contributions of 7.79, 2.60, and 7.79mm. These values generally differ from the corresponding total IOS values of 23.4, 7.79 and 13.0 mm.

Given the moment resistance fraction $M_{\gamma,\gamma_I} / M_{cr}$ calculated from the present finite element solution for threshold displacement values $u_c = L/\gamma = L/360$, $L/270$ and $L/180$ (Columns 8- 10), the predicted IOS L/γ_I are computed from Eq. 4.10: $\gamma_I = \gamma/\left(M_{cr}/M - 1\right)$. The resulting predictions are provided in Columns 18-20 for displacement thresholds $u_c = L/360$, $L/270$ and $L/180$, respectively. The corresponding percentage differences in Columns 21-23 range from to 0.4% respectively for case 1, suggesting that the equation $\gamma_I = \gamma/\left(M_{cr}/M - 1\right)$ is able to estimate the first mode IOS contribution (in a manner similar to the Southwell plot since both methods neglect the contributions of higher modes). In all cases considered, the Southwell plot technique and Eq. (4.10) are unable to capture the contributions of the higher modes.

Table 5.3 Assessment of Southwell plot technique to estimate IOS

(1)	(2)	(3)	(4)	(5)	(6)	(7)	(8)	(9)	(10)	(11)	(12)	(13)	(14)	(15)	(16)	(17)	(18)	(19)	(20)	(21)	(22)	(23)
	IOS information						FEM predicted moment ratio corresponding to			Southwell plot predictions							IOS predicted by Equation*					
					Contribution of ϕ_1												corresponding to					
Case	Peak IOS (γI)(mm)	ϕ_1	ϕ_3	ϕ_5	cenroid IOS at midspan (mm)	IAT at midspan (rad)	additional displacement =L/360	additioal dispalcement = L/270	Additional displacement = L/180	critical moment (kNm)	IOS at extreme fibre (mm)	IOS at cetroid (mm)	IAT (rad)	[(3)-(12)]/(3)	[(6)-(13)]/(6)	[(7)-(14)]/(7)	additional displacement =L/360	additional displacement =L/270	additional displacement =L/180	[(2)-(18)]/(2)	[(2)-(19)]/(2)	[(2)-(20)]/(2)
1	L/1000= 7.79	L/1000	0	0	5.46	0.0175	0.735	0.787	0.848	100.3	7.79	5.46	0.0175	0.0%	0.0%	0.0%	7.80	7.81	7.76	-0.2%	-0.2%	0.4%
2	3L/1000 =23.37	L/1000 =7.79	L/1000	L/1000	5.46	0.0175	0.739	0.790	0.849	100.3	7.78	5.46	0.0174	0.1%	0.0%	0.6%	7.64	7.67	7.70	1.5%	1.9%	1.2%
3	L/1000= 7.79	L/3000	L/3000	L/3000	1.82	0.00583	0.893	0.917	0.944	100.3	2.59	1.82	0.0058	0.4%	0.0%	0.5%	2.59	2.61	2.57	-0.4%	0.3%	1.3%
4	5L/3000 =12.98	L/1000	L/3000	L/3000	5.46	0.0175	0.737	0.788	0.848	100.3	7.79	5.46	0.0174	0.0%	0.0%	0.6%	7.72	7.76	7.76	0.4%	0.9%	0.4%

ϕ_1, ϕ_3 and ϕ_5 amplitudes of first, third, and fifth modes respectively to the IOS

$$^{*}\gamma_i = \gamma \frac{1}{M_{cr}/M - 1}$$

5.6 Effect of higher modes on the response

Figure 5.3 (a) depicts the relation between the applied mid-span point load and the total lateral displacement at the compression flange $\bar{u}_c$, as predicted by the present finite element solution, for the four cases considered in Table 5.3. The plots for all four cases are found to asymptotically approach from below the critical moment obtained predicted from the eigenvalue solution. While cases 1 and 3 share the same total IOS magnitude $u_{0-c} = L/1000$, a large difference is observed between the predicted moment ratio for case 1 is distinctly higher than that of case 3 given that the IOS contribution of the first mode in case 1 is three times higher than that of case 3. To the contrary, Cases 1, 2 and 4 tend to approach one another as the lateral displacement increases, although they happened to have different total IOS. This is due to the fact that the mode 1 contribution to the IOS is equal in all three cases.

In Figure 5.3 (b), the relation between the applied mid-span point load and the additional peak lateral displacement at the compression flange u_c is provided for the all four cases. All four curves are also found to asymptotically approach the critical load predicted by an eigenvalue solution from below. Unlike Figure 5.3(a), the plots for cases 1, 2 and 4 are observed to nearly coincide since they share a common IOS first mode contribution $\phi_1 = L/1000 = 7.79mm$. In contrast, Case 3 has a lower IOS first mode contribution $\phi_1 = L/3000 = 2.59mm$ and thus approaches the eigen value solution faster than the other thee plots. The results suggest that effect of the higher mode contributions to IOS on the moments predicted reduces as the additional lateral displacements decrease.

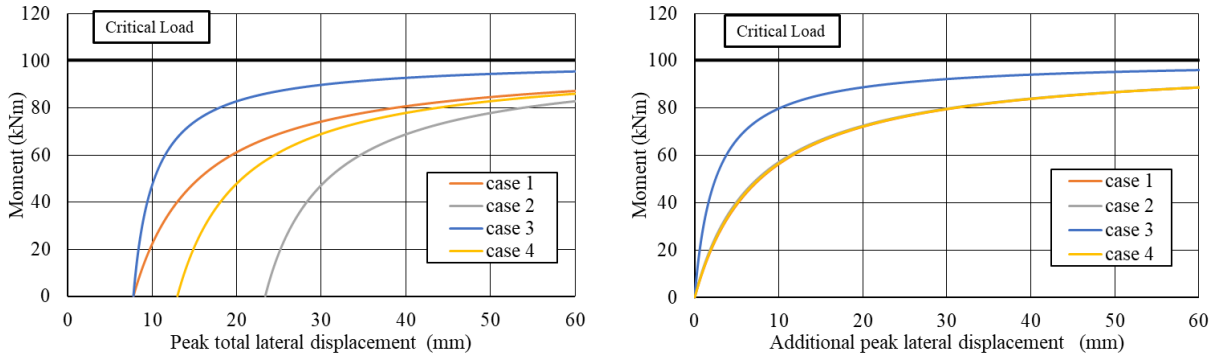

Figure 5.3 Relation between (a) the peak lateral displacement and (b) the additional peak lateral displacement and the applied load for the examined four cases

5.7 Predicting the number of contributing modes

The previous sections suggest that the Southwell plot technique can predict only the magnitude of the first buckling mode to the IOS. The present section proposes a technique to estimate the contributions of all modes by assuming all modes contribute equally to the IOS. In Chapter 3, we recall that the additional displacement at the compression flange u_c was given by summing the amplified IOS for each mode, resulting in the equation

$$u_c(z) = \sum_{m=1}^{\infty} \phi_m \frac{M}{M_{crm} - M} \sin\left(\frac{m\pi z}{L}\right) \tag{5.15}$$

The exact IOS is assumed to be based on a linear combination of the first, third and fifth buckling. In the absence of measurements suggesting otherwise, the contributions of three modes are assumed equal, i.e.,

$$\phi_1 = \phi_3 = \phi_5 = \phi, \phi_2 = \phi_4 = 0 \tag{5.16}$$

From Eq. (5.16) by substituting into Eq. (5.15) and adopting $z = L/2$, and solving for ϕ one obtains

$$\phi = u_c \Big/ \sum_{m=1,3,5} M/\left(M_{crm} - M\right) \tag{5.17}$$

Equation (5.17) is restricted for uniform moments. To extend its applicability to other loading cases, the elastic critical moments M_{crm} $(m = 1,3,5,..)$ are first obtained from the Eigen solutions. For a given moment M , the corresponding lateral displacement u_c is then obtained from the FEM developed in chapter 3. The terms on the right-hand side of Eq. (5.17) are known, which allows the characterization of the contributions $\phi_1 = \phi_3 = \phi_5 = \phi$ of the three modes.

Eq. (5.17) is applied to the IOS pattern corresponding to Case 2 defined in section 5.5. The percentage differences between the IOS predicted by Eq. (5.17) and the input IOS are provided in Figure 5.4. The percentage difference between the predicted and input IOS is found to decreases as the applied moments increase in a nearly linear manner. For example, the percentage difference between the predicted and input IOS is 16.5% at a moment of 40 kNM and reduces to 6.10% at a moment of 80kNm.

The previous example is based on the assumptions that (1) the number of the buckling modes n contributing to the IOS is known, and (2) the buckling modes contribute equally to the IOS. For a real beam, if the second assumption retained, it would be of interest to develop a technique to estimate the number of contributing modes n to the IOS. Equation (5.15) is normalized by dividing both sides by the maximum lateral displacement $u_c\left(L/2\right)$, yielding

$$\left[\frac{u_c\left(z\right)}{u_c\left(L/2\right)}\right]_n = \sum_{m=1}^{n} \frac{\dfrac{M}{M_{crm}-M}}{\displaystyle\sum_{m=1}^{n}\frac{M}{M_{crm}-M}} \sin\left(\frac{m\pi z}{L}\right), \quad m=1,3,5...n \tag{5.18}$$

The normalized lateral displacement distribution $\left[u_c\left(z\right)/u_c\left(L/2\right)\right]_n$ based on $n=1,3,5,...$ modes are compared to the lateral displacements at a relatively low value of the applied moment M (in comparison to the critical moment). Here, the lateral displacements are obtained from the FEM model, while for a real beam, the lateral displacement distribution would be experimentally determined. Figure 5.5 provides a comparison between the normalized lateral displacements for an applied moment $M =$ 39.2 kNm as predicted by Eq. (5.18) based on $n=1,3,5$. Overlaid on the same plot is the FEA predicted additional lateral displacement based on the input IOS. Given that in the present example, only modes 1, 3, and 5 were postulated to contribute to the IOS, the predictions of Eq. (5.18) provide a very close approximation to the FEA predicted additional lateral displacement when $n=5$, correctly predicting that, in this case, n should be taken as five.

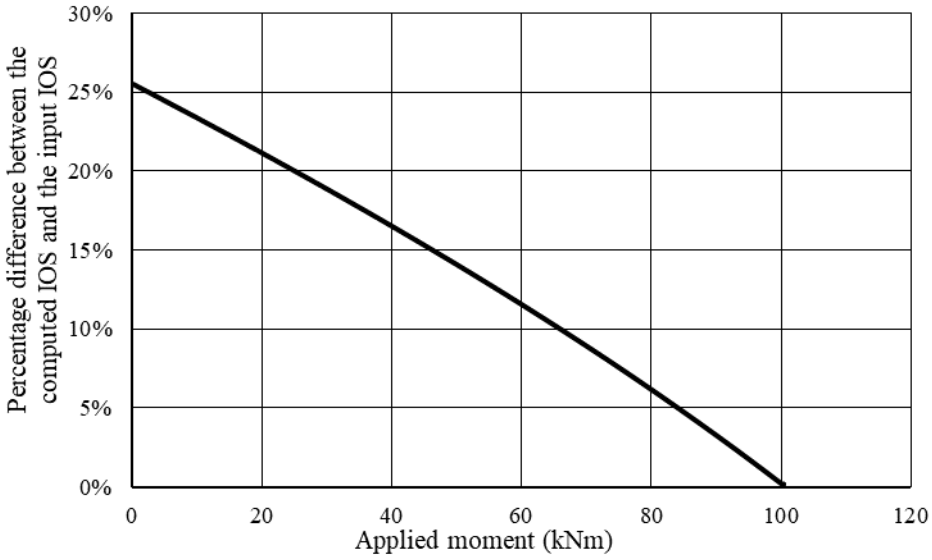

Figure 5.4 Relation between the percentage difference between the predicted IOS and the input IOS and the applied moment for case 2

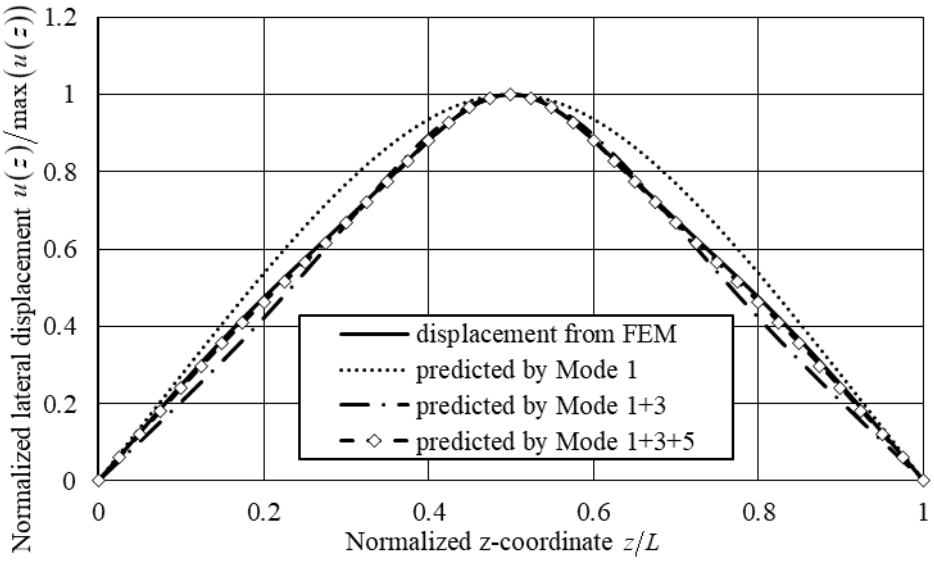

Figure 5.5 Normalized lateral displacement versus normalized coordinate of case 2 under 39.2kNm and the predicted shapes by

5.8 Summary and Conclusions

In this chapter, the theoretical background for the Southwell plot technique was reviewed and extended to the elastic lateral torsional buckling problem. The modified Southwell plot technique was extended for cases of non-uniform moments. The moment lateral displacement plots were developed for various IOS scenarios based on the FEM developed in Chapter 3. The effect of the higher modes on the accuracy of the critical moment and IOS predictions was investigated through

comparison of Southwell plot predictions to the critical moments predictions based on eigenvalue solution and the input in IOS. A method to estimate the contribution of higher modes was provided when the contributions of all modes are assumed equal. The main findings of the study are summarized as follows:

1. The modified Southwell plot technique can predict the elastic critical moment for a perfectly straight beam as well as the magnitude of the first mode contribution to the IOS.
2. When using the extended Southwell plot technique, using the data corresponding to larger loads and displacement was shown to lead to more accurate critical moment predictions.
3. The technique is found applicable and valid for any lateral displacement (or angle of twist) within the beam. Thus, the use of any displacement was found to reliably predict the critical moments and contribution of the first buckling mode to the IOS.
4. A method was devised to estimate the contributions of all modes in situations where the analyst believes that n modes contribute equally to the IOS.

6. Summary and Conclusions

6.1 Summary

1. A variational principle was developed in Chapter 3 for the lateral torsional analysis of beams with initial out-of-straightness (IOS) and initial angle of twist (IAT) subjected to strong axis bending. The variational principle was used to obtain the governing equations and boundary conditions by evoking the stationary conditions. The governing equations were solved for a simply supported beam under uniform moments to obtain a closed form solution for the load-displacement relationship. The variational principle was then used to develop a finite element formulation for crooked beams under general transverse loads and boundary conditions.
2. The validity of the finite element model was assessed through comparisons against the ABAQUS models for the thin walled beam element B31OS, the shell S4R and closed form solutions where applicable, and the present finite element model was found to reliably predict the load-displacement relationship for beams with IOS.
3. The finite element model was used to investigate the effect of the IOS/IAT patterns and the contribution of the higher modes on the load-displacement relationships of the initially crooked beams.
4. Two types of design criteria were proposed based on the threshold displacement and threshold stress values and applied in conjunction with load-displacement curves obtained from the present FEM to propose elastic lateral torsional buckling moments that account for initial imperfections.
5. Chapter 4 developed a closed form solution to determine the moment resistance fraction $M_{\gamma,\gamma_1}/M_{cr}$ based on the displacement based criterion. The expression is limited to simply supported beams under uniform moments. Numerical results were used to modify the expression and extend it to accommodate other loading cases.
6. Another closed form solution was developed in chapter 4 to characterize the moment resistance fraction $M_{\gamma_1,\varepsilon}/M_{cr}$ based on the stress-based criterion. The parameters influencing the moment resistance were identified and systematically investigated on members with common cross-sections.
7. The moment ratios based on the displacement-based criterion were used to propose a modified design curve design for the elastic critical moment resistance that could incorporate the IOS

effect into CAN/CSA S16-14 provisions. The moment ratios corresponding to the stress-based criterion were also used to propose modified design curves by adopting a format similar to the one used for columns in CAN/CSA S16-14.

8. A modified form of the Southwell plot technique was extended for the lateral torsional buckling of simply supported beams under uniform moments, and then the technique was numerically extended for other loading cases in Chapter 5. The technique was shown to be valid for any load versus lateral displacement or versus angle of twist history within the beam.
9. Using the load-displacement relationship obtained from the present FEM, in conjunction with the modified Southwell plot technique, the effect of the moment range on the accuracy of the predicted critical moments was studied.
10. The Southwell plot technique was shown to be able to estimate only the IOS associated to the first buckling mode. A method was proposed to predict the higher mode contributions to IOS, under the assumption that the first n modes contribute equally to the IOS.

6.2 Conclusions

The main conclusions of the work are:

1. When initial imperfections are expresses as a linear combination of the buckling modes, the most detrimental IOS contribution was shown to be associated with the first buckling mode. The relative contributions of higher modes to the lateral displacement (or angle of twist) tend to decrease as the applied loads approach the elastic critical loads.
2. For a specified initial out-of-straightness at the compression flange u_{0-c} , among the initial out-of-straightness scenarios attempted for the tension flange within the range $-u_{0-c} \le u_{0-t} \le u_{0-c}$, the most adverse IOS pattern was found to correspond to the case $u_{0-t} = -u_{0-c}$, which maximizes the initial angle of twist. In particular, for a specified initial out-of-straightness at the compression flange u_{0-c} , the assumption that the IOS follows the first buckling mode is found to be less detrimental.
3. Based the displacement based design criterion, the LTB resistance of a beam is found solely to depend on the magnitude of the initial imperfection and the threshold displacement specified by the designer.

4. In contrast, the LTB resistance $M_{\gamma_1,\varepsilon}/M_{cr}$ based on the stress based design criterion was found to depend upon the IOS coefficient, yield stress fraction, yield-to-critical moment ratio, span-to-section-depth ratio, flange-width-to-depth ratio and depth-to-flange-thickness ratio.
5. For an initially crooked beam under increasing moment, the normal stress ratio σ / F_y induced by minor axis bending and warping were found to increase at a higher rate than the normal stress ratio due to major axis bending as the applied loads are increased.
6. The equation for predicting the moment resistance ratio $M_{\gamma,\gamma_1} / M_{cr}$ based on the displacement criterion, while developed for the case of uniform moments, was found to provide reliable approximate results for non-uniform moments when appropriate moment gradient factors are adopted to modify the critical moment M_{cr} .
7. A modified form of the Southwell plot technique was found to reliably predict the elastic critical moment for a perfectly straight beam and the magnitude of the first buckling mode contribution to the IOS, given the load-displacement data from the lateral torsional buckling experiments (or analyses) on an initially crooked beam.
8. The accuracy of the modified Southwell plot technique is found to increase with the applied load magnitudes. The predicted critical moment is found to be more accurate when using data in the large moment range, as long as the specimen does not undergo yielding.
9. The modified Southwell technique is found to be valid for any displacement (or angle of twist) within the beam and is able to capture the contribution of the first buckling mode.

6.3 Recommendations for Future Research

Possible extensions of the present study include

1. While the finite element solution developed in Chapter 3 is applicable for any loading and boundary conditions, subsequent sections have focused solely on simply supported beams under three loading patterns. It is recommended to use the model developed to extend the study to other loading and boundary conditions.
2. The present developments were limited to doubly symmetric cross-sections. It is recommended to extend the model to mono-symmetric cross-sections.
3. The present model is based on the Vlasov theory which neglects the effect of cross-section distortion, shear deformation, and pre-buckling deformations. It is of interest to expand the work

to incorporate such effects by adopting thin-walled beam theories with more enriched kinematics.

4. The present work was primarily aimed at characterizing the effect of initial out of straightness on the elastic lateral torsional buckling resistance. It is of practical interest to extend the study within the inelastic range by incorporating the effects of plasticity, and the contribution of the residual stresses into the inelastic lateral torsional buckling range.
5. The present work was based on postulating initial out-of-straightness limits in line with manufacturing tolerances. While the above approach is conservative, it is of practical interest to supplement the information by measuring the initial out-of-straightness in real steel beams to possibly determine more representative initial out-of-straightness values. For such beams, it would be of interest to conduct full-scale testing to experimentally determine the load-lateral displacement relations and assess the applicability of the modified Southwell plot technique proposed in the present study.

Reference

[1] Ayrton, W. E., and Perry, F., (1886), On Struts, The Engineer, 62, 464

[2] Ariaratnam, S.T., (1963), The Southwell method for predicting critical loads of elastic structures, Quart. Journ. Mech. And Applied Math., XIV (2), 137-153

[3] American Institute for Steel Construction (1966): Specification for the Design, Fabrication and erection of structural Steel for Buildings, AISC, Chicago, Illinois

[4] American Institute for Steel Construction (1986): Manual of Steel Construction, Load and Resistance Factor Design, AISC, Chicago, Illinois

[5] Australian Standard (1998): Steel Structures, ABCB, Homebush, NSW

[6] Aguero, A. and Pallares, F.J., (2007) Proposal to evaluate the ultimate limit state of slender structures. Part 1: Technical aspects, Engineering Structures, 29, 483-497

[7] Ascione, F., (2014), Influence of initial geometric imperfections in the lateral buckling problem of thin walled pultruded GFRP I-profiles, Composite Structures, 112, 85-99

[8] Aguero, A. and Pallares, F.J., (2015a), Equivalent geometric imperfection definition in steel structures sensitive to lateral torsional buckling due to bending moment." Engineering Structures, 96, 41-55

[9] Aguero, A. and Pallares, L., (2015b) Equivalent geometric imperfection definition in steel structures sensitive to flexural and/or torsional buckling due to compression, Engineering structures, 96, 160-177

[10] American institute of steel construction (2016): Specification for structural steel buildings, AISC, Chicago, Illinois, America

[11] Barsoum, R. S., and Gallagher, R. H., (1970), Finite element analysis of torsional and torsional-flexural stability problems, International Journal for Numerical Methods in Engineering, 2, 335-52

[12] Boissonnade, N. and Jaspart, J.-P., (2002), Improvement of the interaction formulae for beam columns in Eurocode 3, Computers and Structures, 80, 2375-2385

[13] Canadian standard association (2014): Design of steel structures, CSA, Mississauga, Ontario, Canada

[14] Canadian institute of steel construction (2016): Handbook of Steel Construction, CISC, Willowdale, Ontario, Canada

[15] Dutheil, J., (1952), The theory of instability through disturbance of equilibrium. In: IABSE, 4th congress

[16] Dubina, D. and Ungureanu, V., (2002), Effect of imperfections on numerical simulation of instability behaviour of cold-formed steel members, Thin-Walled Structures, 40, 239-262

[17] DIN 18800 (1988): German Standard Organization, Teil 1-Stahlbauten, Bemessung and Konstrktion. Beth Verlag Gmbh, Berlin

[18] Eurocode 3 (1993): Design of steel structure. Part 1-1: General rules and rules for buildings, ENV 1993-1-1

[19] European committee for standardization (2005): Design of steel structures-Part 1-1: General rules and rules for buildings, Brussels

[20] Hasham, A.S. and Rasmussen, K. J. R., (1995), Member capacity of thin-walled I-sections in combined compression and major axis bending, Structural stability and design: proceedings of the international conference on structural stability and design, 1, 135-142

[21] Kala, Z. and Melcher, J., (2009), Material and geometrical characteristics of structural steels based on statistical analysis of metallurgical products, Journal of civil engineering and management, 15, 299-307

[22] Kala, Z., (2013), Elastic lateral-torsional buckling of simply supported hot-rolled steel I-beams with random imperfections, 11th International Conference on Modern Building Material, Structures and Techniques MBMST, 57, 504-514

[23] Massey, C., (1963), Elastic and inelastic lateral instability of I-beams, The Engineer, 216, 672-674

[24] Meck, H. R., (1977), Experimental evaluation of lateral buckling loads. Journal of the Engineering Mechanics Division, 103, 331-337

[25] Maquoi, R., and Rondal, J., (1982), Sur la force portante des poutres colonnes, Annales des travaux publics de Belgique, 5, 413-442

[26] Maquoi, R., Boissonnade, N., Muzeau, J. P., Jaspart, J.P., and Villette, M., (2001), The interaction formulae for beam-columns: a new step of a yet long story. Proceeding of the 2001 SSRC Annual Technical Session and Meeting, 63-68

[27] Mandal, P, and Calladine, C. R., (2002), Lateral-torsional buckling of beams and the Southwell plot, International Journal of Mechanical Sciences, 44, 2557-2571

[28] McCann, F., Wadee, M.A., and Gardner, L., (2013), Lateral stability of imperfect discretely braced steel beams, Journal of Engineering Mechanics, 139, 1341-1349

[29] NBE-EA-1995 (1995): Estructuras de acero en edification, Servicio de pubilicaciones, Ed. Ministerio de foment, Spain

[30] Nguyen, T.T., Chan, T.M., and Mottram, J.T., (2013), Influence of boundary conditions and geometric imperfection on lateral-torsional buckling resistance of a pultruded FRP I-Beam by FEA, Composite Structures, 100, 233-242

[31] Papadopoulos, V., Soimiris, G., and Papadrakakis, M., (2013), Buckling analysis of I-section portal frames with stochastic imperfections, Engineering Structures, 47, 54-66

[32] Southwell, R. V., (1931), On the analysis of experimental observation in the problems of elastic stability, Proceedings of the Royal Philosophical Society of London, 135(A), 601-616

[33] Standard association of Australia (1998): Steel structures, Homebush, NSW, Australia

[34] Szalai, J. and Papp, F., (2010), On the theoretical background of the generalization of Ayrton-Perry type resistance formulas, Journal of constructional steel research, 66, 670-679

[35] Timoshenko, S. P. and Gere, J. M., (1961), Theory of elastic stability, McGraw-Hill, New York

[36] Trahair, N. S. and Bradford, M. A., (1993), Flexural-Torsional buckling of structures, CRC Press, Boca Raton, Florida

[37] Taras, A. and Greiner, R., (2010), New design curves for lateral-torsional buckling-Proposal based on a consistent derivation, Journal of constructional steel research, 66, 648-663

[38] Vlasov, V. Z., (1961), Thin-walled elastic beams, 2nd edn, National science foundation, Washinton

[39] Yoshida, H. and Maegawa, K., (1983), Ultimate strength analysis of curved I-beams, Journal of Engineering Mechanics, 109, 192-214

[40] Yoshida, H. and Maegawa, K., (1984), Lateral instability of I-beams with imperfections, Journal of Structural Engineering, 110

[41] Yu, C. and Schafer, B.W., (2006), Distortional buckling tests on cold-formed steel beams, J. Struct. Eng, 132, 515-528